Q. J. R. Meteorol. Soc. (1992), **118**, pp. 877–926 551.553.21:551.513.7

Monsoon and ENSO: Selectively interactive systems

By PETER J. WEBSTER and SONG YANG*

Program in Atmospheric and Oceanic Sciences, University of Colorado, Boulder, Colorado, 80309, *USA*

(Received 11 September 1991; revised 4 March 1992)

SUMMARY

We attempt to construct a logical framework for the deciphering of the physical processes that determine the interannual variability of the coupled climate system. Of particular interest are the causes of the 'predictability barrier' in the boreal spring when observation–prediction correlations rapidly decline. The barrier is a property of many models and occurs irrespective of what time of year a forecast is initiated. Noting that most models used in interannual prediction emphasize the coupled physics of the Pacific Ocean basin, with the intent of encapsulating the essential structure of the El Niño–Southern Oscillation (ENSO) system, lagged Southern Oscillation Index (SOI) correlations are compared with the model results. The lagged SOI correlations also decrease rapidly in springtime. In that sense, the coupled ocean–atmosphere models are behaving in a manner very similar to the real system, at least as it is defined by the SOI.

We propose that (i) the springtime is a period where errors may grow most rapidly in a coupled ocean–atmosphere forecast model or (ii) there are other influences on the system that are not included in the simple coupled-model formulations. Both propositions are based on observations. By examining the period of correlation decrease, it is noticed that the equatorial pressure gradients tend to be a minimum at the time of the correlation decrease, suggesting that the ocean–atmosphere system may be least robust during the spring and, thus, subject to error growth. At the same time the south Asian summer monsoon is growing very rapidly. As the monsoon circulation is highly variable in both phase and amplitude from year to year, the ocean–atmosphere system may be subject to variable and impulsive forcing each spring.

A monsoon intensity index, based on the magnitude of the mean summer vertical shear in the 'South Asia' region, was defined for the broad-scale monsoon. 'Strong' and 'weak' monsoon seasons were determined by the index and were shown to be consistent with the independent broad-scale outgoing long-wave-radiation fields. Associated with the anomalous monsoons were global scale, coherent summer circulation patterns. Of particular importance was that stronger (weaker) than average summer trade winds were associated with strong (weak) monsoon periods. Thus, a signal of the variable monsoon was detected in the low-level wind fields over the Pacific Ocean that would be communicated to the Pacific Ocean through surface stresses.

A longer-period context for the anomalous summer monsoon circulation fields was sought. Based on the summer monsoon index, annual cycles for the years in which there were strong and weak monsoon seasons were composited. Large-scale coherent differences were apparent in the circulation fields over most of the globe including south Asia and the tropical Indian Ocean as far as the previous winter and spring. Although the limited data period renders the absoluteness of the conclusions difficult to confirm, the results indicate that the variable monsoon (and hence the signal in the Pacific Ocean trade regime) are immersed in a larger scale and slowly evolving circulation system. Based on the observation that the monsoon and the Walker circulation appear to be in quadrature, it is proposed that these two circulations are selectively interactive. During the springtime, the rapidly growing monsoon dominates the near-equatorial Walker circulation. During autumn and winter, the monsoon is weakest with convection fairly close to the equator; the Walker circulation is then strongest and may dominate the winter monsoon. During the summer the monsoon may dominate. Numerical experiments are proposed to test both propositions.

1. INTRODUCTION

Early studies identified the monsoon as a regional physical entity and, naturally, attempts to understand its structure and variability focussed on local effects. As global observations became more readily available to researchers, indications emerged that the monsoon was a macro-scale phenomenon which was intertwined and interactive with other global-scale circulations (Kutzbach 1987). In recent decades, with the advent of a more homogeneous data set from satellites and a more substantial conventional data base, there has been little to counteract this global view of the monsoon. A number of questions remain, however, such as: what is the role of the monsoon in the global climate and does the variability in the monsoon lag, lead or occur simultaneously with the interannual variability of other global phenomena?

* Present affiliation: Atmospheric and Environmental Research Incorporated, Cambridge, MA, 02139, USA.

Sir Gilbert Walker showed that the global atmosphere possesses coherent and fairly reproducible patterns of low-frequency variability (Walker 1923, 1924, 1928; Walker and Bliss 1932 (corroborated by Troup 1965; Berlage 1966; and many others)). Of the many interrelated patterns found by Walker, the Southern Oscillation (SO) was thought to be of particular relevance to the monsoon. Walker described the SO '. . . a swaying of pressure on a big scale backwards and forwards between the Pacific Ocean and the Indian Ocean . . .'. With the aid of such slowly varying circulations, Walker hoped to 'foreshadow' the variability of the Indian monsoon by seeking relationships with other aspects of the general circulation which he termed '. . . strategic points of world weather . . .'. Indeed, Walker's slow rhythms, most notably the SO, adumbrated the possibility of forecasting climate variations which would be of singular importance to the agrarian society of India. Yet, the ability to predict the future course of these rhythms was severely hampered by a vagueness in the observational relationships and by the failure to identify underlying physical processes which might have allowed the relationships to become unravelled.

To make use of the observations of large-scale coherent rhythms for predicting the intensity of the subsequent monsoon, Walker would have had to satisfy three basic criteria:

(i) The precursor circulation (the SO) should possess a spatial scale that encompasses the circulation or the phenomenon (the monsoon) that is to be predicted.

(ii) The precursor should possess a time-scale that is very much longer than that which is being predicted in order to provide sufficient lead time for the prediction to be useful.

(iii) The precursor circulation should be the 'active' circulation and the circulation to be forecast should be 'passive'. That is, an obvious cause and effect relationship should be apparent.

Walker's SO fulfilled the first two criteria. Figure 1(a) shows the spatial distribution of the simultaneous Southern Oscillation Index (SOI) (the normalized and detrended surface pressure difference between Papeete and Darwin[1]). The pattern resembles a dipole with the extrema spanning the Indian and the Pacific Oceans with scales larger than the monsoon region shown as the shaded rectangle in accord with the definition of Ramage (1971). Clearly, the summer and winter monsoon regions (we will use a northern-hemisphere chronology) are close to the locations of the positive extrema of the SOI. Whereas there are many time-scales embedded in the series (e.g. Rasmusson *et al.* 1990), the predominant period is four to five years; a scale consistent with basin-scale ocean–atmosphere dynamics (Philander 1990). Higher-frequency components of the SOI may result from complex interactions of related or independent phenomena. However, the low-frequency character of the SOI is far longer than the annual cycle and, thus, the monsoon period.

The third criterion has proven much more difficult to satisfy. Walker found that Indian summer rainfall, while weakly correlated with pressure variations some months earlier in locations as far away as South America, was more strongly correlated with *subsequent* events. In fact, as Normand (1953) summarized: 'Unfortunately for India, the Southern Oscillation in June–August, at the height of the monsoon, has many significant correlations with later events and relatively few with earlier events. . . . The Indian monsoon therefore stands out as an active, not a passive, feature in world weather, more efficient as a broadcasting tool than an event to be forecast. . . . On the whole,

[1] Walker's original SOI was a complicated combination of a number of parameters. Troup (1965) noted that the SOI was effectively the pressure difference between Papeete and Darwin, thus rendering a much simpler index.

(a) Zero-Lag Correlation of MSL Pressure with Darwin MSL Pressure

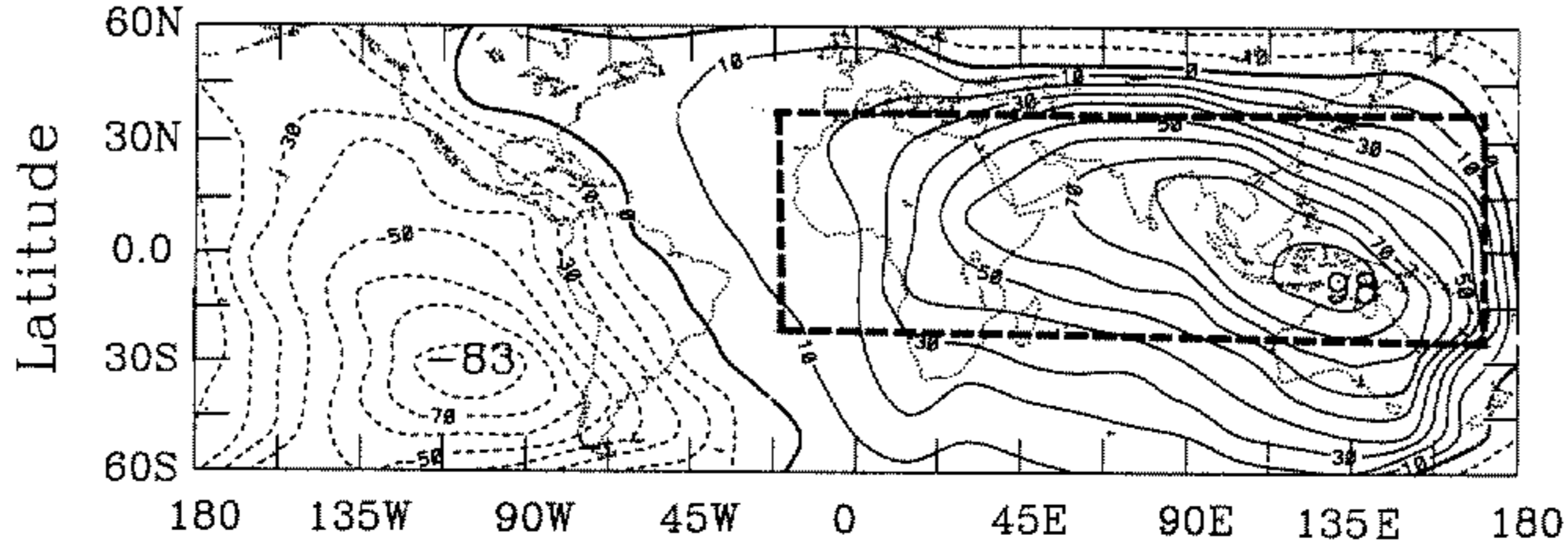

(b) Departures of MSL Pressure (June-August)

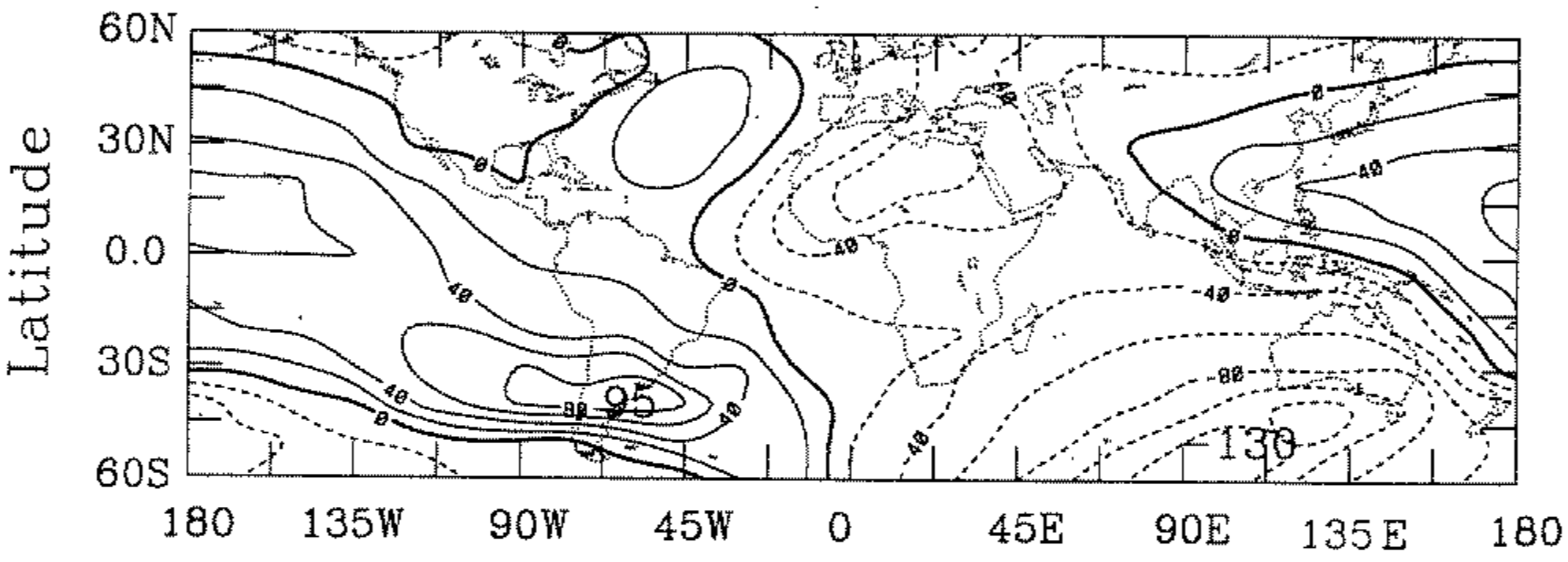

(c) Departures of MSL Pressure (December-February)

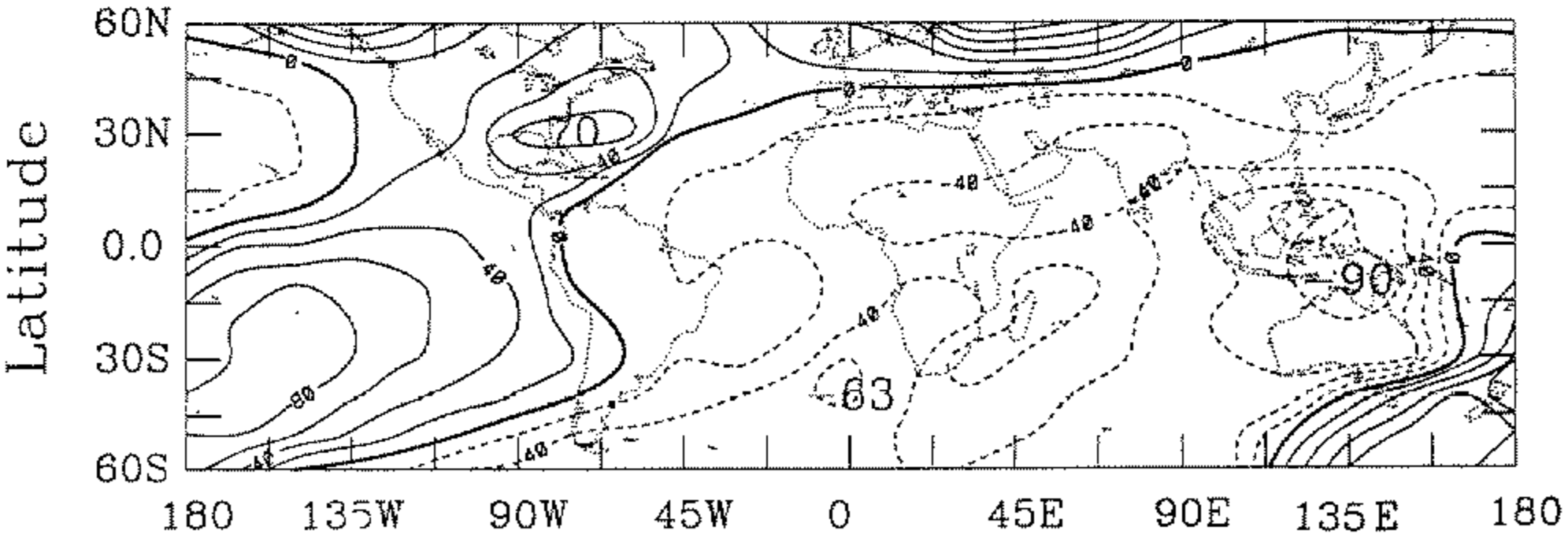

Longitude

Figure 1. (a) Global distribution of the zero-lag correlation of surface pressure variations with the Darwin surface pressure. The distribution defines the Southern Oscillation Index (SOI). The large negative and positive extrema in the Pacific and Indian Oceans are the centres of Walker's 'swayings'. The dashed rectangle outlines the area designated as 'monsoonal' by Ramage (1971). (b) The departure of the surface pressures (tenths of mb) from the long-term boreal summer mean value when the SOI is at +1 standard deviation (June–August). (c) The boreal winter surface pressure departure when the SOI is at +1 standard deviation (December–February). After Troup (1965). For the opposite extreme of the SOI the sign of the pressure anomalies would be reversed.

Walker's worldwide survey ended offering promise for the prediction of events in other regions rather than in India. . . .' Normand noted, however, that the failure of the SOI as a predictor for the monsoon referred specifically to the summer monsoon and that there had been some success in foreshadowing the winter monsoon.

Troup (1965) suggested why it it difficult to expect clear relationships between the SOI and Indian summer monsoon precipitation. Walker's correlations were re-examined by stratifying the deviations of surface pressure at the extremes of the SO from the long-term means by season. Planetary-scale regions of negative and positive sea level pressure are clearly evident in both summer (Fig. 1(b)) and winter (Fig. 1(c)). However, in the boreal summer the zero anomaly line passes very close to the Indian subcontinent. That is, India is located near a node in the pressure pattern and well away from the regions of anomaly extrema! Troup's diagrams suggest why the contemporaneous correlations of Indian rainfall and the SOI are spatially complicated and relatively weak, and why forecasting variations of the monsoon using the SOI may be difficult. Small displacements of the node would place India in either a weak-positive or weak-negative pressure regime. Given the uncertainties in the observations, it is not clear if the pressure anomalies over India would exclude zero with any statistical confidence. Thus, even with a perfect forecast of the SOI, a discriminating foreshadowing of the summer monsoon over India would be rather difficult. On the other hand, the major precipitating regions of the winter monsoon occur well away from the nodes and near the extrema of the anomalies. Therefore, *a priori*, one may expect that forecasting the variability of the winter monsoon using the SOI might have a better chance of success simply because the wintertime precipitation regions are located within a broad extremum of surface pressure and not near a node in the anomalous surface-pressure field.

Relationships between the SOI and monsoon precipitation, particularly over India, have been studied exhaustively. Angell (1981), Rasmusson and Carpenter (1983), Ropelewski and Halpert (1987, 1989), and many others, found less precipitation over India when the SOI was negative. Shukla (1987a) summarizes these studies by noting that, in the period 1900 to 1981, 14 out of 34 of the summer seasons with below average rainfall were years of warm events in the Pacific Ocean. Yet, only 2 of the 47 summers with above average precipitation were warm event years! Thus, it would seem that in warm event years the Indian subcontinent tends towards drought, although there are also serious rainfall deficiencies in non-El Niño years.

Whereas most of the research has concentrated on simultaneous relationships between the SOI and Indian summer rainfall, many studies have persisted in attempting to use the SOI as a base predictor for monsoon variability, despite the conclusions reached by Normand and Troup. For example, Shukla and Paolino (1983) have suggested that the *trend* of the SOI in the preceding spring appears to be more important as an indicator of Indian monsoon precipitation than the absolute value of the SOI itself. However, lagged correlations between the trend in the SOI and the subsequent mean June, July, August (JJA) SOI are very weak and led Shukla (1987b) to suggest that '. . . the largest negative correlations are found in November following the monsoon season. This suggests a possible role of monsoon rainfall fluctuations . . . in affecting the subsequent global circulation . . .' thus tending to support conclusions of Normand. Shukla and Mooley (1987) extended their analysis by configuring a regression equation comprised of the January to April Darwin pressure trend and the latitude of the 500 mb ridge over the Indian subcontinent. We will comment on the predictive utility of the SOI trend and the circulation characteristics in section 7.

In most studies, the emphasis has been on the relationship of the Indian summer rainfall with gross-scale rhythms such as the El Niño–Southern Oscillation (ENSO).

Although there are critical socio-economic concerns that have driven the regional emphasis, India represents only a moderate fraction of the monsoon area of Asia. It is not clear what the relationship is between rainfall on the Indian subcontinent and elsewhere in Asia (Ramage 1971). By extension, the extent of the relationship between the gross external rhythms and the broad-scale monsoon is also unclear. Thus, it is important that some measure of the broad-scale monsoon intensity is obtained.

Other relationships have been made with the interannual variability of the monsoon besides the ENSO. Blanford (1884) was the first to suggest that the intensity of the monsoon was governed by the extent of the previous winter snowfall over Eurasia. Early successes were replaced by failure (Kutzbach 1987). Hahn and Shukla (1976) suggested that Blanford's failure may have been a result of unreliable data and showed strong relationships between snow extent and monsoon rain. Barnett (1984, 1985) showed that limited snowfall during the winter was associated with a stronger than average monsoon in the following winter. Excessive snowfall, on the other hand, was related to a weak monsoon. Dickson (1984) with a more extensive data set confirmed the analysis. Barnett (1984, 1985) and Barnett *et al.* (1989) noted that variability in the monsoons and the ENSO appeared to be related. A large-scale propagating surface-pressure signal was detected to move through the Indian Ocean region into the Pacific Ocean with time-scales greater than two years. The genesis region of the signal appeared to be in the Asian region and Barnett (1985) suggested that it was associated with Blanford's winter snowfall mechanism. Thus, there have been a number of suggestions which have attempted to unify the variability of a number of circulation patterns.

With respect to gross-scale rhythms, Bjerknes (1969) made a key deduction that allowed a physical interpretation of the SO. Interannual variability, Bjerknes reasoned, was the result of interactive processes occurring between the tropical ocean and the atmosphere. Bjerknes was able to relate the quasi-periodic warmings of the Pacific Ocean (the El Niño) and Walker's SO, creating the concept of the ENSO phenomenon. Armed with Bjerknes's vital clue, and with the realization that the long 'memory' of the ocean might allow a predictive capability of the joint system, the international scientific community launched the Tropical Ocean Global Atmosphere (TOGA) monitoring and modelling program. The essential purpose of TOGA was to produce a model-based predictive capability of the coupled system for interannual time-scales.

The predominant phenomena identified early in the TOGA project were the same as those recognized by Walker, the SO and the monsoon, both of which undergo considerable interannual variability. To a large degree, emphasis within TOGA has been directed towards the physical processes contained within the Pacific Ocean basin; a focus which has led to the identification of basic processes that control the longer-term aspects of the ENSO cycle (see Philander (1990), National Research Council (1990) and McCreary and Anderson (1991)). Theories of the ENSO fall into two basic classes. These are: that the coupled system is a lagged oscillator (e.g. Schopf and Suarez 1988; Cane and Zebiak 1985; Battisti 1988) or that the modulation is the result of unstable modes (e.g. Neelin 1988; Battisti and Hirst 1989). The extent of the understanding is illustrated in the moderately successful forecasts of the coupled ocean–atmosphere system in the Pacific Ocean (e.g. Zebiak and Cane 1987; Cane *et al.* 1986; Latif and Graham 1991). So far the models used in these endeavours have been relatively simple and their success has allowed Cane (1991) to make the erudite statement: 'The degree of forecasting skill obtained, despite the crudeness of the model, is telling. It suggests that the mechanism responsible for the generation of El Niño events and, by extension, the entire ENSO cycle, is large-scale, robust and simple: if it were complex, delicate or dependent on small-scale details, this model would not succeed.' There is some justification for Cane's

statement. Many coupled ocean–atmosphere models show ENSO-like variations and support rotational theories involving the joint interaction of the ocean and the atmosphere. There can be little doubt that the models do take into account fundamental physical processes.

Simulation of a phenomenon, though, does not necessarily translate into predictive skill. In fact, the simple ocean–atmosphere prototypes appear to possess distinct prediction limits that are tied very strongly to the time of the year at which the model was initialized. Figure 2 plots the correlations between predictions and observations of the eastern Pacific Ocean as a function of time of year for forecasts starting in April, July, October and January (after Latif and Graham 1991). The curves have been offset so that they are aligned to show the observation–prediction correlations at specific times of the year. Forecasts initiated in April possess a moderately high correlation throughout the year before decreasing rapidly in the following spring. High correlations are maintained for July forecasts for nearly nine months before they also decrease rapidly in the subsequent April and May. Forecasts initiated in October possess only a six-month period of high correlation before they also diminish in spring. High correlations for the January forecast last only for a very short time. Similar decreases across the spring period appear in the results of other models (see for example Cane (1991)).

The models described in Cane (1991) and Latif and Graham (1991) are effectively Pacific Ocean basin models. The models are 'spun up' using observed wind distributions, but after a particular time a simple atmospheric model provides feedbacks to the ocean. Generally an annual cycle is added analytically to the system. However, the models appear to be very sensitive to any system or process that disturbs the wind strength over the Pacific Ocean of the model. For example, Barnett *et al.* (1989) found that a weak

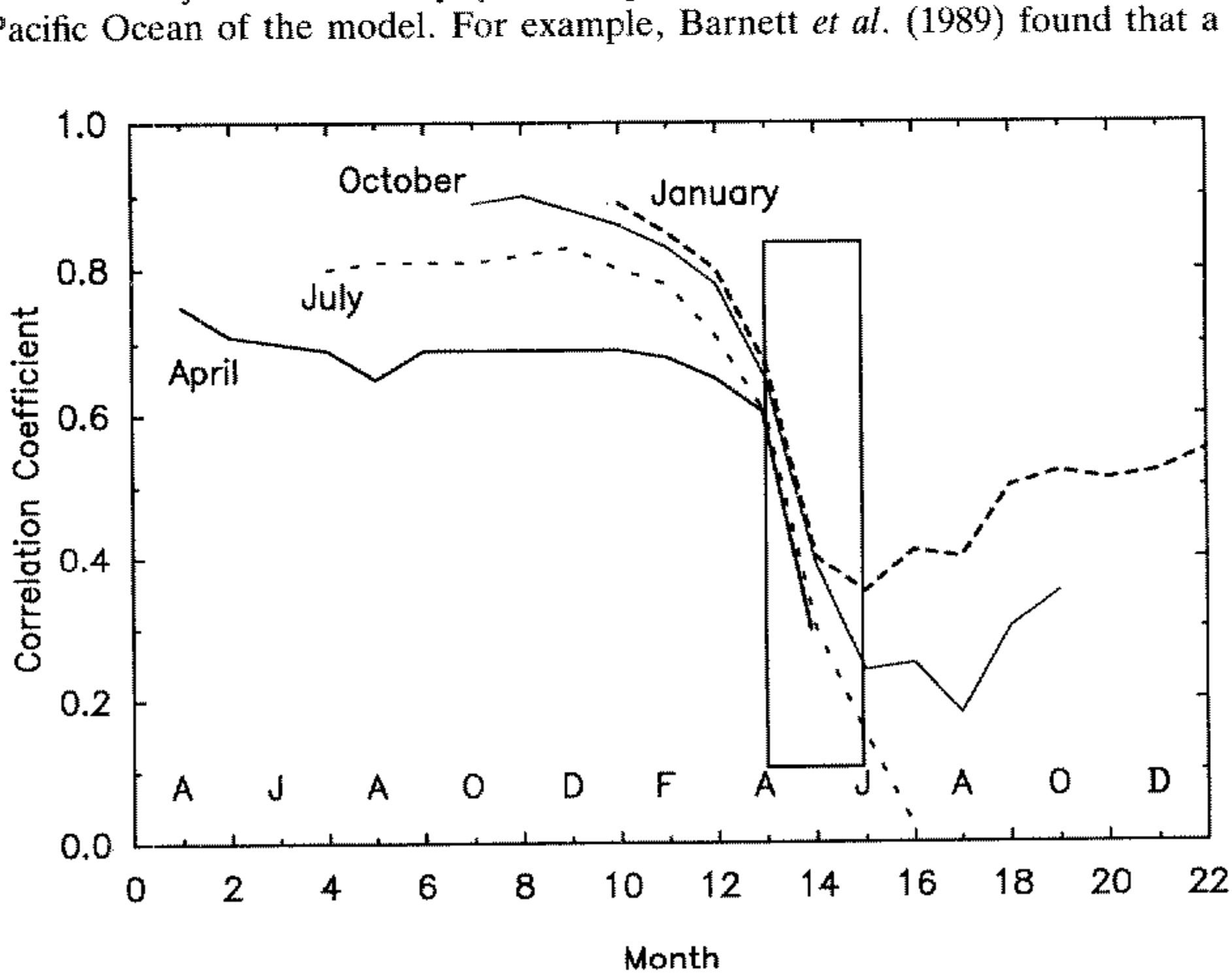

Figure 2. The variation of the correlations between observations and predictions of the sea surface temperature of the coupled system of the Pacific Ocean (adapted from Latif and Graham 1991). Correlates are observed and predicted sea surface temperatures of the Pacific Ocean. The curves denote correlations for forecasts commencing at four different times of the year: April, July, October and January. Irrespective of when the prediction was commenced, the correlation coefficients decrease rapidly between April and June (boxed area).

trade wind, when imposed on an ocean model, produced a weak El Niño system. The weak trade winds introduced into the model were associated with a heavy winter snowfall regime and a weak subsequent summer monsoon. Thus there appears evidence that the coupled ocean–atmosphere response in the Pacific Ocean is coupled strongly with events occurring outside the basin.

The Latif–Graham forecasts show clear evidence that the distinct limitation on the length of useful forecasts using the simple models is tied strongly to the annual cycle. In this context, around the time of the vernal equinox there appears to exist a 'predictability barrier'. The boxed region outlines the period of rapid diminution of the correlation coefficients. How the low-frequency events are influenced by the annual cycle or why that influence is manifested at a particular time of the year is not understood. It should be noted that there is not a similar correlation decrease near the autumnal equinox. That is, the barrier occurs only at one time of the year! In order to proceed there are a number of questions that require answers. These are:

(i) *What are the unique aspects of the spring period of the annual cycle of the tropics?* Modelling studies show a distinct drop in predictability across the boreal spring equinox. A similar decrease does not seem to occur across the boreal autumnal equinox or at any other time of the year.

(ii) *Is the predictability barrier a result of model inadequacies or simplifications, or does it point to an absolute limit to interannual predictability*? The coupled prediction models used to date are relatively simple. Thus, can we expect the predictability barrier to be bridged with more complete models? On the other hand, are these current models sufficiently complete that they are really reflecting a limit on the predictability of the natural system?

(iii) *To what degree are the variabilities of the broad-scale monsoon and the ENSO related*? Variations are observed in the period of the ENSO and the amplitude and phase of the monsoon both in terms of their circulation features and precipitation patterns. The SOI possesses a fairly high simultaneous correlation with the Indian summer monsoon rainfall, at least during drought years. However, the lag and lead correlations about the period of monsoon rains are not symmetric, with a short lead and a long lag relative to events occurring around the Indian summer monsoon. What is the cause of the lag–lead asymmetry? Is the variability of the monsoon and the ENSO a joint venture as suggested by Barnett (1984, 1985) and is the cause of dual variability the snowfall over the Asian continent?

(iv) *How variable is the amplitude and the phase of the broad-scale monsoon*? There appear to be secular variations of the Indian summer monsoon, but are these variations indicative of variations in the entire Asia-wide monsoon system? How can the variability of the monsoon circulation be quantified? Fairly unambiguous measures exist for the variability of the ENSO but an equally simple picture does appear to exist for the planetary-scale monsoon. A definition and a measure or index of the broad-scale monsoon intensity is required.

(v) *How predictable are the variations of the large-scale monsoon*? Despite the conclusions of Normand (1953), most prediction schemes of the large-scale monsoon are still based on associations with the ENSO. But are there other predictors which provide clues to the interannual variability of the monsoon? Would such predictors satisfy the three basic precursor-antecedent criteria listed earlier?

(vi) *From where do the higher-frequency components of the ENSO signal arise*? Higher-frequency components (e.g. the biennial period found by Rasmusson *et al.* (1990) and Barnett (1991)) exist in the SOI besides the basic four- to five-year period

that may be expected from simple wave or lagged-oscillator theories of the Pacific Ocean. Do the higher-frequency components suggest that the annual cycle plays a key role in the modulation of the long-period ENSO cycle through, for example, the imposition of a variable monsoon signal on the coupled system?

The principal purpose of the ensuing study is to provide a logical framework for the deciphering of the physical processes that determine the interannual variability of the coupled system and for answering the questions listed above. Whereas we will attempt to come to closure on the questions listed above using diagnostic methods, it is clear that there are limitations to the technique. Either the data are insufficient for absolute determinations or diagnostic techniques alone cannot reach closure on certain issues. However, the diagnostic approaches do have the utility in suggesting theoretical and numerical studies which may lead to closure in combination with the data studies. In the final section and appendix B we will suggest a suite of modelling studies that are required to bolster the results of the diagnostic studies.

In the second section, we consider characteristics of the circulation that appear anomalous during the boreal spring. We propose two hypotheses which allow for the existence of a predictability barrier at that time of the year. In the third section we define the 'broad-scale' monsoon and configure an intensity index related to the monsoon circulation. In the fourth section simultaneous relationships between the monsoon and the SOI are examined. Lag–lead relationships are discussed in the following section. In section 6 a stratification of the circulation is made relative to the monsoon intensity index, and anomalous annual cycles developed relative to 'strong' and 'weak' summer monsoons. In the final section the concept of 'selective interaction' is developed. A series of numerical experiments are proposed to test the hypotheses.

2. Aspects of the annual cycle in the tropics

The asymmetry in the observation–prediction curves relative to the annual cycle (Fig. 2) suggests either that there exists anomalous forcing of the system occurring at one particular time of the year or that particular processes such as error growth occur more prolifically during spring. Thus a range of possibilities exist to explain the predictability barrier, ranging from external forcing functions influencing the coupled Pacific system to the frailness or robustness of the system itself.

To study the annual cycle of the tropics we make use of satellite-derived outgoing long-wave-radiation (OLR) data. Figures 3(a) and (b) show aspects of the June and December OLR fields. The upper panels show the mean fields averaged between 1974 and 1987. To facilitate the identification of the near-equatorial and monsoon heating fields, and to show features indicative of the Walker circulation and the monsoons, asymmetric and symmetric components of the OLR with respect to the equator were calculated and are shown in the middle and lower panels of each diagram.

During June, minimum OLR emittance occurs over southern Asia. Richards and Arkin (1981) showed that OLR values less than 240 $W\,m^{-2}$ (shaded) represent mean broad-scale precipitation and, thus, net tropospheric heating. In addition, gradients in OLR are indicative of horizontal gradients in columnar radiative flux divergence, a forcing function of large-scale circulations which is in phase with the latent-heating gradient and about one third its size (Webster 1991). Thus, one can infer from the OLR distributions that the majority of the atmospheric heating lies across the equator and over southern Asia. In June, monsoonal heating is reflected in the relatively large value of the asymmetric heating component, with maximum amplitude occurring along the

90°E meridian and a strong latitudinal gradient of about 25 W m^{-2} per 10° latitude towards the equator. The December fields are quite different. The monsoon heating gradient decreases by at least a factor of five, and major heating is now located much closer to the equator. In fact, the asymmetric component almost disappears over the Asian–Australasian sector. However, at this time of year, the equatorial heating gradient is much stronger than during June. The symmetric OLR values over Indonesia have decreased by nearly 20 W m^{-2} from summer to winter, with corresponding increases in the longitudinal gradients from 5 W m^{-2} in summer to nearly 10 W m^{-2} in winter.

It is clear that both the asymmetric and symmetric components of the circulation undergo a strong annual cycle. Emphasis is normally given to the annual cycle of the monsoon circulation. The annual cycle of the Walker circulation has received less attention. Yet its sub-annual variability is substantial. There are two symmetric heating maxima; over the eastern Indian Ocean and over the western Pacific Ocean. Throughout the year, the relative amplitude of the two maxima vary, producing variations in the direction of the zonal wind along the equator. In a sense, the annual variation of the Walker circulation is so strong that it may be termed a symmetric monsoon.

Summarizing the characteristics of the OLR fields in Fig. 3, we find that in the Indian–Pacific region, the boreal winter fields are dominated by a strong equatorial heating gradient. In summer, the equatorial heating gradient along the equator weakens and the latitudinal, asymmetric gradient dominates. In other words, the maxima of near-equatorial and cross-equatorial heating gradients, the forcing which drives the symmetric Walker circulation and the asymmetric monsoon, are about six months out-of-phase. The two orthogonal heating gradients are in quadrature.

To determine the transition between the extremes, we plot time–longitude plots of the symmetric (Fig. 4(a)) and the asymmetric heating (Fig. 4(b)) along the latitudes of maximum amplitude. The diagrams essentially show the mean annual cycle of the heating associated with the symmetric Walker circulation and the asymmetric monsoon. The symmetric fields show a minimum in intensity during the boreal summer and a maximum during the autumn and winter. However, the asymmetric fields show exceedingly rapid growth during spring and early summer. Once having reached a maximum value it is maintained through summer and across the autumnal equinox, at which stage it slowly decreases. The dashed rectangles on the two figures (and also Fig. 5) show the Latif and Graham (1991) predictability barrier transposed from Fig. 2.

The rapid transition of the monsoon can be seen by the mean composite annual cycle of the asymmetric OLR along the 90°E meridian (Fig. 5). The meridian chosen corresponds to the region of maximum summer asymmetric heating (Fig. 3(a)). Very strong trends extend across the spring equinox. However, the decrease in heating during the autumn is much slower. Thus the asymmetric heating imposes a strong asymmetric signal into the annual cycle. Similar asymmetries in the annual cycle have been found in numerical studies of the monsoon (e.g. Webster 1983; Srinvasian *et al.* 1992).

The rapid development of the monsoon is also apparent in circulation statistics. Figure 6 illustrates the annual evolution of the broad-scale monsoon kinetic energy defined as: $\overline{KE} = KE_{850\text{mb}} + KE_{200\text{mb}}$, where $KE_i = (u_i^2 + v_i^2)/2$, calculated over the region 5°N–15°N and 40°E–100°E to provide an indication of the strength of the broad-scale monsoon. u_i and v_i represent the zonal and meridional components at level i. The region is chosen to encompass the maximum heating region noted in Figs. 3 and 4 and the monsoon region defined by Ramage (1971) shown in Fig 1.

The evolution of the $\overline{KE}$ in the form of 20-day running means are shown for each of the four years. The heavy line shows the four-year average. During spring the south Asian summer broad-scale monsoon circulation develops explosively, yet during the

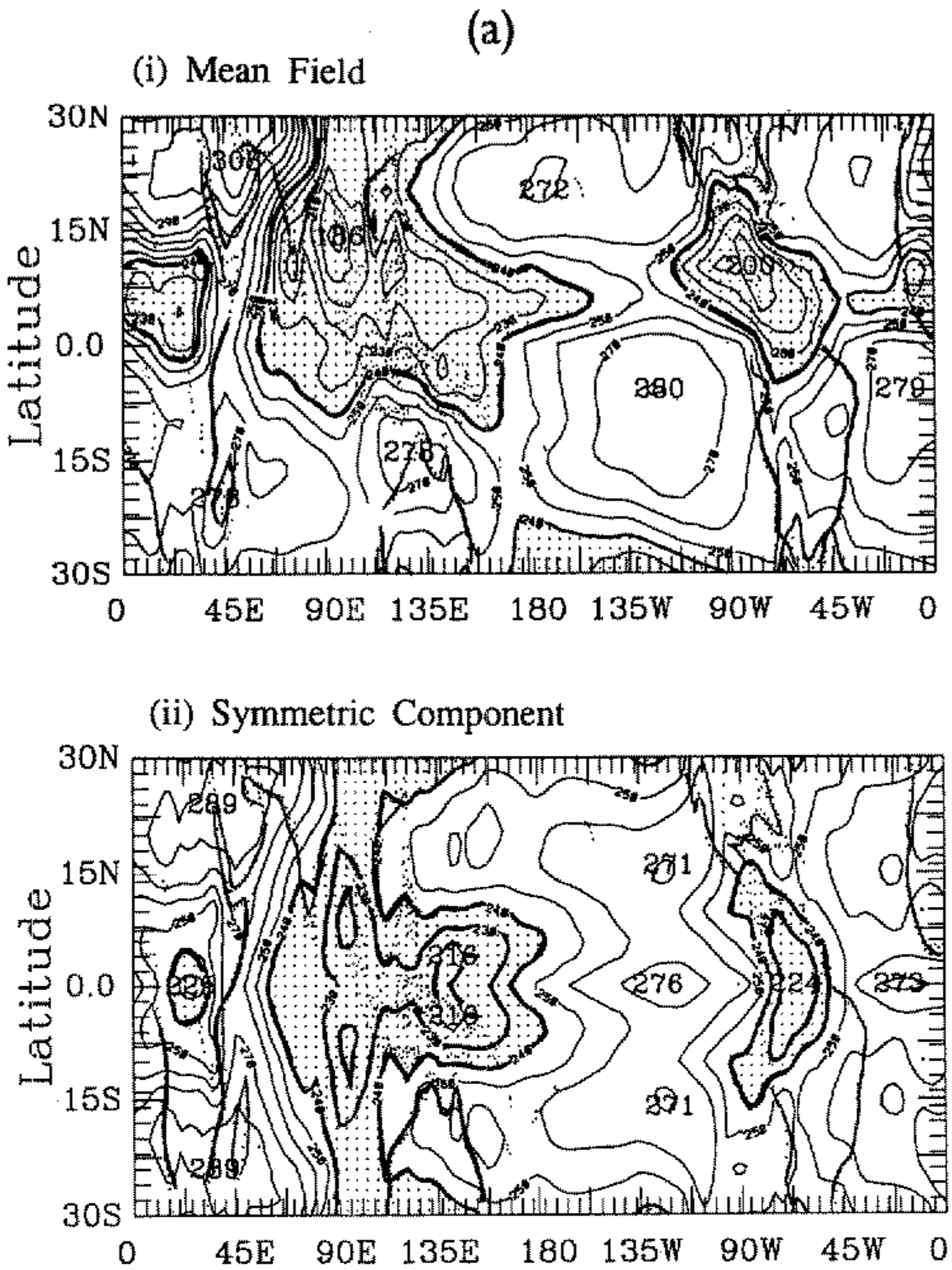

Figure 3. Structure of the (a) June, and (b) December outgoing long-wave-radiation (OLR) fields. The upper panels, (i), show the long-term (1974–87) mean distributions and the lower panels, (ii) and (iii), show the symmetric and asymmetric components of the OLR fields about the equator. Units are $W\,m^{-2}$ with intervals every 10 units. Shaded regions indicate OLR $< 240\,W\,m^{-2}$ (upper two panels) or negative values (bottom panels).

(b)

(i) Mean Field

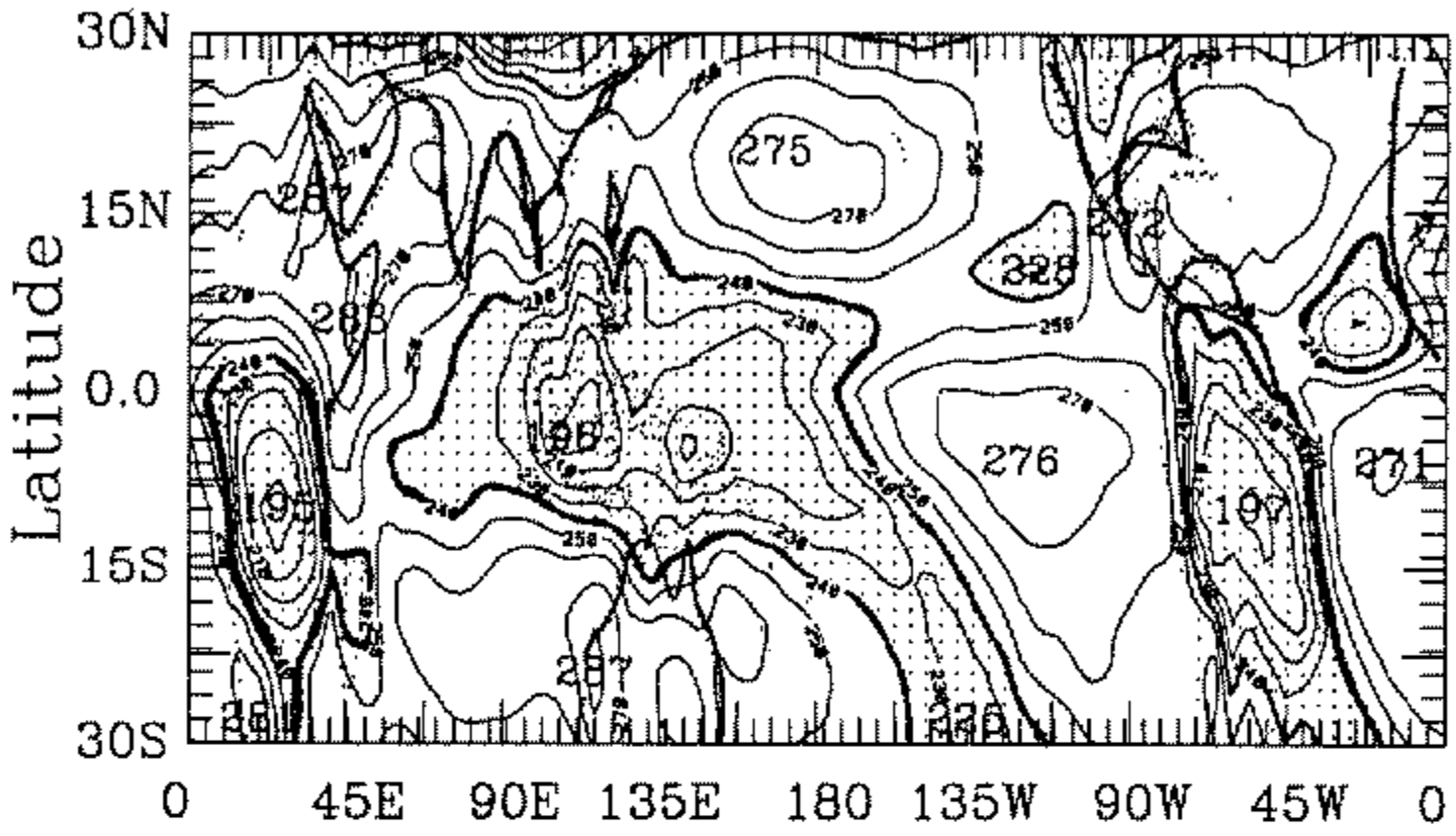

(ii) Symmetric Component

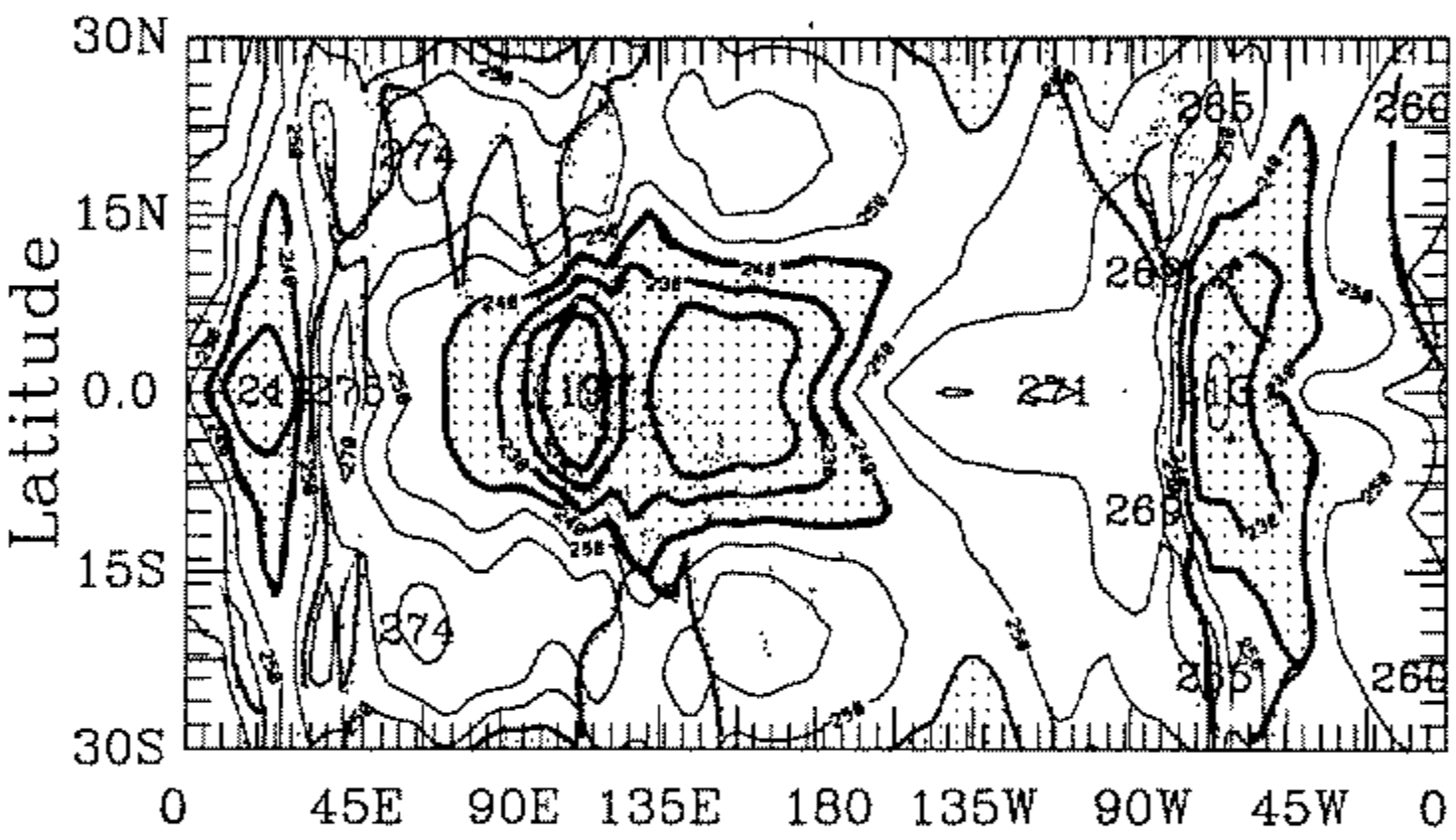

(iii) Asymmetric Component

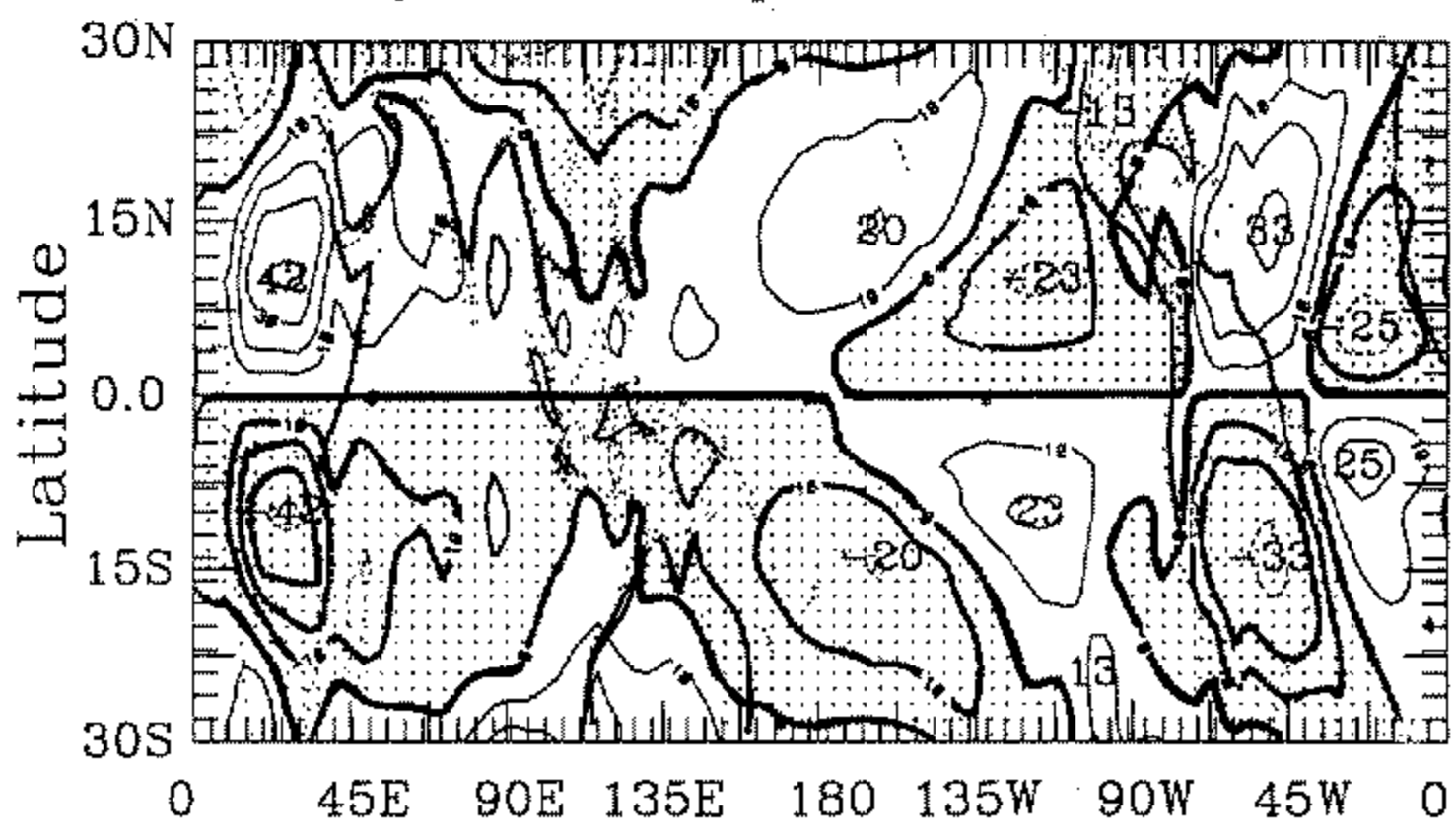

Figure 3. Continued.

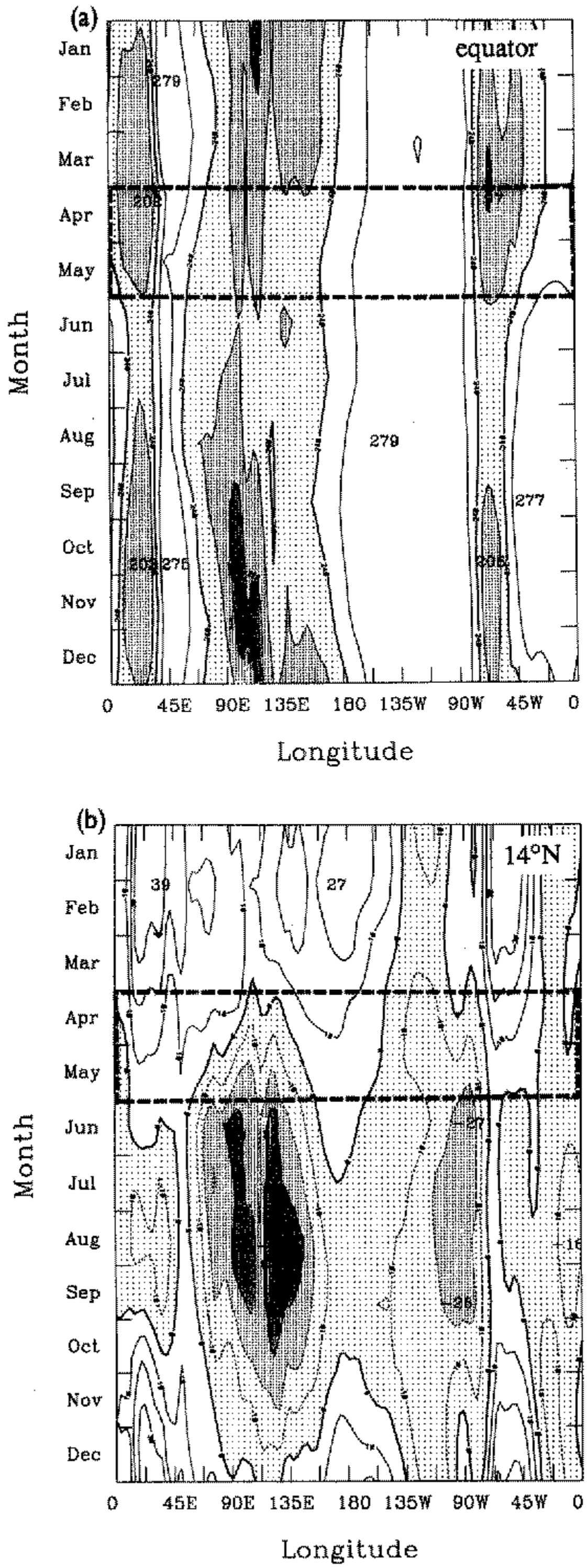

Figure 4. The mean annual cycle of the components of the outgoing long-wave-radiation (OLR) field ($W\ m^{-2}$). (a) The symmetric part along the equator (contour interval $20\ W\ m^{-2}$; regions where OLR $< 240\ W\ m^{-2}$ are shaded). (b) The asymmetric part along 14°N (contour interval $10\ W\ m^{-2}$; negative OLR values shaded). The symmetric and asymmetric parts of the OLR field are associated with the near-equatorial Walker circulation and the monsoon circulation, respectively. The heavy dashed rectangle outlines the time period of the correlation decrease shown in Fig. 2.

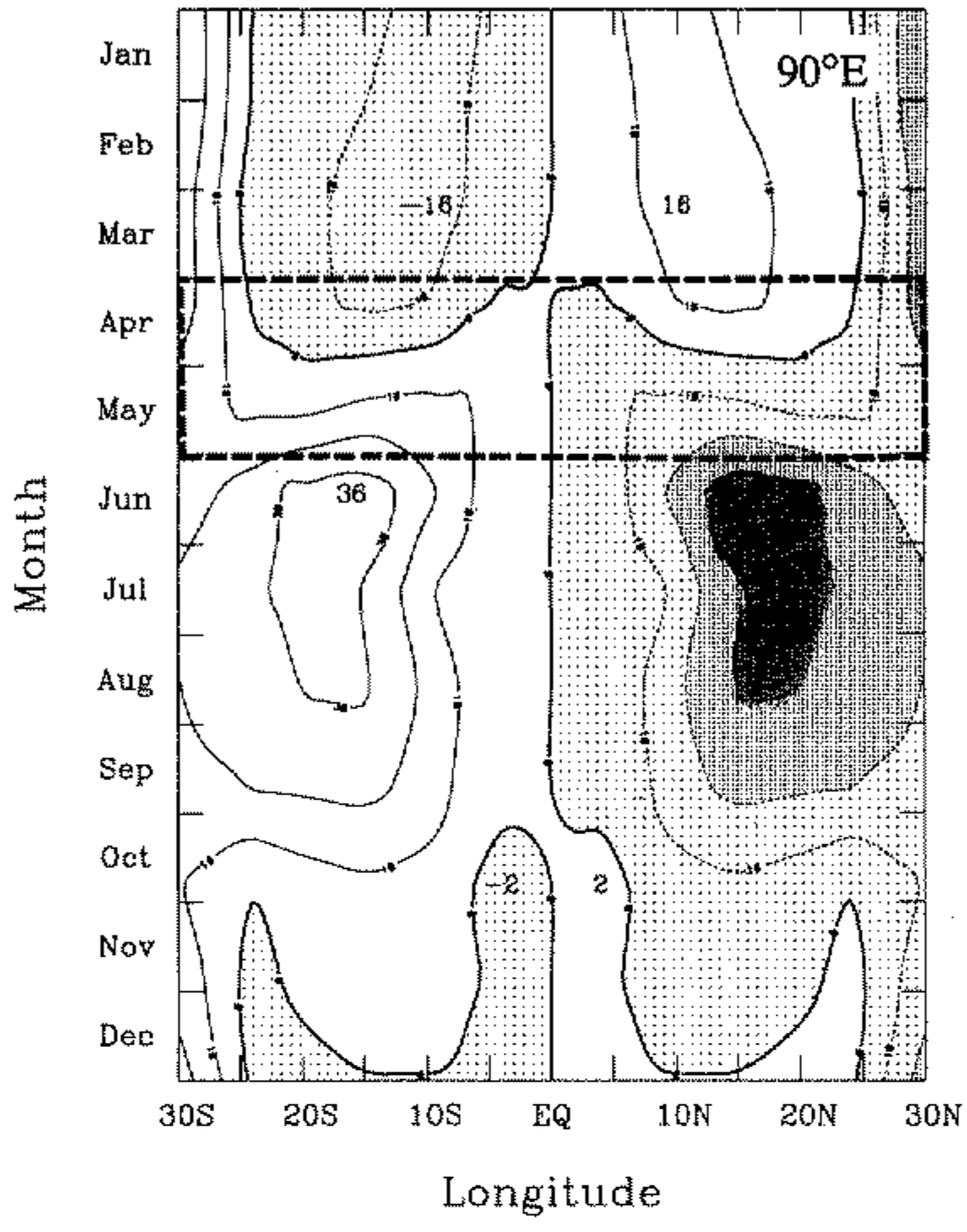

Figure 5. The mean annual cycle of the asymmetric part (monsoon) of the outgoing long-wave-radiation field (units W m^{-2}; contour interval 10 W m^{-2}) along the 90°E meridian. Negative areas are shaded. The heavy dashed rectangle outlines the time period of the correlation decrease shown in Fig. 2.

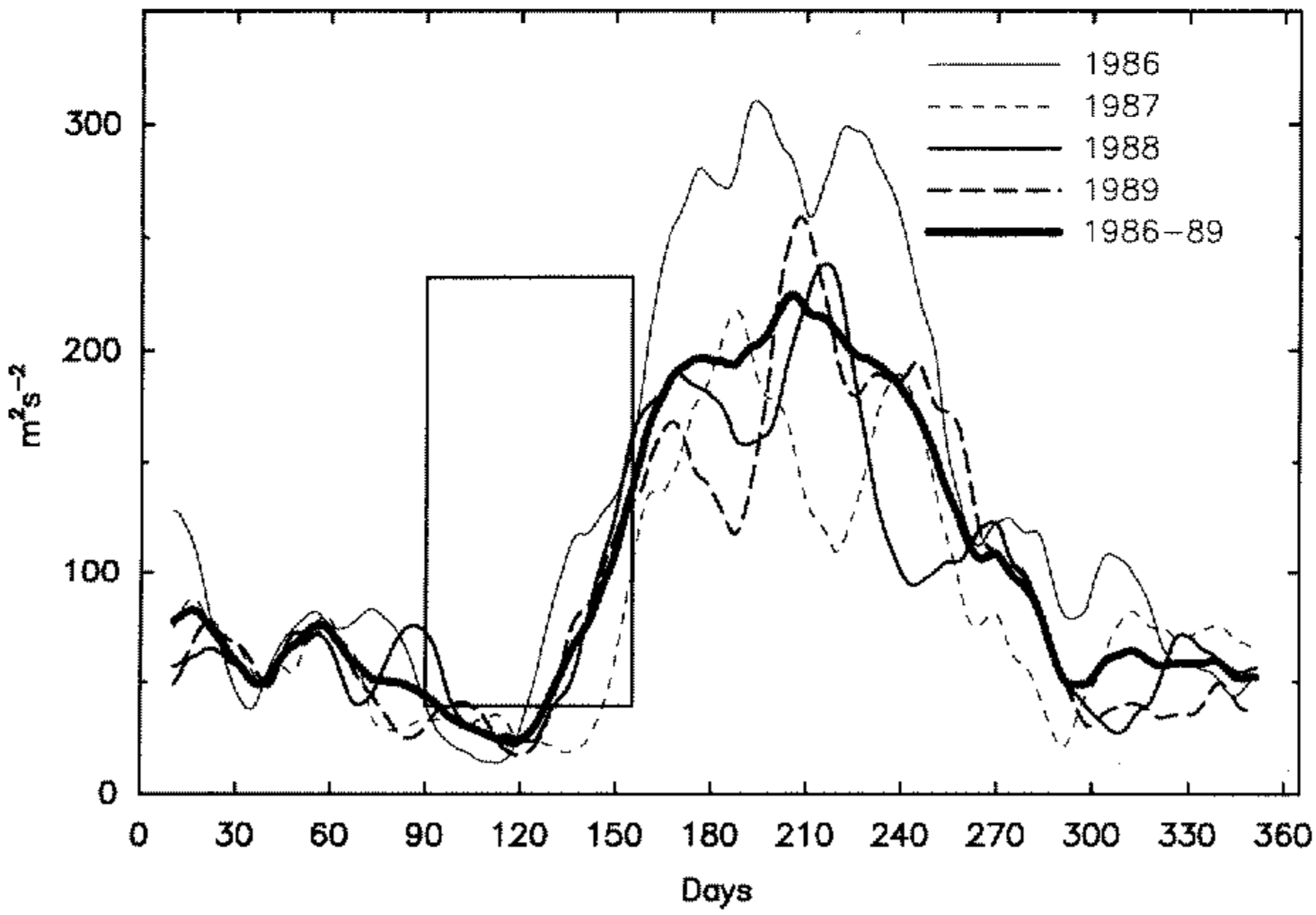

Figure 6. Annual variation of the monsoon kinetic energy (defined in the text) for four years (1986–89) for the region 5°N–15°N, 40°E–110°E plotted as 20-day running averages. The heavy solid curve defines the four-year average. Large differences in the intensity, phase and variability of the monsoon kinetic energy are apparent. The most intense and earliest monsoon occurred in 1986 while the latest and weakest occurred in 1987. Note the low-frequency variability within each monsoon season. The box defines the period of predictability decline (see Fig. 2). ECMWF data were used.

autumn $\overline{KE}$ decreases more gradually, The phase and the amplitude vary considerably from year to year. For example, 1986 contained the most energetic broad-scale monsoon of the four years and also developed at the earliest time of the year. On the other hand the kinetic energy of the 1987 season was the lowest and developed the latest. In fact almost a thirty-day difference exists between the commencement of rapid growth of the monsoon in these two years, and about a 30% difference in the summer kinetic energy. Once the monsoon has developed, the $\overline{KE}$ varies substantially on intraseasonal time-scales. All four years show low-frequency variations which are apparently associated with breaks (i.e. dry periods) within the broad-scale monsoon.

While the boreal summer monsoon is growing in strength, the equatorial zonal pressure gradient across the Pacific ocean is decreasing sharply. The slackening is not apparent in the SOI though, which purposely removes the annual cycle from the index in order to facilitate a clearer signal of the interannual variability of the tropical atmosphere. However, the removal masks a strong annual cycle with a magnitude far larger than the interannual signal. Figure 7 shows the mean annual cycle of the Darwin (12.4°S, 130.9°E) and Tahiti (17.5°S, 149.6°W) surface pressures, their standard deviations and their differences (data from Trenberth (1984)). Within one standard deviation, Tahiti's mean pressure is always higher than Darwin's except during the late boreal spring and summer. Near the vernal equinox, the zonal equatorial pressure gradient is at a minimum and may even reverse. Thus, while the surface pressures of the Indian and Pacific Oceans are 'swaying' on interannual time-scales, they are also swaying within the annual cycle. The amplitude of these intra-annual swayings possess much higher amplitude than their interannual counterparts.

The growth of the summer monsoon and the slackening of the equatorial pressure gradient at the same time as the rapid observation–prediction correlation decline suggest two propositions or hypotheses which might explain the sensitivity of the coupled system in particular phases of the annual cycle or, at least, suggest a framework for their investigation. These are:

(i) The magnitude of the monsoon circulation grows very rapidly between April and June. Variability in the amplitude and phase of the monsoon system influences the ocean–atmosphere interaction in the Pacific Ocean through alteration of the planetary-scale surface-wind-stress field. The anomalous wind-stress field modulates the basic ENSO period which, otherwise, would be set by the basin-scale dynamics of the coupled system of the Pacific Ocean.

(ii) In the boreal spring and early summer, while the near-equatorial circulation is weakest and the ocean–atmosphere system least robust, external influences produce random error growth in the system. Such influences may be unpredictable climatic noise, such as extratropical weather events or, indeed, the variable phase and amplitude of the monsoon as described in (i), above.

The first proposition heeds the Normand (1953) conclusion that variability in the monsoon heralds changes in the circulation of other parts of the globe. The proposition is also supported by the observations and deductions of Meehl (1987, 1989) and Yasunari (1987, 1991) who showed that the monsoon could be categorized into 'strong' and 'weak' years by the anomalous precipitation in India and the South Pacific Convergence Zone.

The second proposition depends on near-equatorial coupled circulations being more susceptible to outside influences at particular phases of the annual cycle. There is some experimental support for the proposition. Discussing the variability of forecast skill as a function of time of year, Cane (1991) noted that the stability of the ocean–atmosphere system varies throughout the year, rendering certain periods more susceptible to error growth by 'noise' in the initial conditions.

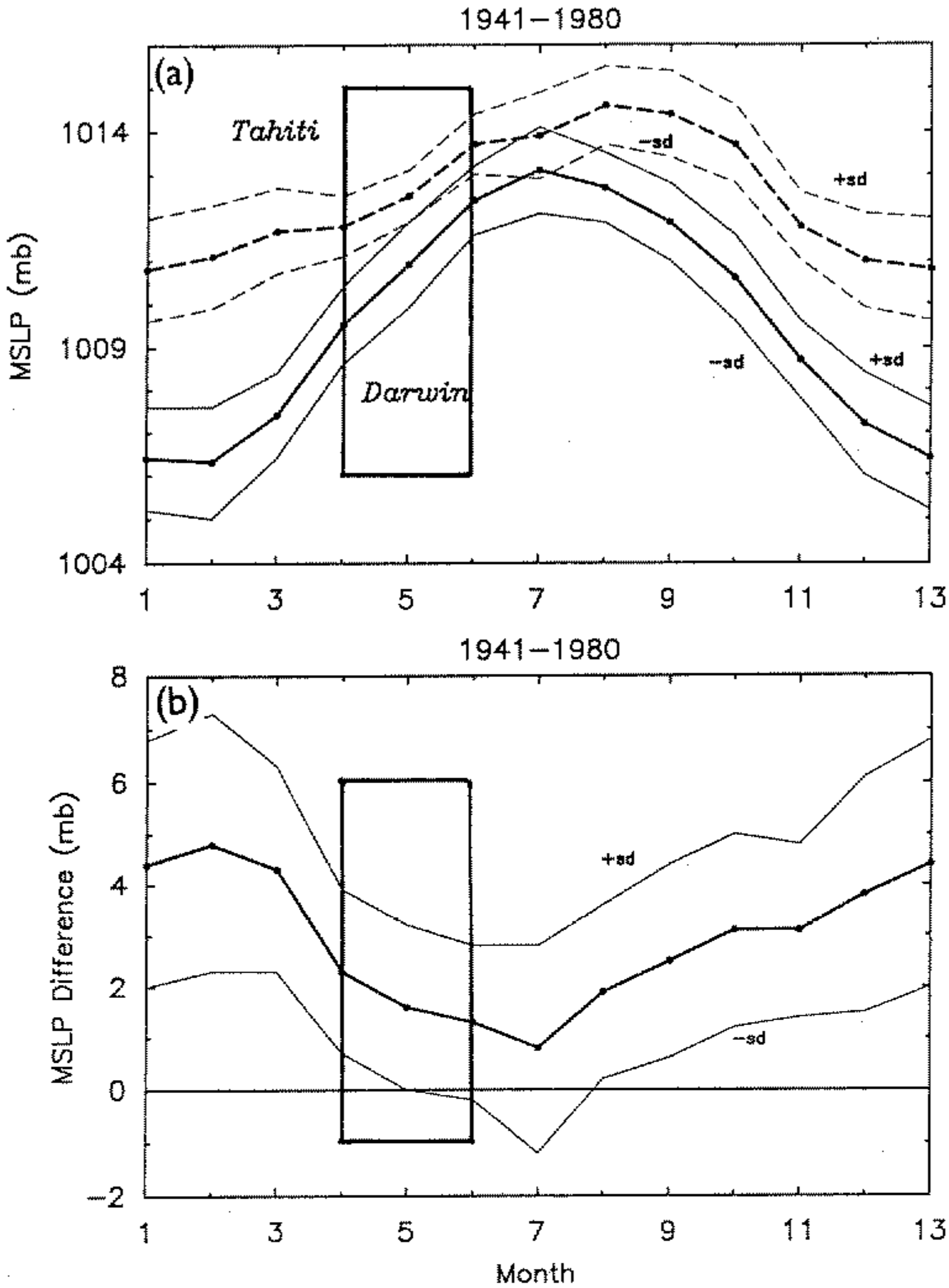

Figure 7. (a) The annual cycle of the mean monthly surface pressures at Darwin (solid line) and Tahiti (dashed line). The secondary curves show the standard deviation about the monthly means. (b) The differences in the mean monthly pressures and their standard deviations. The pressure difference defines the annual variation of the zonal pressure gradient along the equator. The difference curve is the annual cycle signal that would be subtracted from the pressure record to produce the Southern Oscillation Index. The boxes outline the period in which the predictability of the coupled ocean–atmosphere system appears to diminish very rapidly (see Fig. 2).

Cane's noise could originate from many factors, such as variability in the phase and the amplitude of the monsoons, or random synoptic influences from higher latitudes. If it is the former, or a similar large-scale and definable phenomenon, and if it can be demonstrated that there is a deterministic relationship between (say) the strength of the monsoon and the period of the ENSO, then one may be able to seek physical processes which determine the variability of the monsoon; thus extending the predictability of the system beyond the limits indicated in Fig. 2. This would be the optimistic outcome to the first proposition where one could perhaps envision a grander model that might account for processes that would simulate monsoon variability. However, if no 'linear' relationship between monsoon phase and amplitude and the characteristics of ENSO can be demonstrated, or if it seems that unpredictable events (e.g. extratropical synoptic noise) are the major perturbers of the ENSO cycle, then Fig. 2 probably would provide

natural limits of predictability of interannual variability *even* if better and grander models were available. Thus the legacy of the second proposition would be interannual predictability limited by the annual cycle!

3. Measures of broad-scale monsoon variability

The categorization of the strength of the monsoon has been generally associated with precipitation amount averaged over a particular region during a particular period (e.g. Shukla 1987a, b; Meehl 1987; Krishnamurti *et al.* 1989a, b). But while precipitation is arguably the most societally important climate variable, it is also the most difficult to measure and interpret. Interpretation is difficult as it is necessary to differentiate between factors such as geography, which may emphasize even the smallest circulation changes, and the influence of secular changes in the climate. In Asia the problem is exacerbated by the lack of a homogeneous data set over the scale of the continental monsoon. Long-term data sets exist for India and for China but, even together, the data sets cover only a small percentage of the land area under the influence of the monsoon and none of the adjacent ocean (see Fig. 1(a)).

Two independent data sets lend themselves to the definition of the intensity of the monsoon. These are the satellite OLR fields which exist in fairly continuous form from 1974, and circulation statistics which have been compiled and archived at a number of numerical meteorology centres throughout the world. In addition to OLR fields we will utilize data from the European Centre for Medium-range Weather Forecasts (ECMWF) and the National Meteorological Center (NMC). The data are critical and discussed in appendix A.

Figure 8 shows the variation of the mean OLR during the period from 1974 to 1988 for three key sectors: South Asia (5°N–20°N, 40°E–110°E), North Africa (10°N–30°N, 0°E–40°E) and the South Indian Ocean (10°S–5°N, 40°E–110°E). Strong annual cycles in the OLR occur in each of the areas while the largest amplitude occurs in the South Asian sector (dashed). The amplitude of the annual cycle is slightly less in the South Indian Ocean sector (solid) and smallest over the North African sector (bold). At any time of the year the OLR or heating gradient in the monsoon region is very complicated. From January to June the OLR gradient between the South Asian and North African sectors varies from about $-5\,\mathrm{W\,m^{-2}}$ to $-60\,\mathrm{W\,m^{-2}}$. Between South Asia and the South Indian Ocean the gradient changes sign from $30\,\mathrm{W\,m^{-2}}$ in winter to $-20\,\mathrm{W\,m^{-2}}$ in summer. Thus, at the height of the monsoon, the largest radiative heating gradient is between Asia and north Africa.

The OLR also contains considerable interannual variability. For example, Fig. 8 shows that the amplitude of the annual signal over the South Asian sector varies by $\pm 15\,\mathrm{W\,m^{-2}}$ from year to year which is about 25% of the mean annual variability. Similar variability is also apparent in the North African and South Indian Ocean sectors, although with amplitudes that are larger fractions of their mean annual amplitudes. Both sectors possess interannual variability of about $\pm 10\,\mathrm{W\,m^{-2}}$ or about 50% of their mean annual amplitude. In summary, in the monsoon regions, large-scale differences exist in the OLR fields. As spatial variability of the OLR fields is associated with heating gradients (e.g. Webster 1991) it is probable that the interannual variability is indicative of temporal variations in the circulation strength of the broad-scale monsoon.

The use of the circulation as an indicator of the vigour of the broad-scale monsoon is based on a rather simple theory. Using simple linear models with prescribed heating, Webster (1972) and Gill (1980) established a clear relationship between the strength of the heating over the South Asian region and the magnitude of the regional vertical shear.

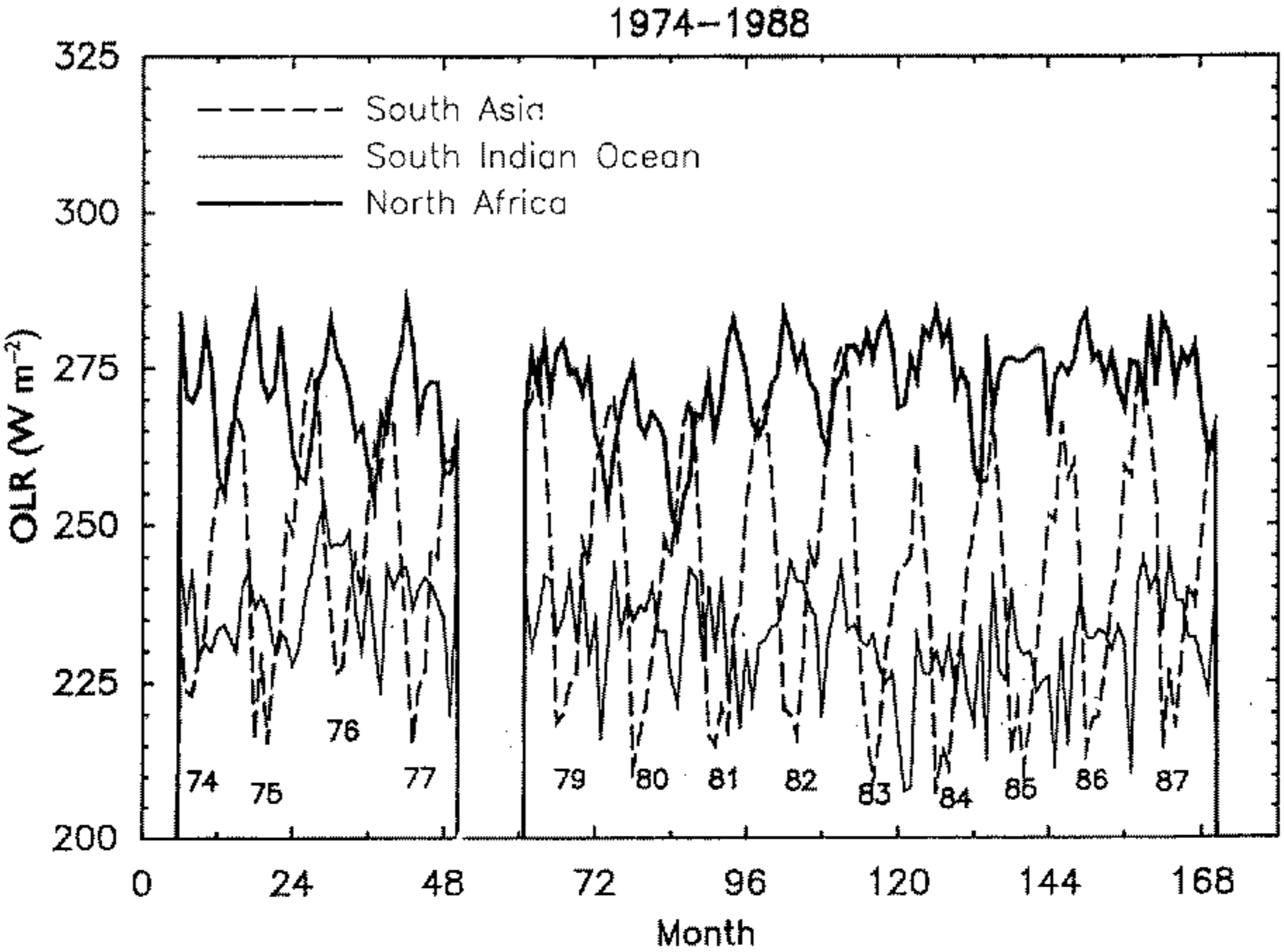

Figure 8. Time series of the mean monthly outgoing long-wave-radiation (OLR) for 1974–88 averaged over three areas: South Asia (5°N–20°N, 40°E–110°E), North Africa (10°N–30°N, 0°–40°E) and the South Indian Ocean (10°S–5°N, 40°E–110°E). Blank regions indicate missing data. The numbers next to the OLR minimum indicate the years of each South Asian summer.

In this simplest context, monsoon flow may be thought of as the low-frequency baroclinic Rossby-wave response to the monsoon heating. However, there are data problems which make the checking of the relationship difficult. OLR data are only available from 1974 onwards; 200 mb wind fields exist from 1968, but 850 mb data were only archived after 1974. Before 1975, only 700 mb data were archived. However, despite these limitations, and noting the data problems that existed before 1979, it is possible to produce a 22-year index sequence, albeit a patchy one.

Like the OLR fields, the monsoon wind field possesses a combination of interannual and intraseasonal variability. Figure 9(a) shows 5-day running means of the 200 mb and 850 mb zonal wind fields averaged in the band 5°N–10°N along the 80°E meridian for the four-year period 1986–89. In the late boreal spring or early summer the lower tropospheric winds switch rapidly from weak easterlies to rather strong westerlies over a very short period, and are accompanied by an equally rapid acceleration of the upper tropospheric easterlies. In the late summer and the early fall the winds decrease more gradually in intensity at both levels, in contrast to the rapidity of their onset in early summer. In each of the four years there is a strong temporal correspondence between the demise and the rapid growth of the monsoon winds. The winds are also very highly negatively correlated in the vertical at all times of the year. Figure 9(b) shows a scatter plot of the 850 mb and 200 mb winds. Over the four-year period the correlation is −0.83. It is this shear that forms the basis of a monsoon intensity index.

Table 1 lists a number of quantities which may be useful in the definition of the intensity of the monsoon circulation and in the validation of an index. The deviations of a particular quantity, X, are defined by:

$$X^* = X - \overline{X}$$

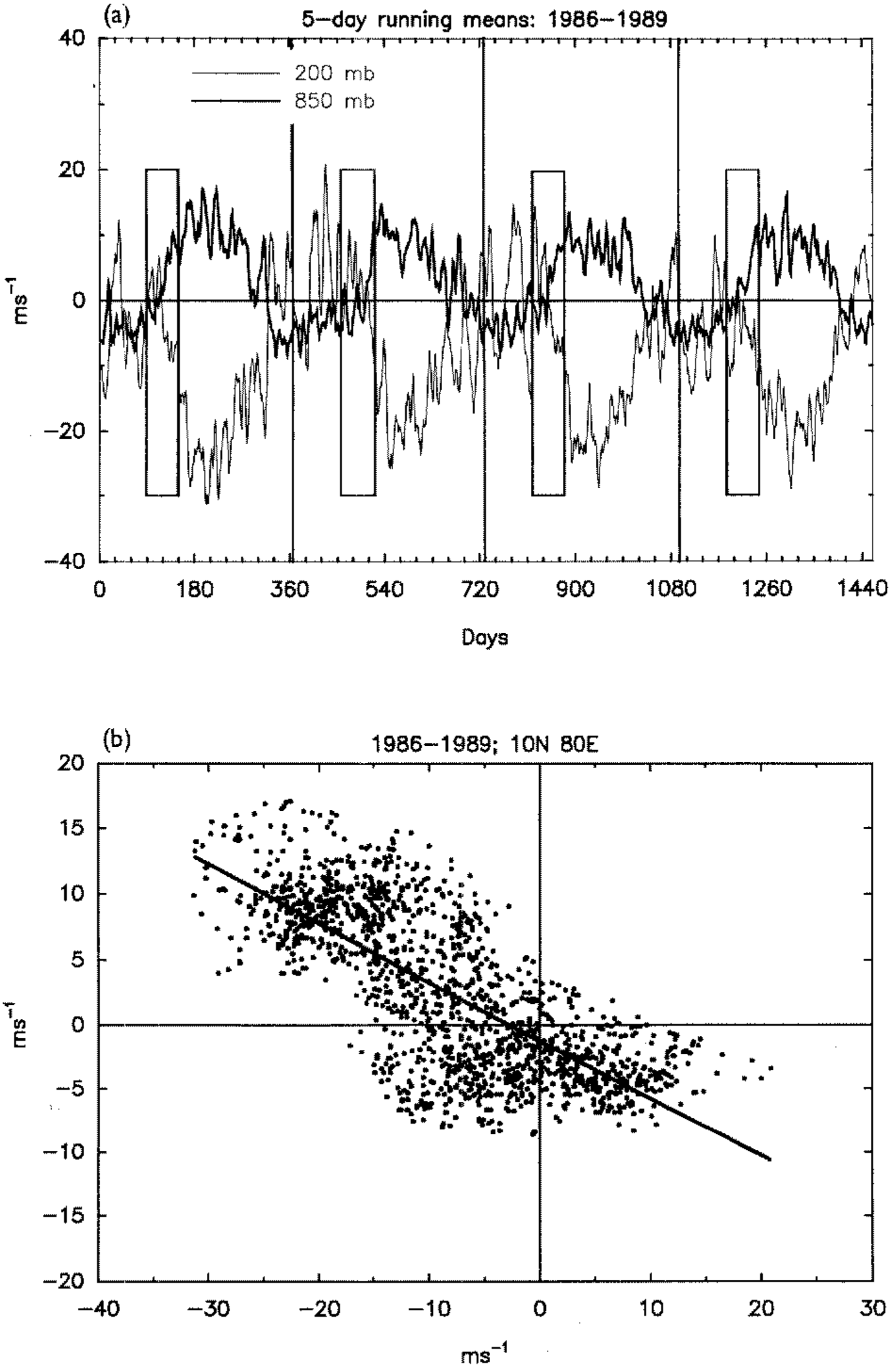

Figure 9. (a) Variation of the 5-day running average zonal wind field at 200 mb and 850 mb at 80°E and averaged between 5°N and 10°N along the 80°E meridian for 1986–89. Curves indicate a very rapid transition of flow regime in late spring at the same times as the predictability of the coupled system decreases (boxes, from Fig. 2). ECMWF data were used. (b) Scatter plot of the 200 mb (abscissa) and 850 mb (ordinate) zonal wind field using the 1986–89 data at 80°E and averaged between 5°N and 10°N. Solid line denotes the linear regression curve.

TABLE 1. INDICES FOR THE DEFINITION OF THE INTENSITY OF THE BROAD-SCALE MONSOON CIRCULATION FOR THE PERIOD 1968–1987 FOR THE BOREAL SUMMER, JUNE, JULY, AUGUST

	OLR* (W m^{-2})			U^* (m s^{-1})			Index			
Year	As	Af	IO	850	700	200	M_1^*	M_2^*	R	SOI
1968					−0.1	1.4	−1.6	−1.5	−10	0.6
1969					−0.1	−0.2	0.0	0.1	−5	−0.5
1970					0.1	−1.9	1.9	2.0	10	0.3
1971					0.9	−1.7	2.4	2.5	2	0.6
1972					−0.5	1.1	−1.7	−1.6	−21	−1.6
1973					−0.7	−2.0	1.2	1.4	11	1.0
1974	6.7	3.9	−1.7		−0.7	−2.3	1.5	1.6	−9	0.6
1975	0.6	0.3	0.0	0.3	0.1	2.2	−2.0	−2.1	18	1.9
1976	10.5	9.7	1.9	0.4	0.4	1.3	−0.9	−0.9	6	−1.0
1977	3.8	2.9	0.3	0.4	0.3	1.5	−1.0	−1.2	5	−1.7
1978				0.6	0.2	0.4	0.3	−0.2	8	0.3
1979 (W)	1.4	−0.2	0.6	−1.0	−1.0	1.2	−2.2	−2.2	−16	0.4
1980	−3.3	−0.9	−8.0	−0.3	−0.7	0.7	−1.0	−1.4	4	−0.3
1981	−2.2	0.2	−7.4	0.2	−0.3	1.4	−1.2	−1.9	1	0.9
1982 (W)	−0.7	4.0	3.3	−0.1	−0.6	2.2	−2.3	−2.8	−12	−3.4
1983 (W)	−1.7	−5.5	1.4	−1.0	−1.1	1.9	−2.9	−3.1	16	−0.6
1984 (S)	−8.6	−8.1	5.2	1.2	0.0	−4.9	6.1	4.9	−2	−0.4
1985 (S)	−4.5	−3.8	−0.2	1.6	0.4	−2.8	4.4	3.2	−6	−0.3
1986 (S)	−2.1	−4.7	2.7	0.4	0.2	−1.3	1.7	1.5	−12	0.1
1987 (W)	0.0	2.1	1.9	−1.0	−0.8	1.7	−2.7	−2.5	−15	−2.1

Lists of OLR*, the seasonal anomalies of the outgoing longwave radiation from 1974 to 1987 for the South Asian sector (As: 5°N–20°N, 40°E–110°E), the North African sector (Af: 10°N–30°N, 0°E–40°E) and the South Indian Ocean sector (IO: 10°S–5°N, 40°E–110°E), the anomalous zonal wind field, U^* for 850, 700 and 200 mb, the two monsoon intensity indices, M_1^* and M_2^*, the Indian rainfall index, R, and the Southern Oscillation Index (SOI) are presented. The circulation statistics are calculated over the area 0°–20°N, 40°E–110°E. Because of the data discontinuity in 1978, the U^*-fields are calculated relative to two mean values, 1968–78 and 1979–87. 'Weak' (W) and 'strong' (S) monsoon seasons (see text for discussion) are listed in the left column. Absence of data is left blank.

where $\overline{X}$ is the long-term seasonal mean of a quantity. OLR* is the OLR anomaly calculated in the South Asian region relative to averages for the period from 1974 to 1987. M_1^* and M_2^* are wind shear indices given by:

$$M_1^* = U_{850}^* - U_{200}^*$$

$$M_2^* = U_{700}^* - U_{200}^*.$$

Deviations of the zonal wind field (U^*) are calculated relative to two separate mean summer values: 1968–78 and 1979–87. The different averaging periods acknowledge the different initialization schemes used in the creation of the data set (see appendix A). The last columns show a mean summer rainfall index for the Indian subcontinent (Krishnamurti *et al.* 1989a, b) and the mean summer SOI for the particular year.

Correlations between a number of the items listed in Table 1 provide some useful insight. The two indices M_1^* and M_2^* correlate at 0.95, indicating that even with the data problems we can have some confidence that the index can be extended back to 1968, although with some caution. Correlations between M_1^* and M_2^* and the upper tropospheric wind are also very high (−0.93) suggesting that we could quite adequately use U_{200}^* as well as either M_1^* or M_2^* to indicate the monsoon intensity. Correlations between the OLR fields and the indices are not very strong (−0.46 and −0.41, respectively) but they are, at least, of a sign which is consistent with the simple theories. That is, when

the OLR is a minimum (convection maximum) the shear should be a maximum. Thus we may view the correlation in an *a posteriori* perspective (Webster and Keller 1975) and have more confidence in the relationship suggested by the correlation.

The distribution of monthly values of actual monsoon intensity function, M_2 (i.e. the difference between the actual winds $U_{850} - U_{200}$) and M_2^* are plotted in Fig. 10 for the period March 1968 through February 1988. The numbers refer to the year of the summer of the positive extrema in M. The vertical lines in Fig. A.1 show the separation of the two data periods defined in appendix A. In both periods the index shows considerable variability both in the summer (positive) and winter (negative). The anomalous intensity function is shown as the heavier lines. Generally, the values of M in the first data period are smaller in each extreme. The inset in Fig. 10 compares the mean monthly values of the index. The greatest difference between the two data periods occurs in the summer where the divergent part of the wind field becomes more important (see appendix A).

Large positive values of M^* should correspond to strong circulation characteristics of the monsoon; negative values should reflect weak monsoon circulations. In the second period of the data (i.e. 1979–87) the average summer values of M_1^* for years 1984, 1985 and 1986 are 6.1, 4.4 and 1.7. We will refer to these seasons as possessing 'strong' broad-scale monsoons. Years 1979, 1982, 1983 and 1987 have values of −2.2, −2.3, −2.9 and −2.7, respectively. These will be referred to as 'weak' broad-scale monsoon years.

Whereas the indices M_1^* and M_2^* are calculated over substantial areas (15° latitude by 70° longitude) it will be shown in section 6, when composite analyses are made for both strong and weak monsoons, that the regions of anomalous easterlies and westerlies associated with the extremes of the indices exist over a much larger scale again. In fact,

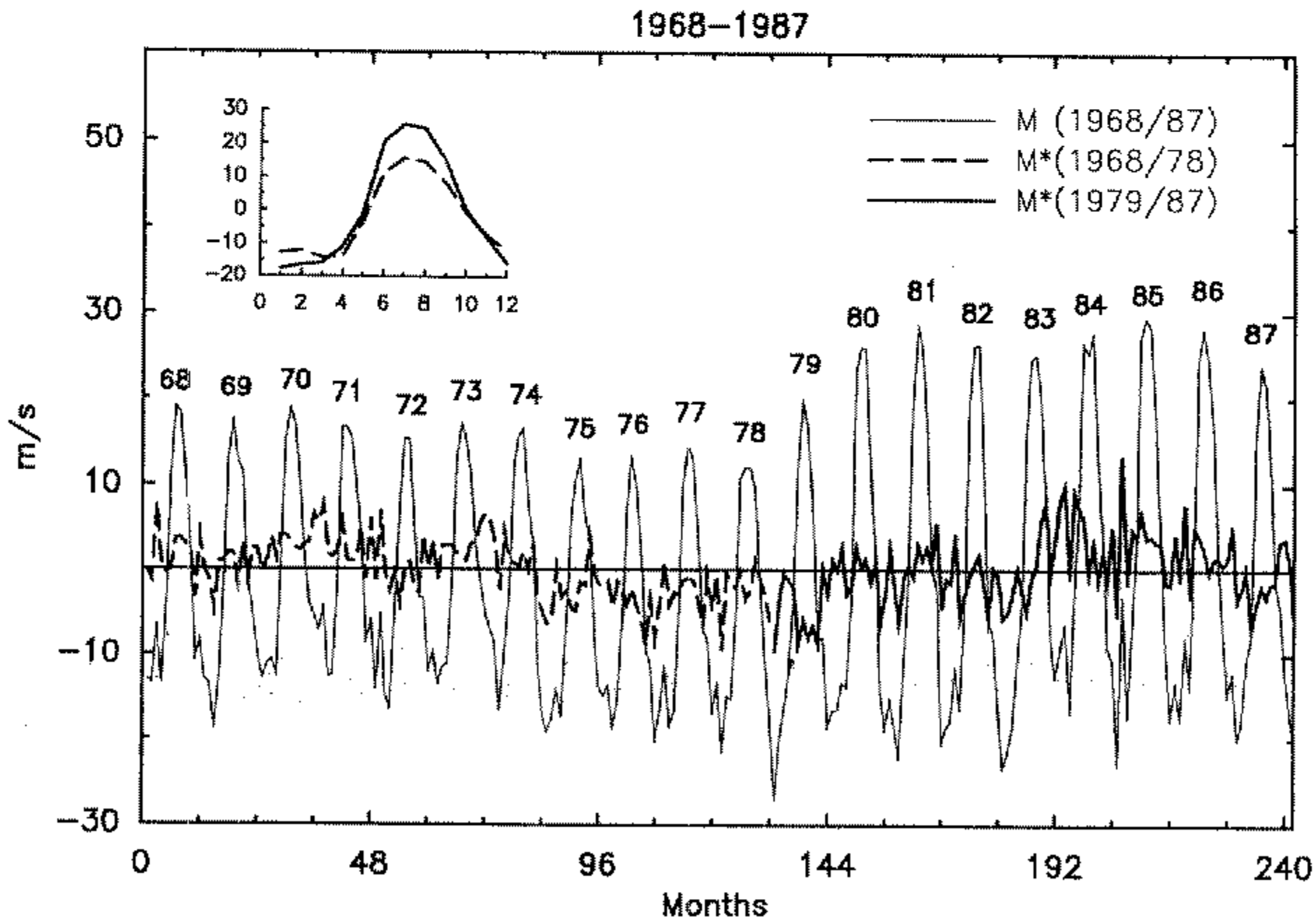

Figure 10. The evolution of the broad-scale monsoon intensity function M_2 (i.e. non-anomaly; solid line) and the anomaly M_2^* (heavier dashed and solid lines) for the period 1968 through 1987. The indices were calculated from data averaged over the area 0°–20°N, 40°E–110°E. Large positive values occur in the boreal summers which are labelled by year. The change from a dashed to a solid line denotes the data discontinuity in the NMC data set introduced by the change in initialization schemes (see appendix A). The inset shows the comparison of the mean monthly intensity functions for the two data periods 1968–78 (dashed) and 1979–87 (solid line).

the anomalous circulations are of such a scale that they project coherent signals over the entire Pacific Ocean.

In the first period of data (i.e. 1968–78) there are three weak monsoon seasons (1975–77) when OLR data exists. For these three years M_1^* has values of −2.0, −0.9 and −1.0. As these values of M^* were constructed with circulation data of dubious quality, the OLR distribution is used as an independent check on the intensity of the monsoon. Figure 11 shows the mean 1975–77 mean summer distribution of OLR* relative to the long-term 1974–87 summer average. It is clear that over much of south Asia and the Indian Ocean OLR* is anomalously positive, suggesting overall weaker convection. Thus, even in the period before 1979, the indices appear to provide some indication of the strength of the broad-scale monsoon.

The data record can be extended slightly in the other direction by using the ECMWF data from 1986–89 which overlaps the NMC set by two years. Over the South Asian sector the ECMWF yields summer mean values of the quantity $(U_{850} - U_{200})$ of 28.6, 21.7, 22.3 and 22.9 m s^{-1}, respectively. Using the NMC 1979–87 mean values, the ECMWF data gave anomaly values of 4.9, −2.0, −1.4 and −0.8. The first two values compare well with the NMC indices of 2.0 and −3.1. Thus two independent data sets show similar relative intensities of the broad-scale monsoon.

As many other monsoon intensity indices depend on regional precipitation, it is difficult to find an independent broad-scale index to compare with the M^* indices that is better than the area-averaged OLR. In fact, over the entire data period, there is almost zero correlation between M_1 and the Krishnamurti *et al.* (1989a, b) rainfall index R. In summary, the indices do not appear to have much in common with indices that define the state of the local monsoon. But the main purpose of this section has been to determine a measure of the variability of the broad-scale monsoon circulation to use in seeking relationships with remote aspects of the general circulation. M_1^*, or equivalently U_{200}^*, emerges as a suitable index for the determination of the broad-scale monsoon intensity. We will determine the global or broader-scale impact of the strong and weak monsoon seasons in section 6.

Given that we have established a measure of broad-scale monsoon intensity which possesses some correspondence with the OLR fields, we are now in a position to assess relationships between the monsoon and the ENSO. A starting point is to see if there are

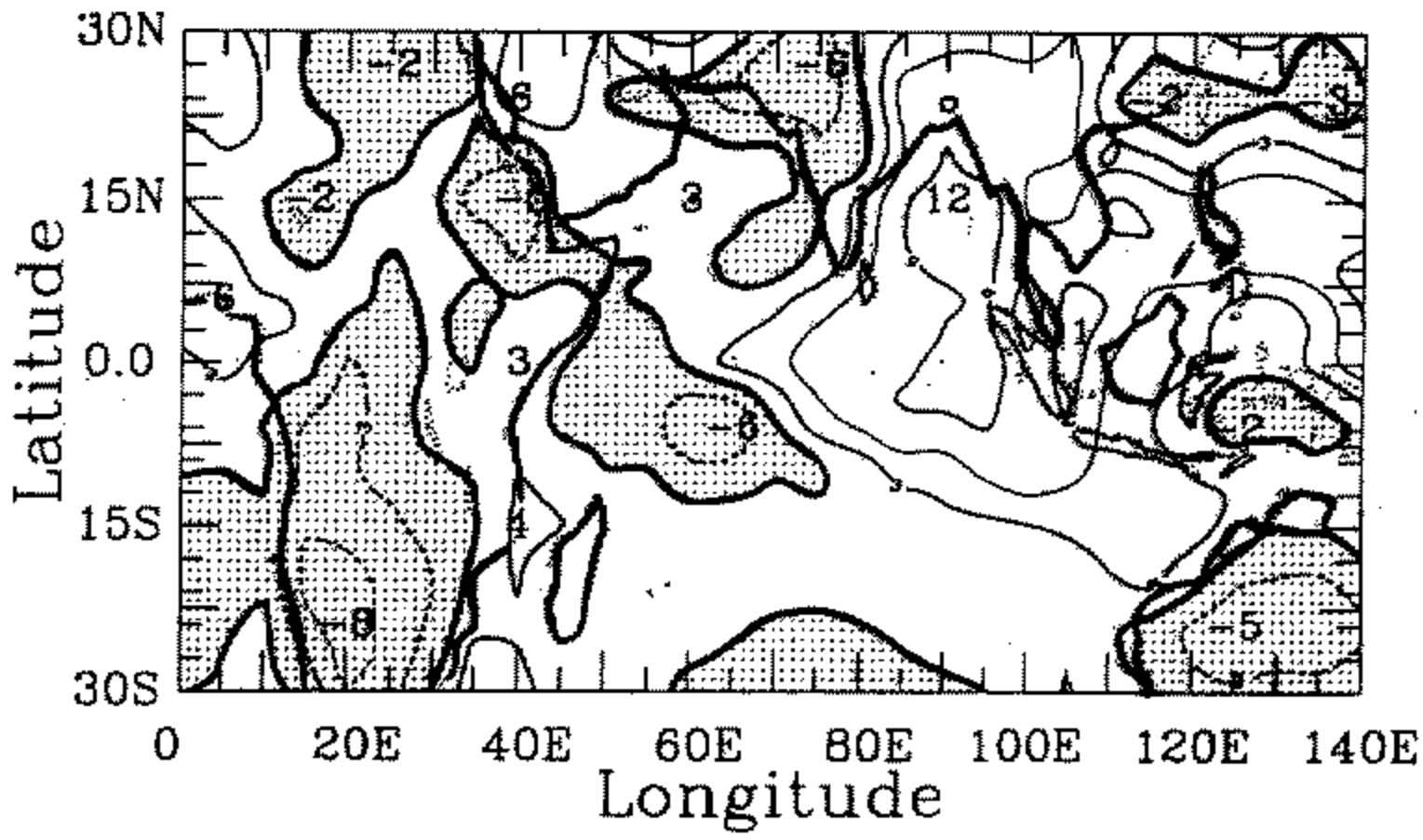

Figure 11. Anomalous outgoing long-wave-radiation fields in the Indian Ocean region averaged over the three 'weak' summers (June, July, August) 1975, 1976 and 1977. Units are W m^{-2} and the heavy lines represent the zero contour.

simultaneous or lagged relationships between the ENSO signal and the fields of OLR and U associated with the monsoon.

4. Simultaneous relationships between the ENSO and monsoons

Simultaneous correlations between the OLR and the SOI (upper panel) and U_{200} (lower panel) are plotted in Fig. 12. The correlations are for summer and winter and over the period 1974–87. Strongest correlation fields occur in the central and eastern Pacific Ocean in summer and winter for both OLR and U_{200}. The correlations confirm that during a warm event in the Pacific Ocean (i.e. SOI < 0) the convection is regionally stronger (OLR < 0) and the upper-level zonal winds in the central and eastern Pacific become more easterly (see for example Gill and Rasmusson (1983)). Furthermore, in both seasons, the convection weakens in a band stretching north-eastwards and south-eastwards out of Indonesia, suggesting an eastward migration of the South Pacific Cloudiness Zone during warm events. Similarly, in accord with the eastward migration of the equatorial convection, the mid-latitude westerlies increase over the central Pacific Ocean in both hemispheres (see for example Yang and Webster (1990)).

In summary, much stronger simultaneous relationships appear to exist between the SOI and U_{200} in winter than in summer. In winter significant correlation patterns of OLR and (especially) U_{200} extend over the Indian Ocean and south Asia. In summer significant simultaneous correlations are absent anywhere to the west of the Pacific basin, in particular over the south Asian monsoon regions.

The weakness of the correlations of the circulation and the heating fields with the SOI over the south Asian monsoon regions during summer poses a serious problem for monsoon prediction. Even a confident prior knowledge of the SOI for the succeeding summer may be of little use in foreshadowing the monsoon intensity, as the *simultaneous* correlations of the SOI and either the OLR or U are weak over the south Asian monsoon regions. On the other hand, an advance knowledge of the SOI would appear to provide a keen indication of the strength of the winter monsoon, because the simultaneous relationships between the SOI and measures of the intensity of the winter monsoon are locally much stronger in the Indonesian–Australian region during winter.

Figure 12 substantiates Troup's view that the influence of the ENSO appears to have a strong annual cycle. It is interesting to note that the U_{200}–SOI correlations possess a node over the Indian subcontinent very similar to that found by Troup (Fig. 1(b)). The annual character may be seen more clearly by stratifying the data from different periods throughout the year in terms of strong negative and positive values of the SOI. The seasonal mean values of the SOI are listed in Table 2 together with the appropriate value of the SOI. In choosing the sample an attempt was made to select the same number of seasons for each composite. The lower part of the table shows the average SOI for each seasonal composite. Unfortunately, the majority of the large positive SOI values come from the early part of the data record which may bias the composites of the U-field somewhat. The potential for bias should be kept in mind when considering the results.

Using the extreme seasons defined in Table 2, composite distributions of the OLR and the U_{200} were calculated. Figure 13 shows the difference fields between these extremes (e.g. $\overline{\mathrm{OLR}}(\mathrm{SOI} \ll 0) - \overline{\mathrm{OLR}}(\mathrm{SOI} \gg 0)$) for each of the four seasons. The purpose of the diagram is to show the annual cycle of the ENSO signal in the OLR and U-fields. Large-scale and coherent signals may be seen throughout the year. In the OLR difference fields the maximum excursions remain in the Pacific Ocean. The characteristic dipole between the western Pacific and Indonesia is evident between autumn and spring. It reaches its maximum amplitude in winter and all but disappears in summer.

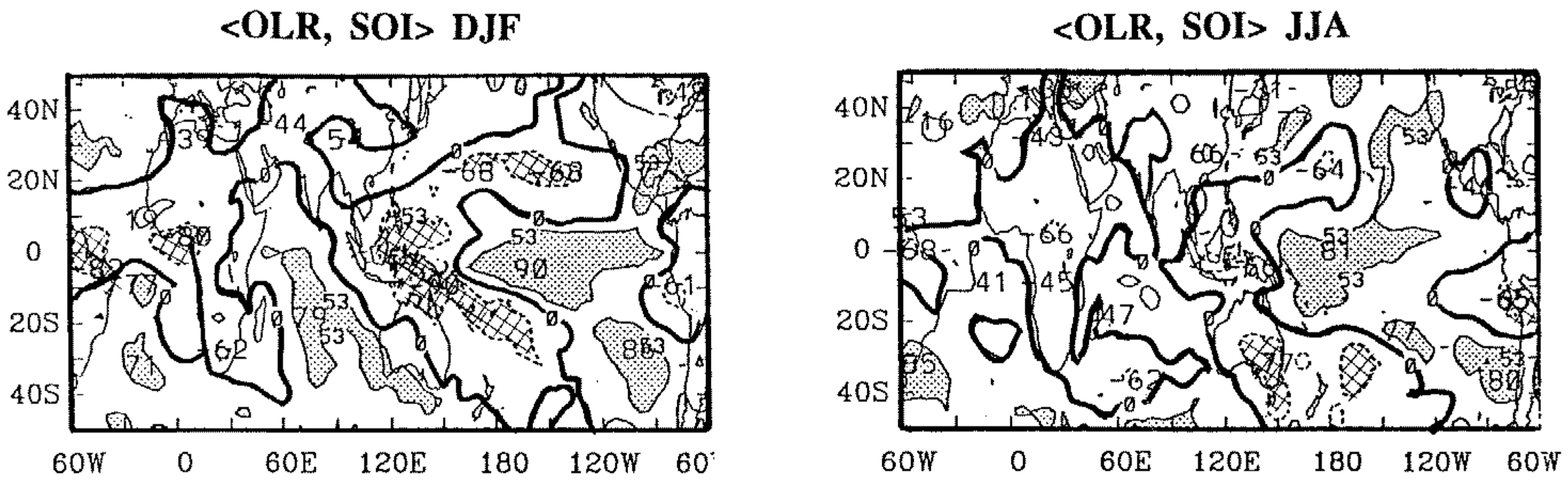

Figure 12. Spatial distributions of the simultaneous correlations between the outgoing long-wave radiation (OLR) and the Southern Oscillation Index (SOI) (upper row) and the 200 mb zonal wind field, U_{200}, and the SOI (lower row) for winter (Dec., Jan., Feb.) and summer (June, July, Aug.) for 1974–87. Correlations with statistical significance > 95% are hatched (negative) or shaded (positive).

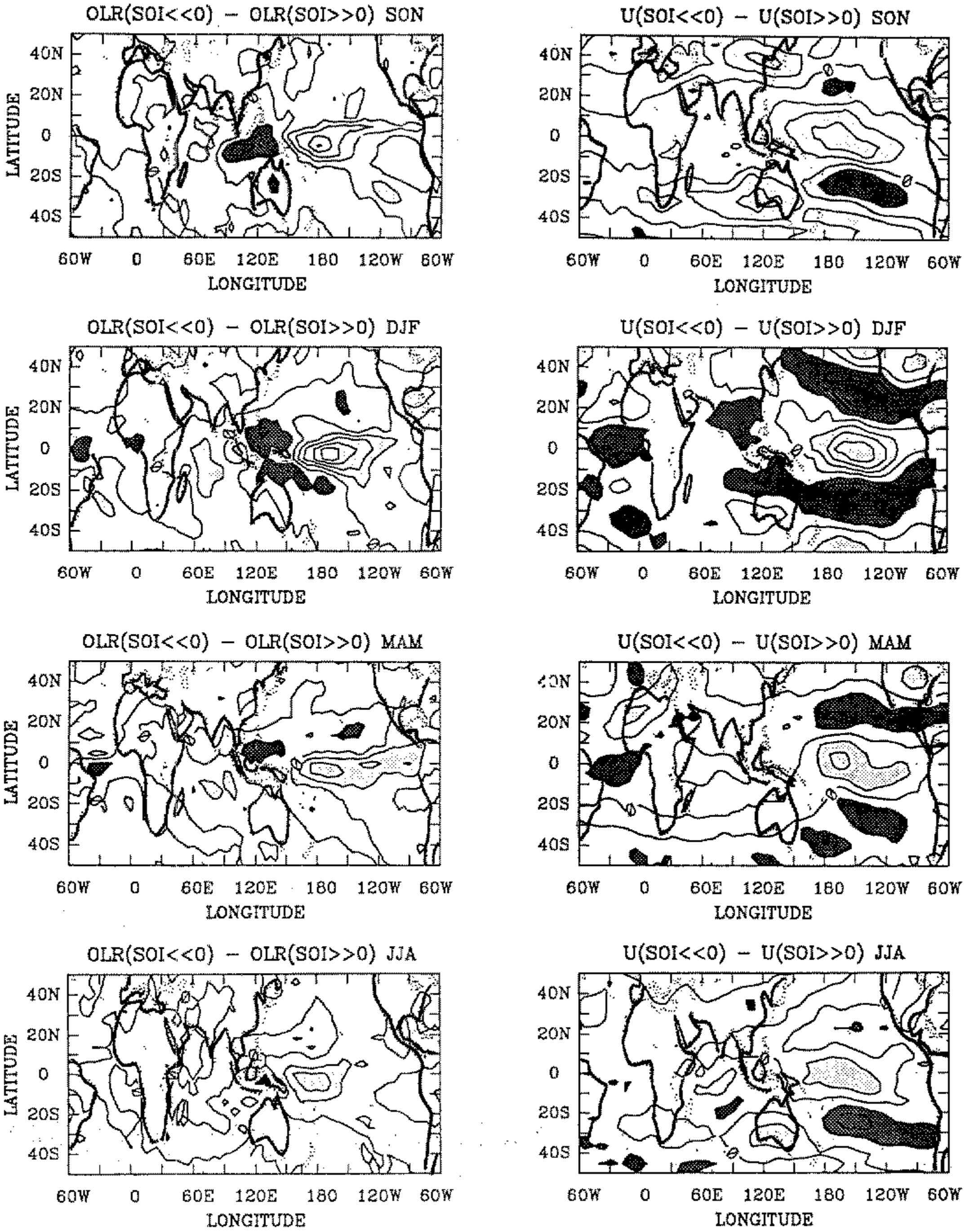

Figure 13. The annual cycle of the ENSO signal depicted as the differences of outgoing long-wave radiation (OLR) (left column) and 200 mb zonal wind (U_{200}) (right column) between the extremes of the SOI. Data are described in Table 3. Heavy shading denotes positive values while light shading indicates negative values. Contour intervals are 3 W m^{-2} and 3 m s^{-1} for the OLR* and U*-fields, respectively.

The U^*-fields are much more widespread and variable. In autumn, large patterns set up over the Pacific basin and around much of the globe at higher latitudes. By winter, the patterns have grown in scale and amplitude over the Pacific Ocean, south Asia and the Atlantic Ocean but have diminished somewhat at higher latitudes. The patterns lose intensity in the spring and almost disappear in the summer. Especially absent are summer patterns with significant amplitude over south Asia during the summer.

Another feature of Fig. 13 is that it shows that the character of the circulation associated with the ENSO cycle changes between spring and summer. The difference fields during the autumnal equinox and winter are very similar and the equinox fields exhibit similar characteristics although they are considerably weaker. Summer, on the other hand, shows a disparate character which, outside the Pacific basin, appears to be independent of the SOI.

Once again there is no indication of there being any significant signal in the convective zones of the summer monsoon region.

TABLE 2. MEAN SEASONAL SOUTHERN OSCILLATION INDEX (SOI) AS A FUNCTION OF YEAR

Year	Mar., Apr., May	June, July, Aug.	Sept., Oct., Nov.	Dec*., Jan., Feb.
1968	0.1	**0.6**	−0.3	−0.7
1969	−0.6	*−0.5*	*−0.8*	−0.7
1970	−0.1	0.3	**1.3**	**1.1**
1971	**1.8**	**0.6**	**1.3**	0.3
1972	*−0.9*	*−1.6*	*−1.0*	*−1.1*
1973	0.0	**1.0**	**1.6**	**1.8**
1974	**1.9**	**0.6**	**0.5**	0.0
1975	**1.0**	**1.9**	**1.7**	**1.5**
1976	**0.7**	*−1.0*	−0.1	−0.1
1977	*−1.2*	*−1.7*	*−1.3*	*−1.5*
1978	−0.1	0.3	−0.3	0.0
1979	−0.2	0.4	−0.3	−0.2
1980	*−1.0*	−0.3	−0.4	−0.1
1981	−0.6	**0.9**	−0.1	**0.5**
1982	−0.2	*−3.4*	*−2.4*	*−3.1*
1983	*−1.5*	−0.6	0.4	0.1
1984	−0.1	−0.4	−0.1	0.0
1985	**0.5**	−0.3	−0.4	−0.1
1986	−0.2	0.1	−0.5	*−1.3*
1987	*−2.2*	*−2.1*	*−0.6*	−0.5
SOI ≫ 0	1.2	1.1	1.3	1.2
SOI ≪ 0	−1.4	−2.1	−1.2	−1.4

* December of year indicated; January and February added from the following year.
Data with strong positive (bold type) and negative (italic type) SOI are used for composites.
Seasons when the outgoing long-wave-radiation data were available are underlined.

5. LAG–LEAD RELATIONSHIPS BETWEEN THE ENSO AND MONSOONS

In order to assess the use of the SOI correlations in a predictive mode, we will now consider lagged correlations between the SOI and the monsoon. Figure 14 shows the lagged autocorrelations between the mean seasonal SOI values lagging or leading by two seasons. SOI data from 1935 to 1990 were used. Figure 14(a) plots the summer SOI with the succeeding winter SOI, and Fig. 14(b) the winter SOI with the succeeding summer SOI. Two very different correlations are found depending upon whether the summer season is leading or lagging; 0.21 with winter leading and 0.7 with summer leading. Thus, if the SOI is known in summer then the SOI in the following winter can be anticipated to a relatively high degree of accuracy. Clearly, the opposite is not true. The winter SOI provides little indication of the SOI in the following summer.

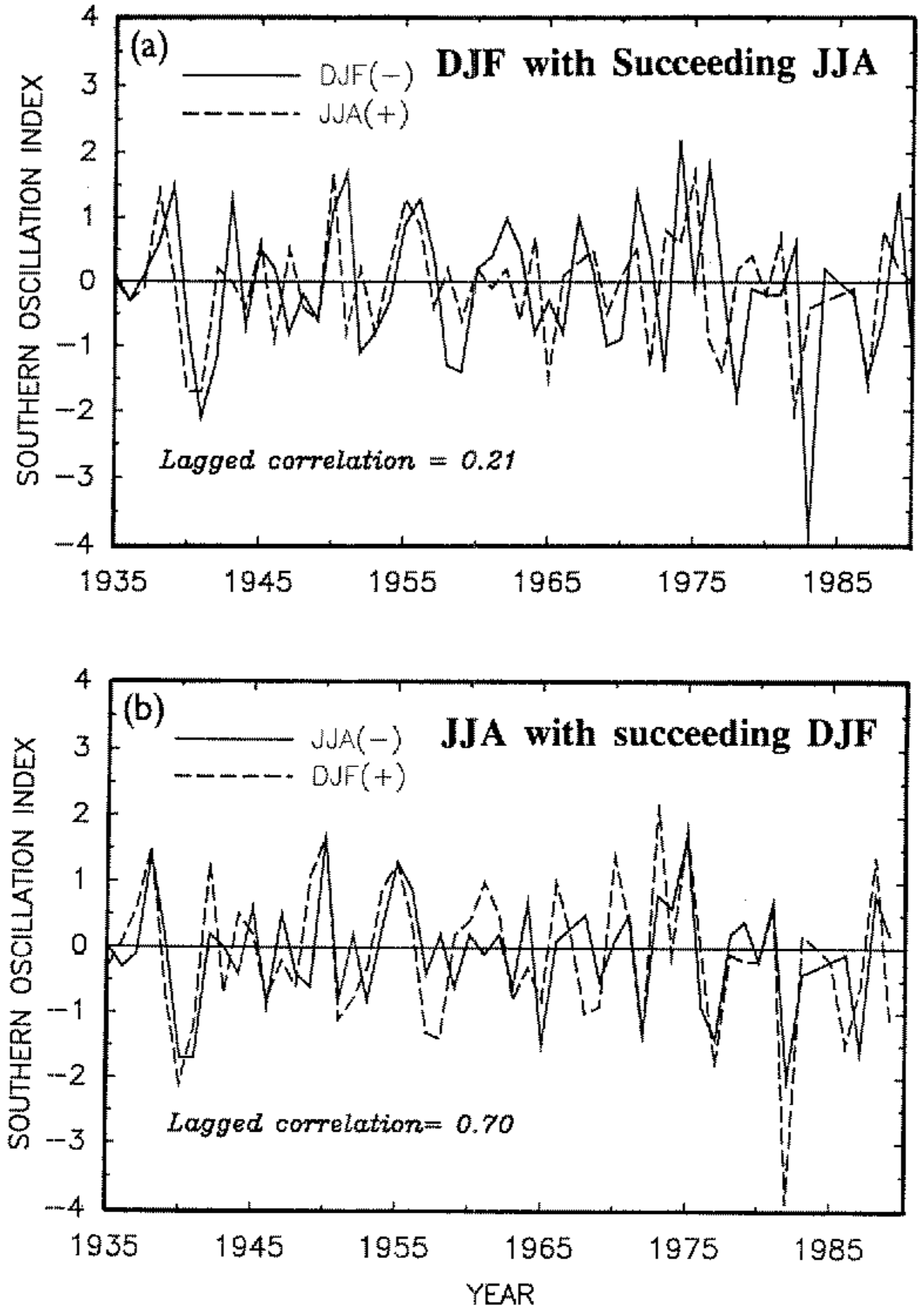

Figure 14. Lagged correlations for the Southern Oscillation Index (SOI) for 1935–90 (a) SOI of winter (Dec., Jan., Feb.) with the SOI of the following summer (June, July, Aug.). (b) Summer SOI with the SOI of the following winter.

Table 3 lists the lagged autocorrelations for the SOI for all seasons. The downward-pointing arrow denotes the primary season and the column underneath shows the lag correlations for the succeeding seasons. The lower stepped line indicates the time at which the correlation halves from the previous season. The 'halving time' provides an arbitrary measure of the rate of decrease of the correlation coefficient with time. The interesting feature is that irrespective of the season in which the lag correlations were commenced, the correlations tend to halve between spring and summer in a manner which is very reminiscent of the Latif–Graham correlation decrease displayed in Fig. 2.

There are some implications for the prediction of monsoon intensity when the SOI is to be used as a predictor. Noting that the winter SOI appears to be correlated to a high degree with the characteristics of the winter monsoon (Fig. 12), it appears that the strength of the winter monsoon may be anticipated with some skill at least six months in

TABLE 3. LAGGED SEASONAL CORRELATIONS BETWEEN THE MEAN SEASONAL SOUTHERN OSCILLATION INDICES

	LAG SEASON			
	Dec., Jan., Feb.	Mar, Apr., May	June, July, Aug.	Sept., Oct., Nov.
Dec., Jan., Feb.	↓ 0.56			
Mar., Apr., May	0.21	↓ 0.61		
June, July, Aug.	0.04	0.54	↓ 0.81	
Sept., Oct., Nov.	−0.01	0.32	0.70	↓ 0.79
Dec., Jan., Feb.		0.03	0.24	0.48
Mar., Apr., May			−0.14	−0.01
June, July, Aug.				−0.06
Sept., Oct., Nov.				

The lag or starting season is shown by an arrow. The lower stepped line denotes the season at which the lagged correlation falls by a factor of two (halves) from one season to another.

advance. However, such skill is not reciprocated between the winter and summer seasons, as the winter SOI does not appear to foretell the SOI in summer. Only a knowledge of the SOI in spring is suggestive of the summer SOI, but then only with a correlation of 0.61 which is less than the correlations between summer and the succeeding autumn and winter (0.81 and 0.70). Thus, if the prediction of the summer monsoon is of primary importance, then an indication of the summer SOI in spring will be of limited utility as it does not fulfil the second criterion for predictors listed in the introduction. However, given the rather poor simultaneous relationships between the summer SOI and the monsoon circulation (Fig. 12), the predictability of the summer monsoon is rather a moot subject. Even if we could predict the summer SOI well ahead of time it may not be useful in providing information about the strength of the summer monsoon. In summary, the results shown here tend to support the conclusions of Walker and Normand discussed earlier.

Given the importance of the correlation drop for interannual predictability, a more precise definition of its occurrence would be helpful. Table 4 lists the results of lag–lead correlations of the monthly SOI values. The lower stepped line indicates the time correlation coefficient halving from one month to another. In most instances, the correlations drop off very rapidly between April and May. In eight out of twelve months the correlation coefficient halves between April and May. In three other months it halves between February and April. That is, in eleven out of twelve months, critical changes occur in the lagged correlations in the spring of the northern hemisphere. Once again there is no evidence of a reciprocal correlation drop in the autumn or at any other time of the year.

Figure 15 plots the lagged correlations of the monthly SOI listed in Table 4. The data are plotted in the fashion of Fig. 2 in order that the lagged correlations of a particular month are lined up along the abscissa. The anchor month of the lagged correlations are shown on the plot. For example, 'A' refers to lagged correlations between the April SOI with the SOI of subsequent months. The plots present a very obvious feature. Irrespective of the anchor month, the lagged correlations decrease at the same time of the year and occur at the same time as the Latif and Graham observation–prediction correlation demise.

Additional insight may be obtained by considering the rows of the data listed in Table 4. The rows of the table indicate the correlation of the SOI of a given month with the SOI of *previous* months. For example, considering the January row, the SOI of all

TABLE 4. LAGGED CORRELATIONS OF THE MEAN MONTHLY SOUTHERN OSCILLATION INDEX VALUES

	LAG MONTH											
Month	Jan.	Feb.	Mar.	Apr.	May	June	July	Aug.	Sept.	Oct.	Nov.	Dec.
Jan.	↓											
Feb.	0.56	↓										
Mar.	0.47	0.51	↓									
Apr.	0.43	0.51	0.59	↓								
May	0.14	0.15	0.22	0.42	↓							
June	0.12	0.16	0.29	0.42	0.59	↓						
July	0.17	0.27	0.33	0.53	0.60	0.79	↓					
Aug.	0.01	0.22	0.35	0.43	0.55	0.65	0.72	↓				
Sept.	−0.10	0.05	0.31	0.35	0.60	0.62	0.69	0.83	↓			
Oct.	0.10	0.16	0.38	0.47	0.55	0.68	0.69	0.69	0.76	↓		
Nov.	−0.14	−0.10	0.16	0.20	0.45	0.48	0.48	0.64	0.64	0.62	↓	
Dec.	−0.17	0.00	0.18	0.23	0.46	0.60	0.53	0.67	0.68	0.60	0.68	↓
Jan.	−0.05	0.06	0.03	0.18	0.41	0.50	0.51	0.57	0.58	0.50	0.61	0.64
Feb.		−0.03	0.17	0.12	0.40	0.45	0.43	0.63	0.65	0.56	0.65	0.66
Mar.			0.08	0.09	0.12	0.20	0.23	0.44	0.41	0.40	0.57	0.44
Apr.				0.09	0.21	0.01	0.24	0.33	0.50	0.40	0.51	0.49
May					−0.11	−0.18	−0.10	0.02	0.20	−0.05	0.17	0.21
June						−0.18	−0.08	0.05	0.01	−0.10	−0.01	0.21
July							−0.03	0.02	0.01	−0.00	0.10	0.22
Aug.								−0.12	−0.03	−0.10	−0.00	0.16
Sept.									−0.15	−0.25	0.02	0.01
Oct.										−0.00	0.14	0.21
Nov.											−0.01	0.06
Dec.												0.01

The starting point (or lag month) is shown by an arrow. The lower stepped line indicates the month when correlation halving occurs.

months after spring correlates with the succeeding January SOI. February, March and, to a lesser extent, April possess similar patterns. The months of June through December show strong correlations with the months of late spring and summer, but not with the preceding winter. But, overall, the anomalous month is May. With the exception of April, with which it is moderately correlated, the SOI of May is not associated with the SOI of any preceding month. Thus May and April emerge as the key months from which the discontinuity in the SOI lag–lead correlations emerge.

The analysis of lag–lead relationships may be taken one step further by introducing circulation as a correlate with the SOI. Figure 16 shows the spatial distributions of the lag–lead correlations between the SOI of December, January and February (DJF) and the preceding and succeeding seasonal fields of U_{200}.

Six sections are shown: three seasons before DJF and two seasons following; these are labelled, successively, −3, −2, −1, 0, +1, +2. Thus, the first panel (−3) of Fig. 16 shows the lagged correlation between the U-field in the previous spring March, April and May (MAM) with the SOI in the following winter. The next panel (−2) shows the lag correlation between the summer U-field and the following winter SOI (−1), and so on. The fourth panel (0) shows the simultaneous relationships between the DJF SOI and the DJF U_{200}. Similar analyses were conducted where lagged correlations were sought between the MAM, June, July, August (JJA) and the September, October, November (SON) SOI and the lagged seasonal fields of U_{200}.

In all four sets of lagged U–SOI correlations, an abrupt decrease occurs through the spring. Thus, the diagrams display the same temporal characteristics in correlation with the SOI alone and in the Latif–Graham observation–prediction comparisons. Note, especially, the change of the character of the correlation patterns between lags '−3' and

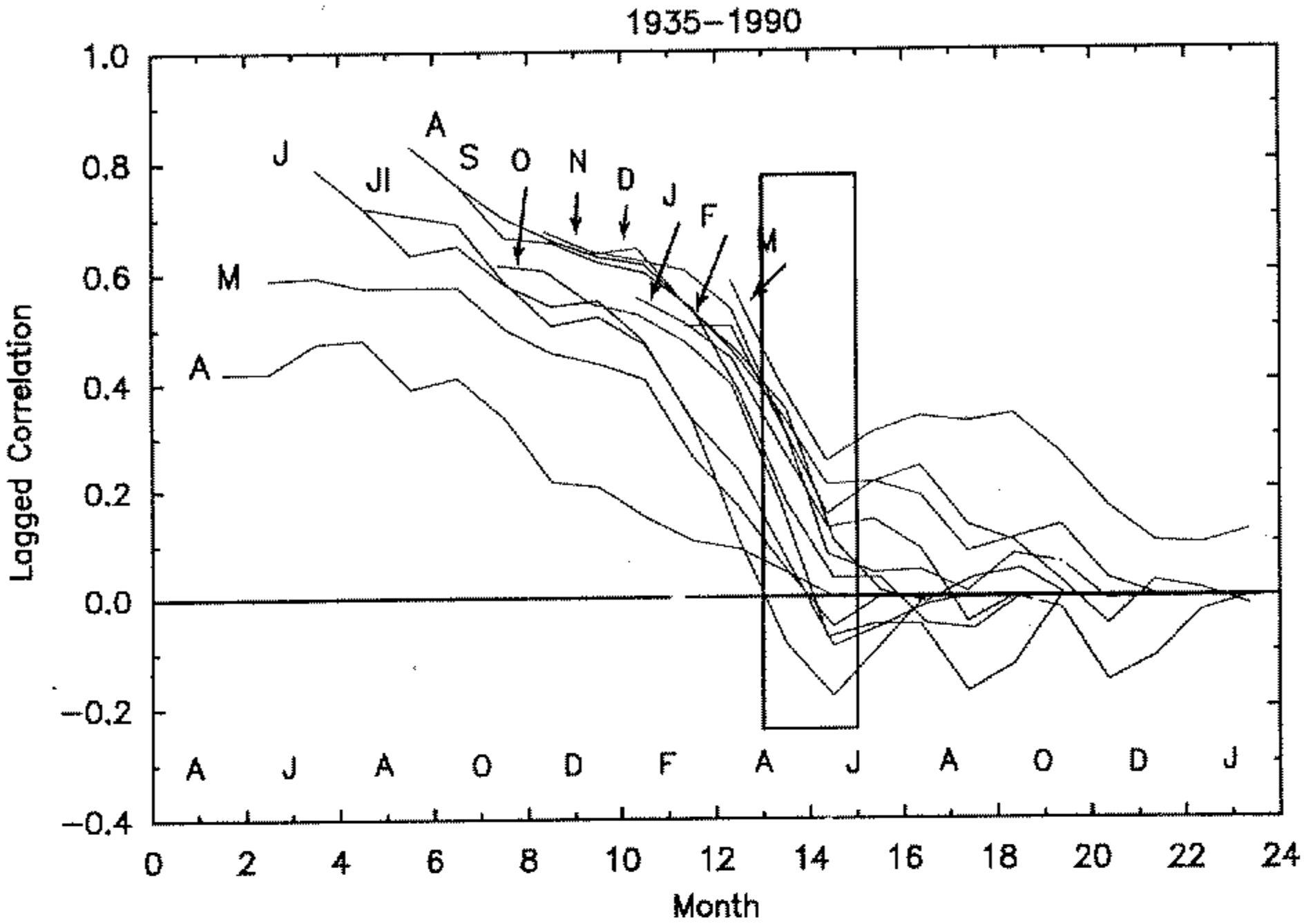

Figure 15. Lagged correlations between the monthly Southern Oscillation Index (SOI). Letters indicate the anchor or starting month of the correlation. The lagged correlation plots have been offset so that the correlations for the same month are lined up along the abscissa. The box shows the period of the Latif–Graham observation–prediction correlation decrease from Fig. 2. Note that the lagged correlations also decrease abruptly in the same period. Data are monthly mean values of the SOI from 1935–90.

'−2' and between lags '+1' and '+2' in Fig. 16. The significant correlation patterns disappear across the preceding and antecedent springs. Figure 17 plots subsequent seasonal correlation maps for MAM, JJA and SON across the vernal spring season. Irrespective of the choice of the base season, correlations decay very rapidly through MAM. Similar calculations to those shown in Figs. 16 and 17 were made using mean monthly data in an attempt to define more precisely the timing of the correlation decrease in the spring. The analysis (not shown) indicates that April and May remain as the major transitional months.

From the discussion above it is apparent that a prediction scheme whose kernel is the SOI will lose statistical connection across the boreal spring. Thus, either the coupled ocean–atmosphere system is inherently unpredictable across spring or some other statistical kernel is required. We now abandon an SOI emphasis and use the monsoon as the basic correlate.

6. Intensity of the broad-scale monsoon and the large-scale circulation

Figure 18 shows composites of anomaly fields for the 'weak' and 'strong' monsoon years. Summer OLR*, U^*_{200} and U^*_{850} fields are shown in the tropical strip between 45°N and 45°S averaged over the years 1979, 1982, 1983 and 1987, for the weak years, and 1984–86 for the strong years. Compared with the composite SOI diagrams (Fig. 13) the monsoon intensity composites show coherent patterns which extend globally and which are not constrained to the monsoon or the Pacific Ocean region.

In the weak monsoon composites (Fig. 18(a)), positive OLR anomalies extend over much of south Asia, Indonesia and the eastern Pacific Ocean. With negative anomalies

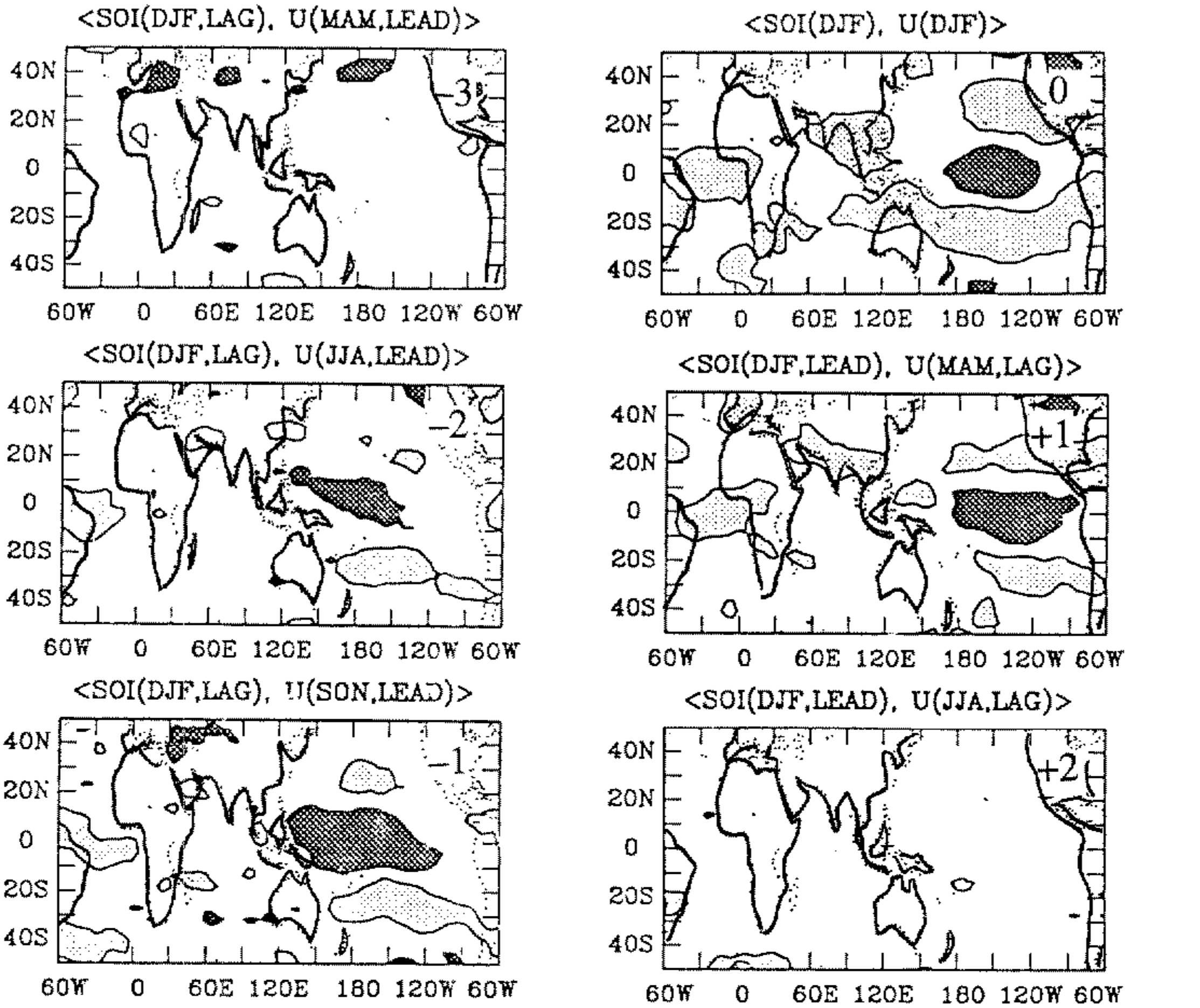

Figure 16. Lag–lead correlation fields between the Dec., Jan., Feb. (DJF) Southern Oscillation Index (SOI) and the preceding and succeeding seasonal 200 mb U-field. Numbers (-3, -2 etc.) refer to the lags in seasons of the U-field relative to the SOI. The simultaneous correlations between the mean seasonal OLR and U-field are shown in the central panels. Heavy and light shading denotes positive and negative correlations beyond the 95% confidence limit, respectively. The zero correlation contour has been omitted for clarity.

in the central Pacific Ocean, the pattern is very characteristic of a warm episode in the Pacific Ocean. In fact two of the years, 1982 and 1987, were El Niño years, although 1979 and 1983 (see Table 2) were not. However, the OLR* patterns for these last two 'non-El Niño' years bear the same signatures as 1982 and 1987. Similarly, the composite of OLR* for the years 1975–77 (i.e. the weak years from the first data period) exhibits similar characteristics. Clearly, the weak monsoon OLR* and the warm event or El Niño patterns are similar, but the signature is not a unique function of the SOI.

Large-scale coherent wind fields are also associated with the weak monsoon category. U^*_{200} is strongly positive over the equatorial Indian Ocean, indicating a weakened upper-tropospheric easterly jet stream in a location consistent with the weakened heating over south Asia. Elsewhere the flow shows generally weak westerlies, especially over the central Pacific Ocean. Poleward of the central Pacific considerable perturbations extend polewards, with maximum values in the winter hemisphere (reasons for which were given by Webster (1981)). Over the monsoon regions U^*_{850} is almost a mirror image of the 200 mb distribution. Weakened monsoonal flow (easterly anomalies of >5 m s^{-1}) matches the weaker upper-level monsoon easterlies. Elsewhere the match between the

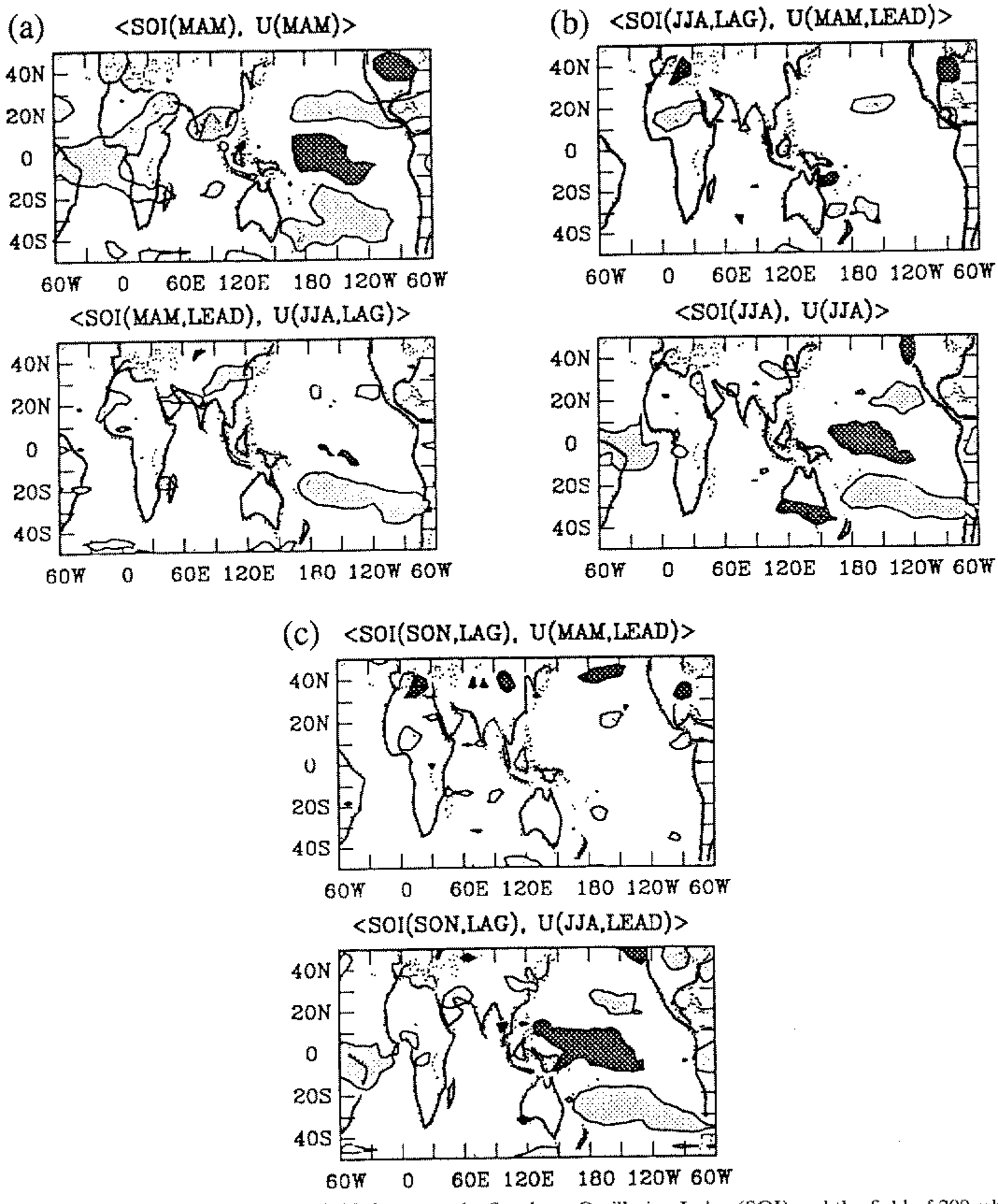

Figure 17. Lag–lead correlation fields between the Southern Oscillation Index (SOI) and the field of 200 mb zonal wind (U_{200}) across the boreal spring. The panels show the lagged correlation fields between the Mar., Apr., May (MAM) and June, July, Aug. (JJA) U-field relative to (a) the MAM SOI, (b) the JJA SOI, and (c) the Sept., Oct., Nov. (SON) SOI. Heavy and light shading denotes positive and negative correlations beyond the 95% confidence limit, respectively. The zero correlation contour has been omitted for clarity.

upper and lower troposphere is less evident. But of particular relevance for this study is that during these weak years the 850 mb winds are anomalously westerly over almost all of the tropical Pacific Ocean basin. That is, weakened trade winds are associated with the weak monsoon year which appears as a coherent signal on the Pacific Ocean basin scale.

The strong-monsoon-year composites (Fig. 18(b)) are in complete contrast to the weak years. Negative OLR anomalies lie over most of the Indian and Pacific Oceans and

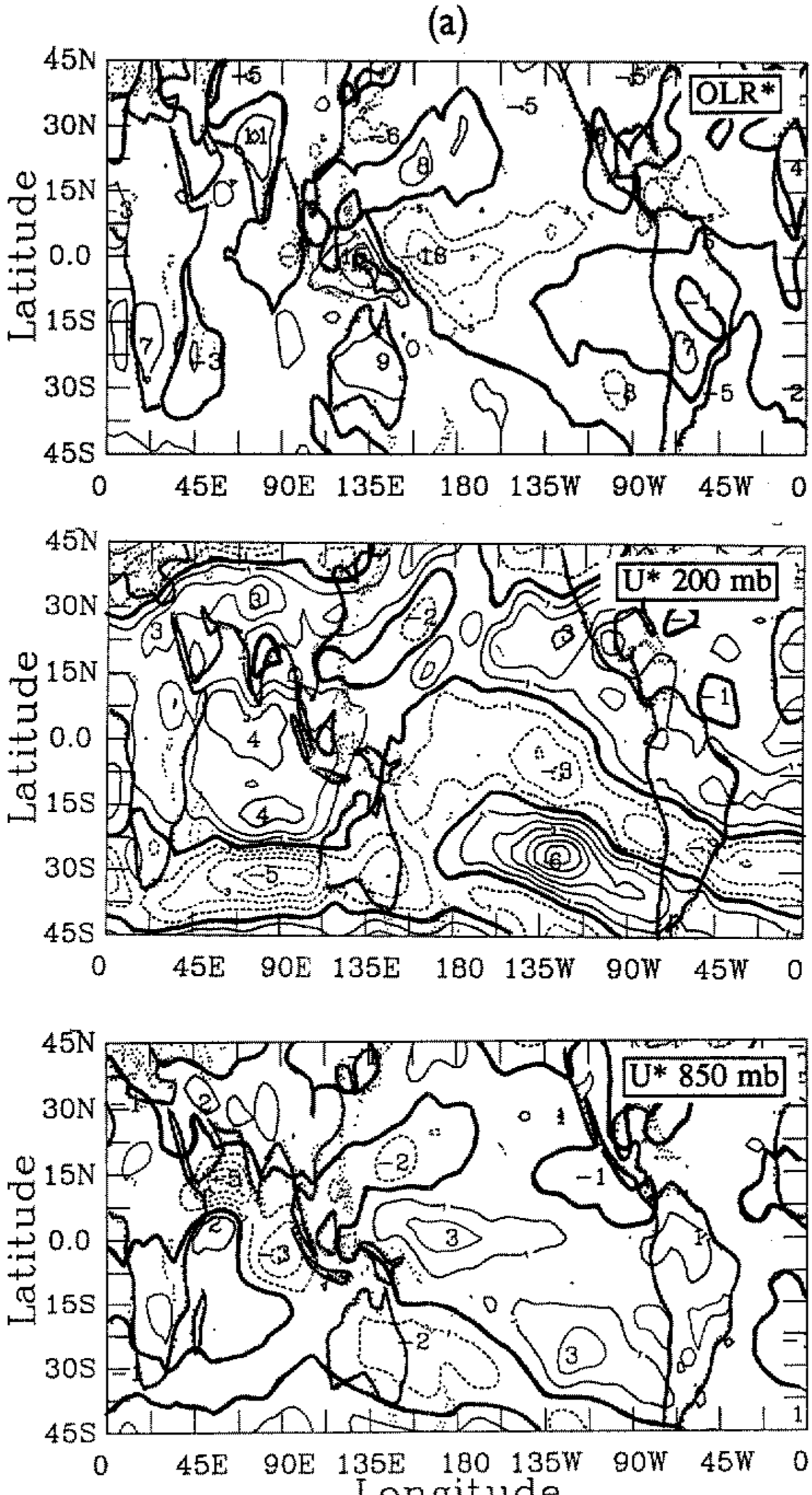

Figure 18. (a) Composites of the anomalous outgoing long-wave-radiation (OLR) field (upper panel), and the anomalous 200 mb and 850 mb zonal wind fields (middle and lower panels) for the 'weak' monsoon years (1979, 1982, 1983, 1987) defined using the monsoon circulation index.

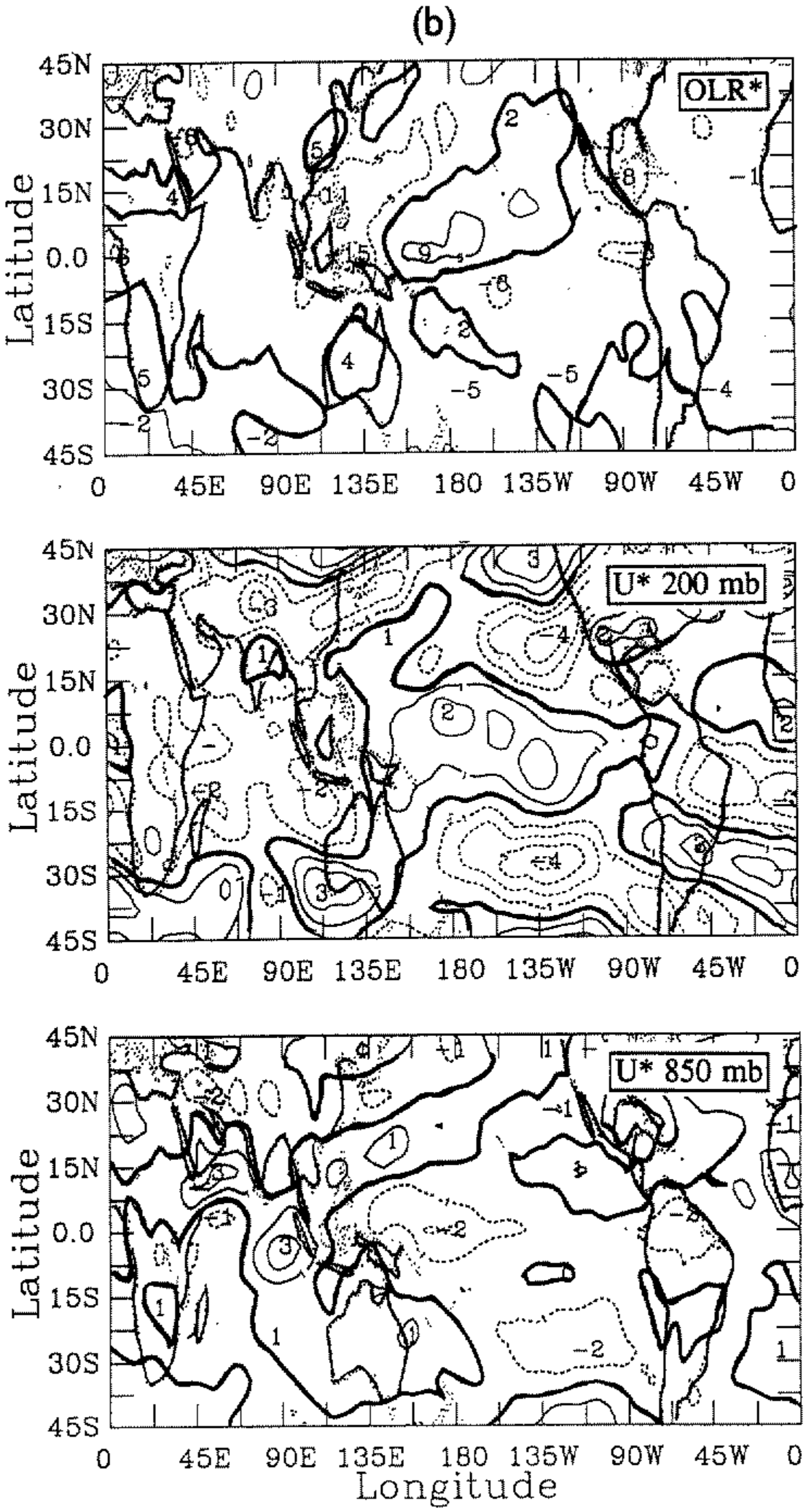

Figure 18. (b) As (a) but for the 'strong' monsoon years (1984, 1985, 1986). Contour intervals are for 5 W m^{-2} for OLR* and 1 m s^{-1} for the wind fields. The zero contours are bold.

Asia except for a positive 'tongue' in the central and western Pacific Ocean which extends across the equator. Maximum negative values (i.e. enhanced convection) occur over south-east Asia and Indonesia. There is some similarity between the cold event (or La Niña) when the SOI $\geqslant 0$ (Fig. 13). However, the values of the SOI for each of the strong years are -0.4, -0.3 and 0.1 (Table 2).

The strong monsoon 200 mb U-field is negative over almost the entire eastern hemisphere and positive along the equator over the central and eastern Pacific. From the latter region anomalies appear to radiate poleward, exhibiting a familiar Pacific–North America teleconnection pattern (e.g. Wallace and Gutzler 1981). The 850 mb field shows a much stronger monsoon with an anomalous westerly monsoon in excess of 3 m s^{-1}. Over the entire Pacific basin the 850 mb flow is anomalously easterly, indicating that a stronger trade wind regime is associated with strong monsoon years.

With what climatic structures are the anomalous strong and weak monsoon periods associated? Are they anomalous patterns which 'emerge' in the summer, or are they part of a longer period and, clearly, a broad-scale circulation? To seek answers to the questions the mean monthly OLR and circulation fields were composited for the weak and strong years. Figure 19(a) shows the composite annual cycles of the OLR for the three areas previously defined: South Asia, North Africa, and the South Indian Ocean. Over North Africa there is little difference between the two composites throughout the year. However, over the South Indian Ocean and South Asian sectors there is a considerable departure, not just at the time of the summer monsoon but for considerable periods on either side. From January through the monsoon season and into autumn the OLR is significantly lower during weak monsoon years. In the spring and early summer the difference is as high as 10 W m^{-2}. Even during the winter months the OLR is anomalously low.

The upper- and lower-tropospheric zonal wind fields in the South Asian sector for the composite annual cycle of the strong and weak monsoons are shown in Fig. 19(b). At the time of the summer monsoon, both the low-level westerlies and the upper-level easterlies are considerably stronger during strong monsoon years than during weak years. But what is very striking is that the anomalous signal of upper-level easterlies during strong years extends back until the previous winter. Then, the 200 mb wind field is about 10 m s^{-1} less westerly during strong years. However, in the lower troposphere, the difference between strong and weak years occurs only in the late spring and summer. Thus there is a suggestion that the anomalies are signifying external influences from a broader scale into the monsoon system. This surmise is supported by what we know about tropical convective regions. Generally, enhanced upper-tropospheric winds will be accompanied by enhanced lower-tropospheric flow of the opposite sign, but, as during the winters before the strong monsoons, this is clearly not the case. This suggests that a modulation of the upper troposphere probably results from remote influences.

Figure 20 shows the time evolution of the 200 and 850 mb wind field in the South Asian sector for the 1979–87 period of the data set. A three-month running average has been applied to the data. Before each of the three strong monsoon periods, the upper-tropospheric winds appeared to be exceptionally weak during the previous winter. The area average value of the upper-tropospheric winds is about 5 m s^{-1} overall. However, before the strong monsoons the winds averaged only a little more than 1 m s^{-1}.

To check if the anomalously weak winds before a strong monsoon were tied to a larger-scale structure, an annual cycle of the U^*_{200}-field was computed relative to the strength of the summer monsoon. Mean seasonal fields were composited relative to the strong and weak summer monsoon. The four seasonal fields for each category are shown in Fig. 21. Considering first the strong monsoon composite (Fig. 21(a)) we note that the

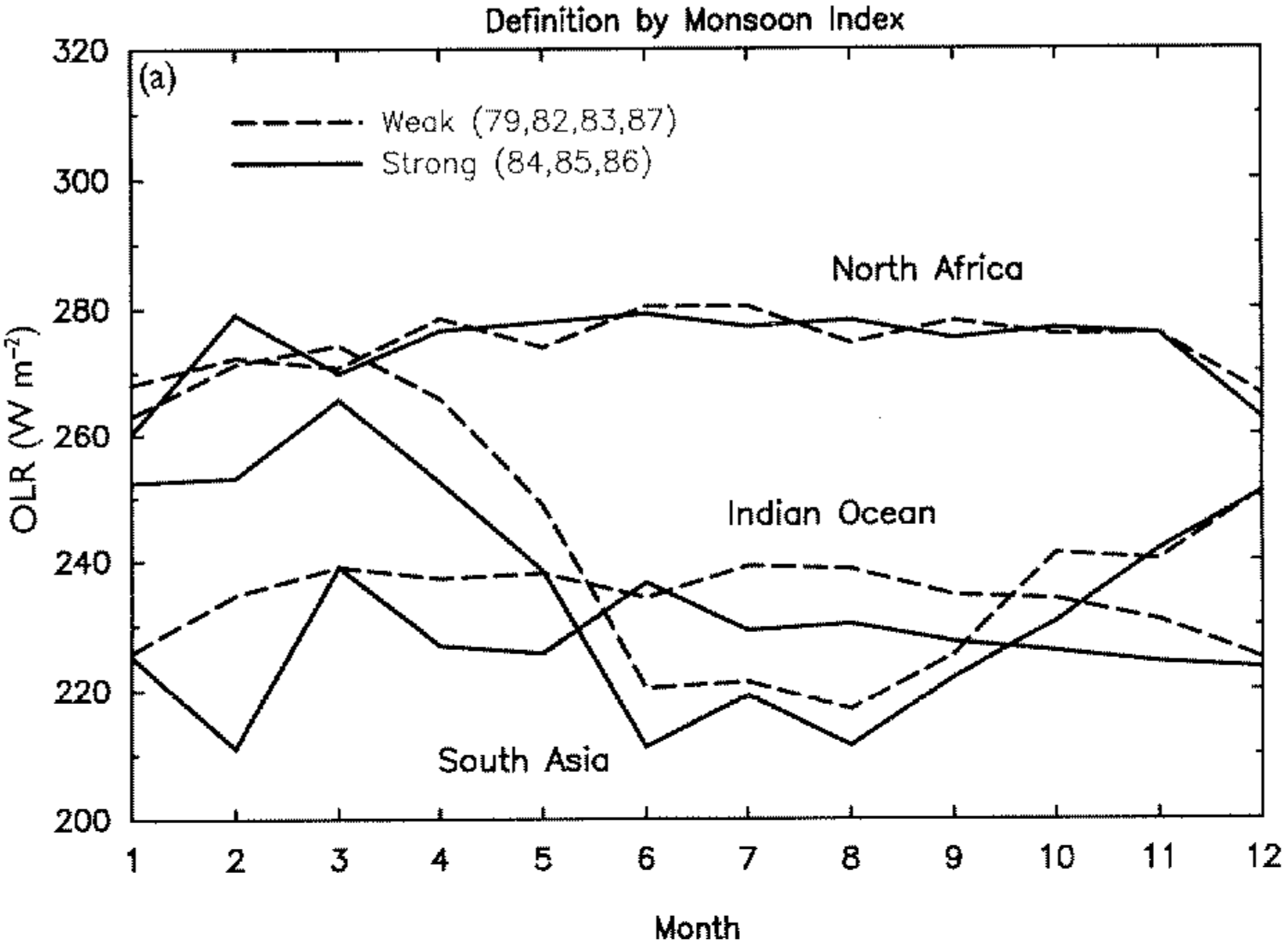

Figure 19. (a) Composite annual variation of the outgoing long-wave radiation (OLR) in the South Asian, North African and South Indian Ocean regions (see text) for years identified by the 'strong' and 'weak' monsoon designations. Strength of the broad-scale monsoon is defined by the monsoon intensity function (M_I^*; see text and Table 1). (b) Composite annual variation of the 850 mb and 200 mb zonal wind component in the South Asian region for years defined by 'strong' and 'weak' monsoons. Note that the signal is not apparent in the lower troposphere at times earlier than the summer.

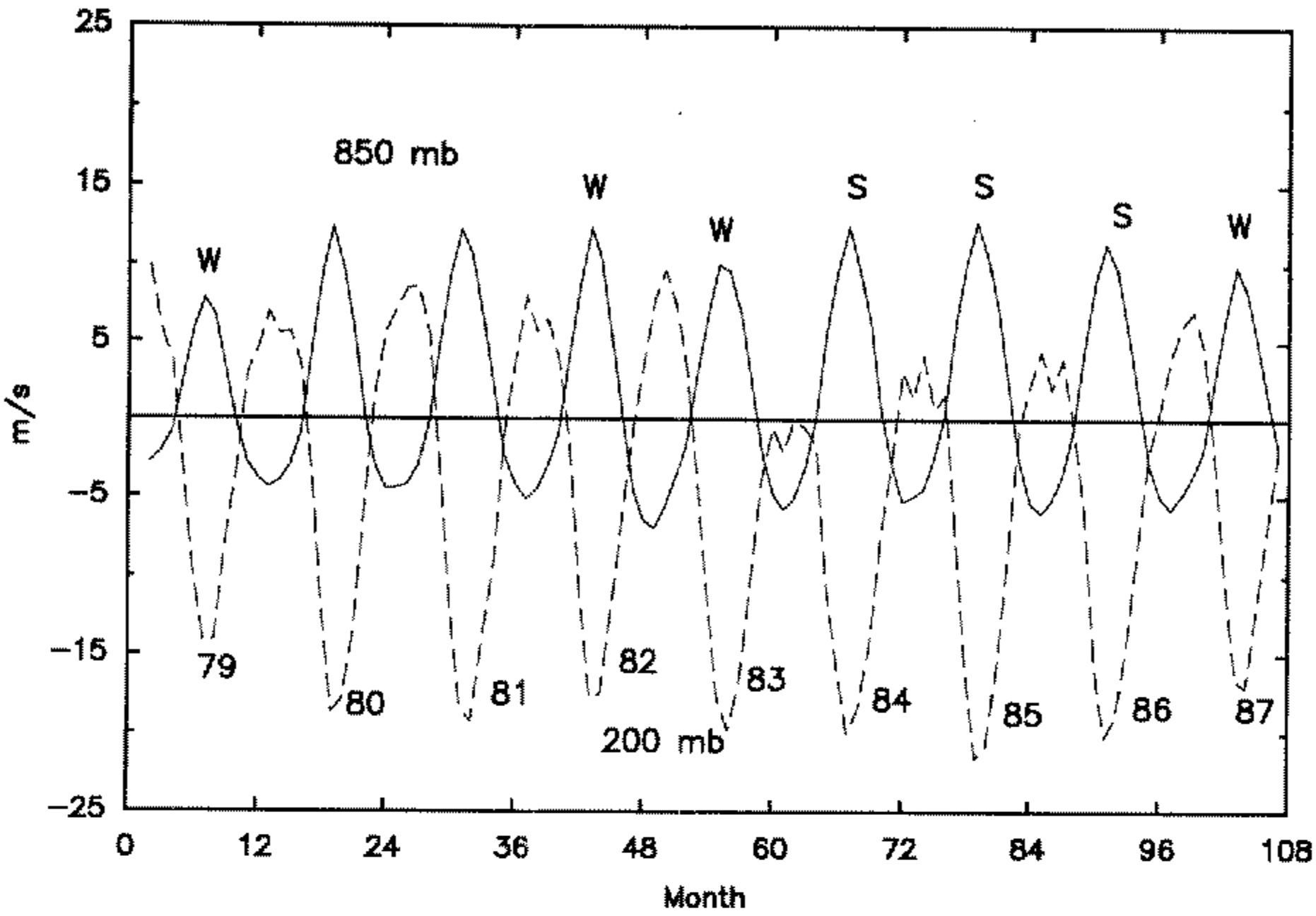

Figure 20. Three-month running average of the 200 mb (dashed) and 850 mb (solid) zonal winds in the South Asian (5°N–20°N, 40°E–110°E) sector for 1979–87. The years and the weak (W) or strong (S) monsoon designations (see text) are indicated on the plot. Note that before a strong summer monsoon the 200 mb winds are remarkably weak. Apparently, strong and weak monsoon periods are functions of a larger-scale and lower-frequency system.

weak winter winds over the monsoon regions (i.e. anomalous easterlies) are coherent over vast areas and persist in a fairly coherent form over the entire composite year. Thus the weaker westerlies over the South Asian sector, which we noted in Fig. 19(b) as preceding a strong monsoon, are part of a much larger anomaly system. Over the Pacific basin the tropical westerlies are enhanced and a strong pattern protrudes poleward in both directions. This teleconnection pattern, which has the opposite phase to the El Niño structure, is strongest in MAM, but is also apparent in the other seasons. Only in the autumn following the strong monsoon does the coherence of the fields start to weaken. The upper-tropospheric wind fields for the weak monsoon year (Fig. 21(b)) show similar spatial coherence but of generally opposite sign. Over southern Asia the winds are anomalously westerly although during the previous winter the fields are less coherent than during the strong case. Over the Pacific basin the 200 mb winds are anomalously easterly.

It is interesting to note that in both the strong and weak monsoon composites a teleconnection pattern extends poleward from a region of minimal convection from the location of the climatological mean upper tropospheric equatorial westerlies. The teleconnection patterns are of opposite phase in the two composites, but they appear as very strong patterns especially in the boreal spring. The eastern Pacific position of the pattern is colocated with the extensive equatorial upper-tropospheric westerlies. Webster and Dong (1991) showed that the strength of the westerlies in this region was a useful correlate in determining flow regimes.

Finally, the statistical significance of the anomaly and difference fields should be addressed. Given the length of the data set (1979–87), it is difficult to determine formally whether or not the anomaly and difference fields are statistically significant. Despite this difficulty, we can add some support regarding their authenticity by noting a number of features about the fields. For example, the circulation fields are dynamically consistent

with the heating fields inferred from the independent OLR fields. Furthermore, the anomaly and difference fields are spatially coherent over very large spatial domains. Together, these checks suggest that strong and weak monsoons are associated with characteristic circulation patterns. Perhaps the most important observation is that the signal associated with the strong and weak monsoons extends across the predictability barrier, at least from as far back as the previous winter.

7. Discussion and conclusions

Modelled predictability (e.g. Latif and Graham 1991) and temporal statistical coherence using the SOI (Fig. 14) have proven to be very strongly tied to the annual cycle. Two hypotheses were posed to account for the springtime correlation demise and to form a framework for study. In essence, the propositions suggested that the correlation demise resulted from either a vulnerability of the coupled ocean–atmosphere system to external perturbation or noise at a time when the tropical circulation was least robust, or from strong external forcing. The second proposition suggested that the near-equatorial circulation was weakest in the spring and that the system was more susceptible to error growth induced by external noise at that time of the year. In the second instance, the external influence was the highly variable south Asian summer monsoon system which possesses a strong asymmetry within its annual cycle.

Initially the SOI was used to explore relationships between the monsoon and the ENSO. With the SOI as the major correlate, significant correlations were restricted to the Pacific Ocean region although in winter the correlations extended to the South Asian region. An annual cycle of the SOI correlations was calculated (Fig. 13) by constructing the differences in the OLR and 200 mb U-fields between the extremes of the SOI. Similar results were found; maximum differences occur in winter and were largely restricted to the Pacific basin.

The utility of the SOI as a predictor of the monsoon presumes that the simultaneous correlation between the SOI and monsoon fields is high. However, only limited correlations were found in the South Asian region in summer. Furthermore, lag correlations using the SOI fail to span the boreal spring period. The absence of lead correlations between the winter and summer suggested that the observation–prediction demise encountered by the numerical modellers (e.g. Latif and Graham 1991) occurred in nature as well. In fact lagged correlations using monthly values of the SOI (Fig. 18) showed that the SOI lagged correlations decreased abruptly at the same time as the models during the April–May period. In summary, the lack of significant correlations across the spring suggested a distinct limitation on the utility of SOI-based prediction schemes for interannual prediction.

The second thrust of the study involved using the monsoon circulation indices as the major correlate, following the abandonment of the SOI as a particularly useful correlate for interannual prediction. A monsoon intensity function (M^*) was defined to be proportional to the vertical shear of the anomalous wind field in a broad-scale monsoon region. Simple tests showed that very-large-scale coherent circulation characteristics in both the upper and lower troposphere were defined by the index. Field composites were made relative to the weak and strong monsoon designations. Summer patterns showed very-large-scale and coherent responses in all fields. Unlike the SOI composites, the anomaly fields were global in extent and they transcended the boreal spring period (Fig. 18). The 200 mb U-field also possessed differences in the previous winter (Fig. 21). In each of the three strong monsoon years the U_{200} during the previous winter and spring was up to 10 m s^{-1} weaker than during weak years and became identifiable in the spring.

(a)

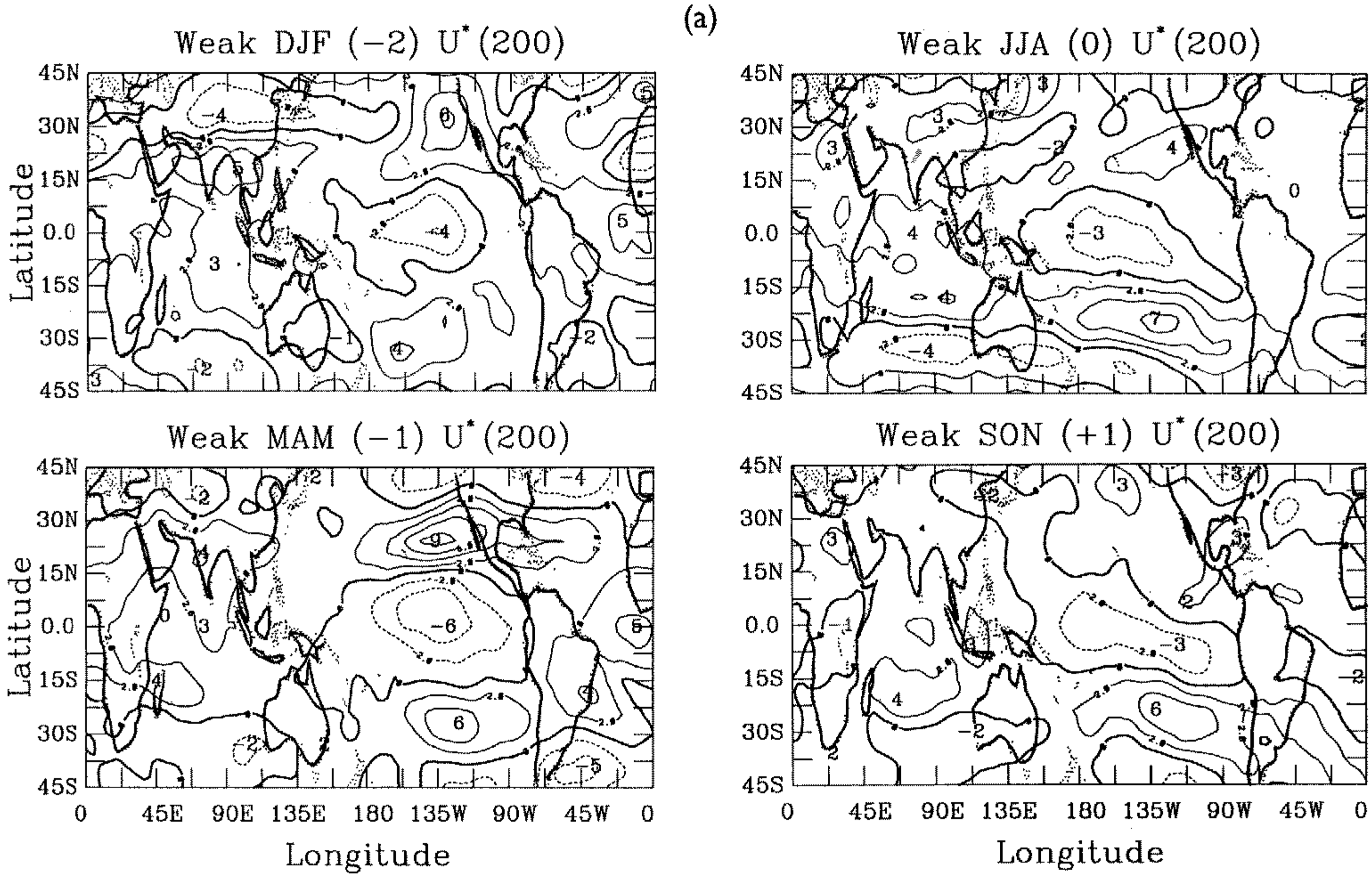

Figure 21. Composite annual cycles of the 200 mb zonal wind component for the year defined by (a) a weak summer monsoon, and (b) a strong summer monsoon. Composite mean seasonal fields are shown from the previous winter (Dec., Jan., Feb. (DJF)—2 seasons) to the following autumn (Sept., Oct., Nov. (SON) + 1 season). Contours intervals are 1 m s^{-1} and negative values are dashed.

(b)

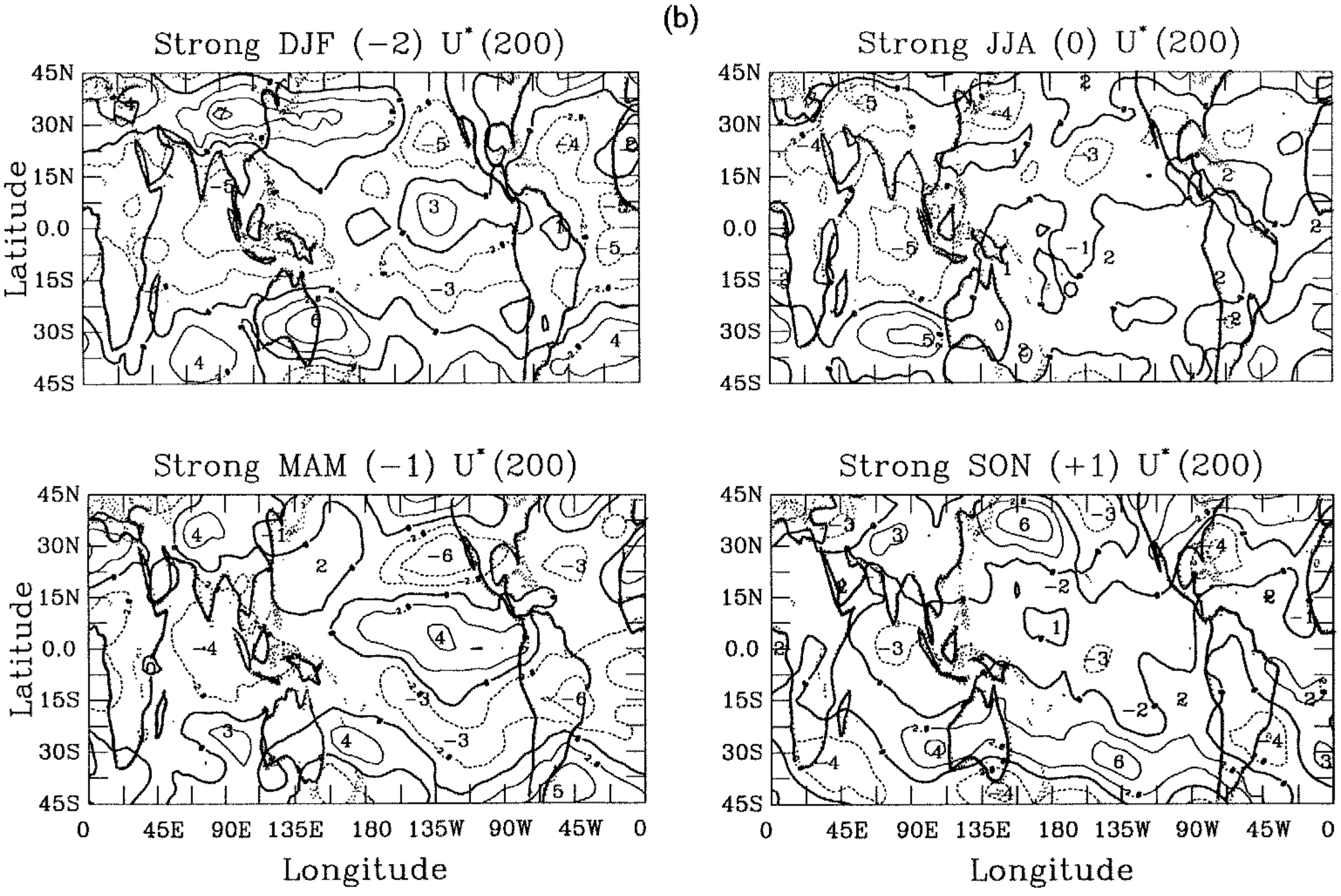

Figure 21. Continued.

Of critical importance to the interaction of the monsoon and the ENSO was the result that strong monsoons were associated with enhanced summer trade winds over the Pacific. On the other hand, the weak monsoon was associated with weak summer trades (Fig. 18). This observation suggests a physical connection between the summer monsoon intensity and the coupled ocean–atmosphere ENSO phenomenon.

The existence of temporal coherence in the atmosphere between summer and the previous winter suggests that monsoon variability is part of a wider and lower-frequency order. In many ways these results are in keeping with the concepts developed by Yasunari (1987, 1991) who proposed relationships between the large-scale monsoon and the ENSO. However, there are some differences. Yasunari uses the definition of a 'monsoon year' in which the year is defined relative to the previous summer monsoon. Within his hypothesis the monsoon is of paramount importance and with its onset the 'characteristic circulations' of the previous year are effectively 'flushed'. From an ENSO or SOI perspective there appears to be some merit in Yasunari's supposition. If anomalous monsoons could impact the coupled system in the Pacific Ocean it could explain the Latif–Graham correlation's decline during spring. However, coherent signals were found in the present study which linked the intensity of the monsoons to anomalous structures in the previous winter circulation (Fig. 21).

The results of the study appear to be consonant with the general-circulation modelling studies of Barnett *et al.* (1989). Before strong monsoon events we found weak upper-tropospheric westerlies over southern Asia in the preceding winter and spring. Barnett *et al.* found weak westerlies to be accompanied with a deficient winter snowfall over Asia because of a reduced latitudinal diabatic heating gradient. They also found that a limited snowfall was followed by strong trades over the Pacific Ocean which is the same general pattern found in Fig. 18(b). The results of the Barnett *et al.* study for the high-snowfall case are also consistent with the weak monsoon composite shown in Fig. 18(a).

It is interesting to check on whether Shukla and Mooley's (1987) second correlate (i.e. the latitude of the mean mid-tropospheric ridge in April over India) is consistent with the large-scale and low-frequency context we have found for the strong and weak monsoon periods. Shukla and Mooley showed that when the monsoon rainfall over India was above average, the April ridge had been located more poleward than normal. When the rainfall was weak the ridge was located to the south. In the averaging domain used to calculate the mean wind fields of Fig. 18(b) (i.e. 5°N–15°N, 40°E–110°E), the Shukla–Mooley ridge locations would translate to weaker 200 mb mean westerlies for the strong monsoon and stronger westerlies for the weak monsoon. Unfortunately, there is only a five-year overlap in the analyses. However, the correspondence is encouraging. In the three strong years (1984–86) the April mean 200 mb wind was 3.6 m s^{-1} while for the four weak years it was 7.3 m s^{-1}. It may be possible that the Shukla–Mooley ridge position is a consequence of the very-large-scale lower-frequency domain (Fig. 21) which also contains the anomalous winter and spring circulations. A comparison of the composite OLR and wind fields (Fig. 18(a) and (b) lends further support. In strong years the OLR fields in the winter and spring are anomalously small in the Indian Ocean region (i.e. 10°S–5°N, 40°E–110°E) indicating greater than normal convection. Stronger convergence in the equatorial area would seem to be consistent with a northward displacement of the mid-tropospheric ridge.

Figure 22 shows the distribution of the 200 mb vector winds for the winter and spring preceding the anomalous summers. Many of the features discussed earlier are evident. The teleconnection patterns extending poleward out of the eastern Pacific Ocean are now seen clearly as alternating cyclones and anticyclones. In addition, the vector distributions point out that before a strong monsoon the Asian continent is dominated by

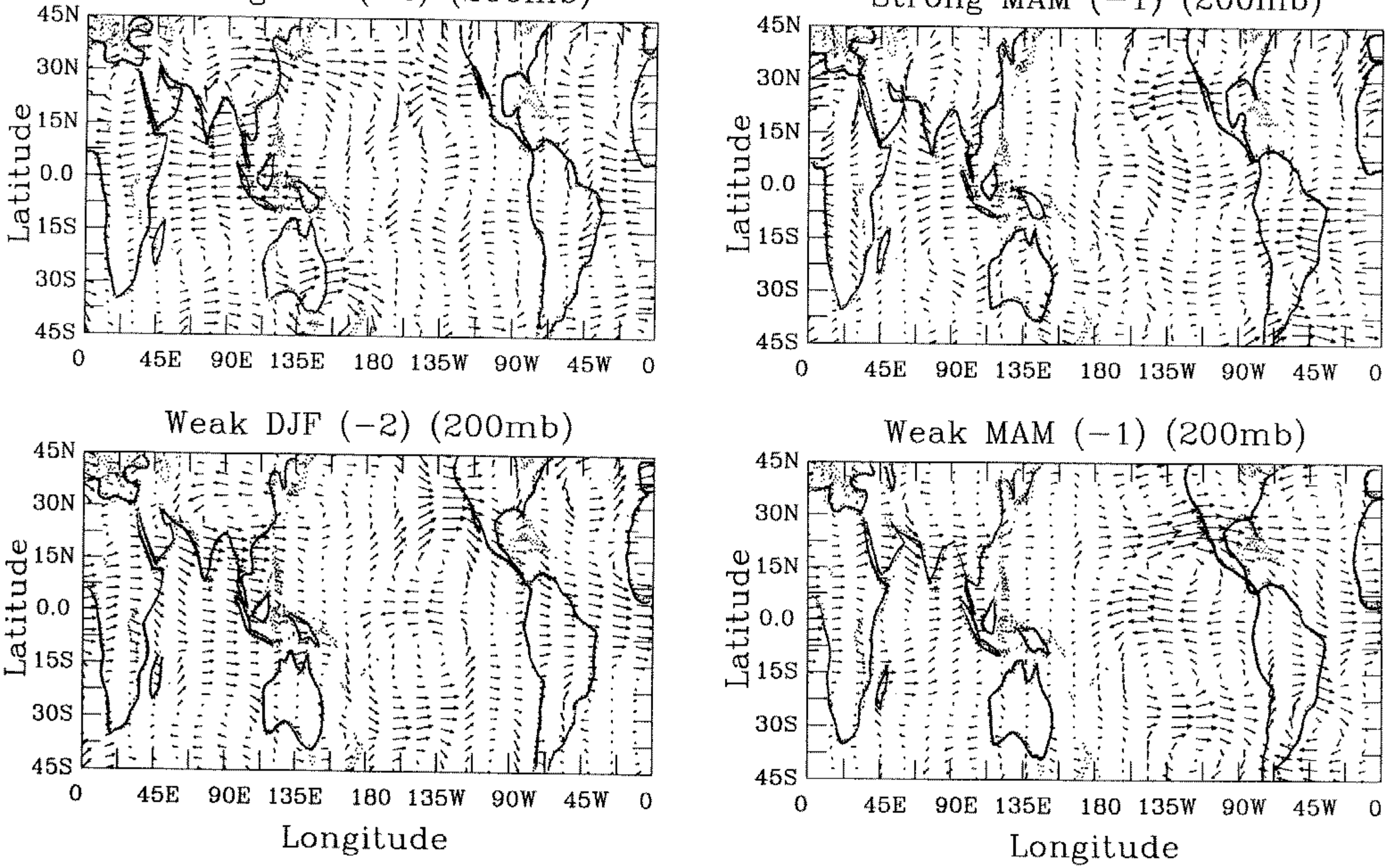

Figure 22. Vector distributions of the anomalous 200 mb vector horizontal wind at 200 mb for the mean winter (Dec., Jan., Feb.) and spring (Mar., Apr., May) preceding the strong (upper panels) and weak (lower panels) monsoons. Maximum vector length denotes 10 m s^{-1}.

a strong anomalous anticyclone, and before a weak monsoon an anomalous cyclonic circulation predominates. The circulations are consistent with both precursor flows suggested by Barnett (1984, 1985) and Shukla and Mooley (1987). Given the lack of predictive value we have found in the SOI across the spring, it would seem that the majority of the skill in the Shukla–Mooley scheme comes from the distribution of the persistent low-frequency circulation patterns which become established in the previous winter.

We are now in a position to return to the questions posed in the introduction.

(i) *What are the unique aspects of the spring period of the annual cycle of the tropics*? Both the asymmetric and symmetric circulation shows distinctive annual cycles. The amplitude of the components are in quadrature with the maximum intensity of the monsoon occurring in summer while the Walker circulation maximizes in the winter. The monsoon grows very rapidly in the spring and reduces its intensity slowly in the fall.

(ii) *Is the predictability barrier the result of model inadequacies or simplifications, or does it signify an absolute limit to interannual predictability*? The similarity between the model prediction–observation correlation curves (Fig. 2) and the SOI lagged correlations (Fig. 15) suggests that the models are emulating well a system that is dominated by the coupled ocean–atmosphere system in the Pacific Ocean. In that sense, we can guardedly agree with Cane (1991) that '. . . the mechanisms responsible for the entire ENSO cycle are large-scale, robust and simple . . .' and are thus included in the intermediate coupled models. Perhaps, though, the question is with regard to the word *entire*.The entire ENSO cycle would include its vagaries of amplitude and phase. And if the calculations made here are correct in any way, the models will have to include considerably more complicated geography, oceanic and continental, be more extensive, perhaps global, and contain moist processes. Thus, it may require the coupling of oceanic and atmospheric general-circulation models to account adequately for the interactive system and to forecast interannual variability.

(iii) *To what degree are the variabilities of the broad-scale monsoon and the ENSO related*? Many of the features of the 'strong' and 'weak' monsoon OLR and circulation distributions resemble El Niño and La Niña characteristics. Whereas some of the years are common (e.g. the weak summers of 1982 and 1987 were also El Niño years), others were not. None of the strong monsoon years (1984, 1985, 1986) were La Niña years and only the spring of 1985 possessed a substantially positive SOI and that was only 0.5. Thus stratification of data in terms of SOI or the monsoon intensity index, M^*, may lead to similar patterns, but not because there is necessarily a causal linkage. Thus patterns that we would normally ascribe to the ENSO are not necessarily unique to the ENSO.

(iv) *How variable is the amplitude and the phase of the broad-scale monsoon*? The length of the two data sets used in this study preclude definitive statements regarding the full range of the amplitude and phase of the broad-scale monsoon. Yet, in the nine years of usable NMC data and the four years of ECMWF data (including two years that overlap), we have encountered wide ranges of circulation and heating differences. In fact, in the eastern hemisphere between 30°N and 30°S, root-mean-square differences of greater than 15 W m^{-2}, 10 m s^{-1} and 5 m s^{-1} in OLR, U_{200} and U_{850}, are apparent. In the western hemisphere the differences are only slightly smaller (10 W m^{-2}, 5 m s^{-1} and 3 m s^{-1}). The anomalous monsoons are associated with large-scale fields with similar differences which extend back through the previous winter. Within each monsoon there exists considerable variability in variance,

amplitude and phase. For example, in the period 1986–89 the time of rapid acceleration of the monsoon (the broad-scale onset) varied within a thirty-day range.

(v) *How predictable are the variations of the large-scale monsoon*? Despite the existence of moderate simultaneous correlation between aspects of the summer monsoon and the SOI, the existence of the predictability barrier in spring precludes the use of the SOI as a useful tool for predicting either the intensity or phase of the succeeding monsoon season. However, we have noted that the anomalous monsoon is part of a larger scale and longer period anomalous system. Thus, if extensions of this data analysis, using longer and more reliable data sets, continue to show the existence of the large-scale character of the monsoon, then some form of prediction may be possible. In any event, the failure of the SOI-based correlation results do say something about the models that will be needed to perform these predictions. Clearly they will have to include a much more complicated geography, and interactive processes that are now included in the Cane–Zebiak and Latif–Graham models. We have also noted that the patterns found in this study are similar to those found in the modeling study of Barnett *et al.* (1989) for high and deficient winter snow extensions over the Asian continent. The degree to which the variations in the snowfall are the instigators or the result of the low-frequency flow within which the monsoon appears to be embedded is difficult to say at this time.

(vi) *From where do the higher frequency components of the ENSO signal arise*? The possible interaction of the monsoon and the ENSO systems provide considerable opportunity for the production of higher-frequency signals in the coupled ocean–atmosphere system. Similarly, the impact of external forcing functions such as the variation of the Asian snowfall may be of consequence. However, the explanation of specific frequencies (e.g. Rasmussen *et al.* 1990; Barnett 1991) requires very careful analysis and numerical experimentation which are discussed below.

The results of the study allow a speculation on a two-layered system which allows, at least, a consistency between the SOI correlation decline in spring on the one hand, and the anomalous monsoon behaviour on the other. Two particular processes can be suggested:

(a) To a large degree the annual cycle of the coupled ocean–atmosphere system can be divided into two components (Fig. 3). But how do these components interact? The symmetric and asymmetric parts of the system both have clear annual cycles. The maximum amplitude of the Walker circulation occurs at the time of the minimum monsoon amplitude and when the monsoon maximum is closest to the equator. On the other hand, the monsoon maxima occur when the Walker circulation is at its weakest state. Thus, these two parts of the annual cycle may exchange their relative ascendancy from one time of the year to another. In that sense, the two components of the system are selectively interactive.

(b) Selective interaction may help in understanding the basis of interannual variability. Besides the dominance of the monsoon circulation during the boreal spring and summer, there are two additional points that should be recalled. The first point is that anomalies in the strength of the summer monsoon tend to lead to anomalies in other regions (e.g. Normand 1953; Barnett 1984, 1985; Meehl 1987; Yasunari 1987). The second point is that strong and weak monsoons appear to be immersed in a slowly evolving system which transcends the spring correlation barrier. During the spring when the Walker circulation is weakest, the symmetric system within the Pacific Ocean is least robust and most susceptible to influence. During any one year this is the time when the asymmetric part of the circulation gains the ascendancy. If

the monsoon is either in a weak or a strong phase, anomalous forcing will be introduced into the system through an anomalous trade-wind regime, and to the ocean through anomalous wind stresses (Fig. 18). That is, the ascendancy of the asymmetric part of the system at that time of the year allows anomalies to be transmitted to the Pacific Ocean system at the time when it is most susceptible to influence. In this manner the ENSO cycle is modulated. Whether or not the broader-scale circulation involved with the monsoon is impacted by the perturbed ENSO cycle at the time when the symmetric part of the system is in the ascendancy is difficult to know from purely diagnostic studies and must await numerical experimentation. The schemata helps to illustrate the form of the annual variation in the tropics and how the annual cycle interacts with longer-term variations. At the same time it suggests a series of numerical experiments which will allow the selective interaction and the random-error-growth hypotheses to be tested. A brief description of the experiments are presented in appendix B.

Acknowledgements

Much of this paper emerges from the writings and earlier conversations with Sandy Troup who foreshadowed the role of the annual cycle in interannual variability of the coupled climate system and the concept of coupled ocean–atmosphere modes. We would like to dedicate our paper to his memory and his contribution to our field. We appreciate discussions with Dr T. Palmer of the ECMWF regarding the role of monsoons in the general circulation and the annual variation of the robustness of the coupled ocean–atmosphere system. Valuable comments on the manuscript were provided by Dr J. Curry of the University of Colorado. We would like to thank Dr P. A. Arkin of the NMC Climate analysis Center and the ECMWF for making the data used in this study available. Much of the work and analyses were accomplished while one of us (PJW) was visiting the ECMWF. We are grateful for their support. This study was supported by NSF Grant ATM 87–03267 and the USDC/NOAA Grant NA89AA-ACO15. Computing was carried out at the National Center for Atmospheric Research which is supported by the National Science Foundation.

Appendix A

Data

The primary data used in this study are the tropical strip winds and outgoing long-wave radiation (OLR) data set from the operational tropical objective analysis of the National Meteorological Center (NMC). The data set consists of monthly mean values of the zonal and meridional wind components at six levels (1000, 850, 700, 500, 300 and 200 mb) from March 1968 to February 1988 and monthly mean values of OLR from June 1974 to February 1988. The sets are incomplete. No 200 mb winds are available for October and November 1972 and the OLR data are missing from March to December 1978. In addition, no 850 mb winds are available before December 1974 although 700 mb wind data is available as a continuous set from 1968 onwards. The data are set on a 72×23 Mercator longitude–latitude grid. The longitudinal spacing is 5°, and the latitudinal spacing is variable, ranging from 5° at the equator to 3.5° at the southern and northern boundaries that are located at 48.1°S and 48.1°N, respectively.

The data sources used in the NMC operational objective analysis include rawinsondes, aircraft reports and cloud-tracked winds from satellite imagery (Arkin 1982). As

the NMC data set is the product of an operational system, a number of different objective analysis and initialization schemes have been used through the years. The Cressman analysis (successive correction scheme) was used from March 1968 through August 1974. The Hough analysis, which employed a spectral representation of first guess and data-generated corrections to the spectral coefficients, was used from September 1974 through August 1978. After September 1978 the optimum interpolation technique, which used three-dimensional correlation functions to make observation-generated corrections to the first-guess fields, was applied. According to Arkin (1982), the effects of the changes in analysis procedure may be noticeable on daily analyses but are small on the large-scale features of the monthly mean fields. However, Webster and Dong (1991) found that, while the rotational part of the wind field was little affected by the changes in analysis procedure, the magnitude of the monthly mean divergent wind was particularly affected by the different schemes. For example, the divergent part of the wind is very small in the period when the data were derived from the Hough analysis which essentially rendered the data non-divergent.

Figure A.1 shows an example of the complete NMC data stream for the period 1968–87 averaged over the area 5°N–20°N, 40°E–110°E. The different analysis–initialization schemes are indicated along the lower abscissa and the data available along the upper abscissa. Three curves are plotted: the evolution of the mean monthly 200 mb zonal wind component, the 850 mb zonal wind component and the monsoon index M_2. A clear demarkation in the magnitude of all three quantities occurs at the time that the optimal

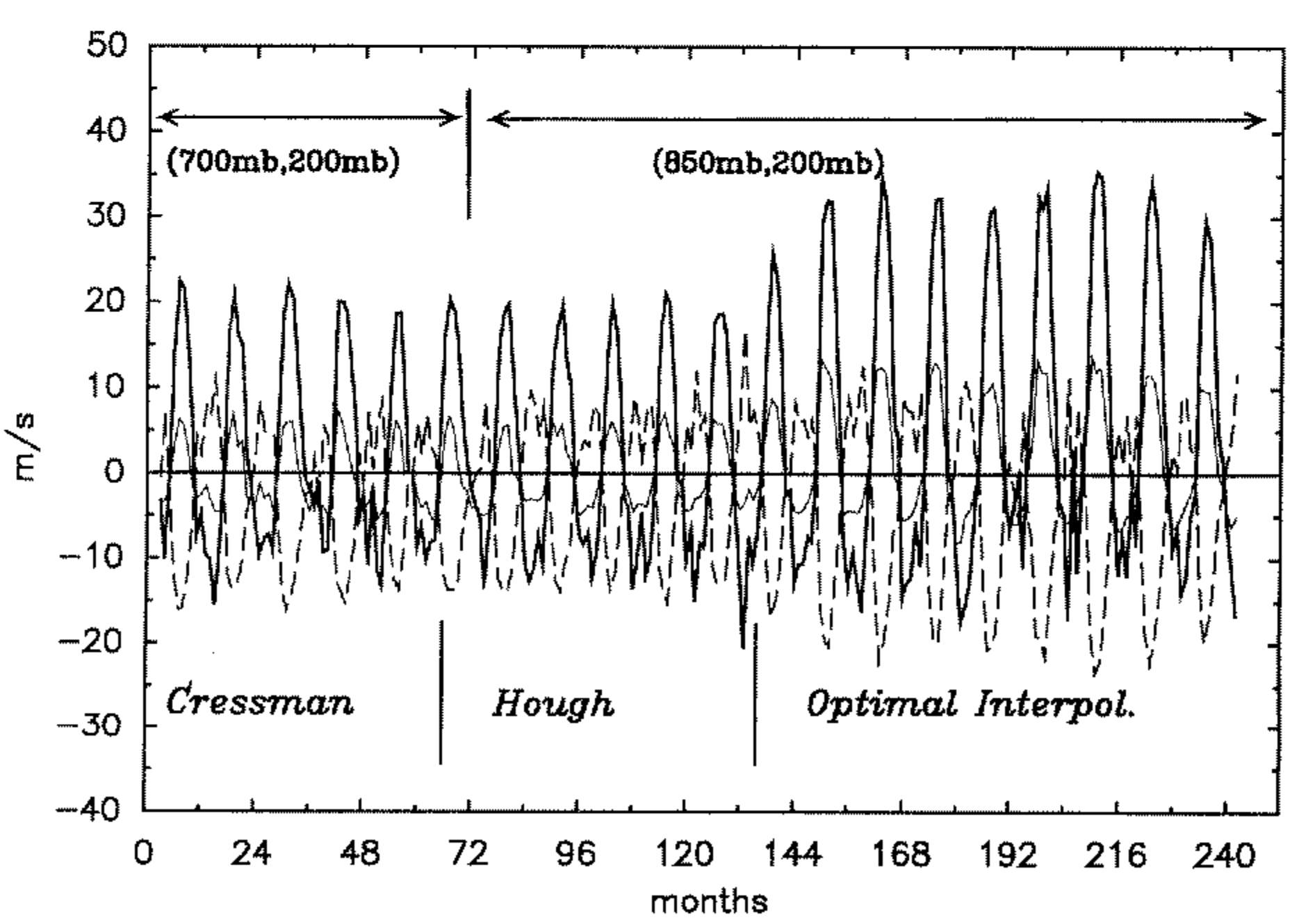

Figure A.1. The characteristics of the NMC data set. The archived data are shown in the upper part of the graph. 200 mb data are available from 1968 through 1987. In the lower troposphere 850 mb data were archived only after 1974; 700 mb data were archived previously. The curves show the 200 mb (dashed) and 850 mb (solid) zonal wind fields in the South Asian sector (5°N–20°N, 40°E–110°E). The heavy solid line shows the M_2^* monsoon intensity index. It is apparent that the character of the data changes drastically in mid 1978 with the introduction of the Optimal Interpretation initialization scheme. The data record was separated relative to the introduction of Optimal Interpolation, and long-term means calculated for the period before and after the introduction. The primary analysis concentrates on the second period when the Optimal Interpolation method was used.

interpolation scheme was implemented. The relative weakness of tropical winds between 1968–78 probably results from the underestimation of the divergent wind in the Cressman scheme and its effective elimination in the Hough scheme. A critical evaluation of the NMC data set has been undertaken by Trenberth and Olson (1988). Besides the discontinuities in the characteristics of the analyses, they pointed out that the quality of the data is questionable in the southern hemisphere, especially in the higher latitudes.

The vastly different character of the NMC data set from one period to the next greatly limits the utility of the entire data set. To allow consistent analysis, the data were divided into two streams: from 1968 to 1978 and 1979 to 1987. Long-term mean fields were calculated for the two periods separately. Difference fields were calculated relative to the appropriate mean field. For example, the anomalous distribution of a field for (say) February 1982 would be calculated relative to the mean February distribution averaged in the period 1979–87. OLR difference fields, on the other hand, would be calculated relative to means from the entire 1974–87 period. The tacit assumption is that the satellite data quality is constant throughout the entire period of its availability.

In a number of instances it has proved convenient to use the ECMWF/WMO data set which covers the period 1986–89. The data are fairly homogeneous and fully divergent during this period. The values of the Southern Oscillation Index (SOI) were obtained from the *Climate Diagnostic Bulletin* which is a monthly climate summary published by the Climate Analysis Center (CAC) of the NMC.

The study is based primarily on the analyses of seasonal mean fields, which are computed from monthly mean fields. When the seasonal means are computed, the criterion of a minimum of two monthly mean data for each season has been set. In a time series, or time section, missing data are linearly interpolated unless the data are missing for two or more successive time periods. The composite analyses used in the study are simply the arithmetic average of the data over a defined period characterized by some criteria. The anomaly of a field, over a time period, stands for the distribution of that field with the long-term time mean removed. The long-term mean chosen for an analysis is described above.

APPENDIX B

Numerical experimentation

In this study we have concentrated on the use of data to test the two propositions regarding the springtime correlation demise. Whereas some progress has been made, the diagnostic technique in the end is limited by the inadequacies of the data and the inability to be able to configure control experiments. However, the hypotheses lend themselves to testing by model experimentation. Such studies are underway.

There are two sets of experiments. Both utilize an interactive ocean–atmosphere model which is an extension of that of Anderson and McCreary (1985). The model includes Indian and Pacific Oceans and Asian and African 'continents'. The atmosphere is linear but linearized relative to a nonlinear zonally symmetric coupled model. Annual forcing is introduced into the system through the nonlinear zonally symmetric models and through the solar heating and wind stress driving of the complicated geography of the model. The geography of the model is shown in Fig. B.1. A complete description of the model will be given in a later paper.

The two sets of experiments are outlined below:

(i) *Robustness of the system*. One of the postulates discussed earlier was that the spring predictability barrier was a result of the frailness of the symmetric part of the circulation during spring which permitted random errors to grow unhindered in the system. Clearly the robustness or frailty of a system cannot be judged solely by diagnostic studies of data. A series of Monte Carlo experiments are in progress as a joint research endeavour with Dr T. Palmer of the ECMWF to see if the coupled system is more susceptible to error growth during springtime than at other times of the year. The model used is the coupled ocean–atmosphere system described above. As will be demonstrated in a sequel paper, the model possesses an annual cycle of the coupled system as well as interannual variability, both of which compare well with observations. A 50-year control run of the unperturbed model is made. For each month of year 30 the model is successively perturbed randomly to produce a set of 12 integrations for that month. The 144 integrations are each run out for 50 years and a difference field (i.e. control minus experiment) calculated for each of the runs. The error growth for each ensemble is mapped to see if the spread of forecasts diverges more at one time of the year than at another. The null hypothesis is that there will be no significant variation of the error spread (and thus the frailty or robustness of the system) as a function of the time of the year.

(ii) *Selective interaction*. There are two aspects of the selective interaction hypothesis which lend themselves to numerical experimentation. These are interactions which take place within an annual cycle and those which take place on interannual time-scales as discussed in section 7. The rather realistic annual cycle produced by the model will allow the interaction of the symmetric and asymmetric parts of the annual cycle to be carefully studied. With respect to the longer-term interaction, we plan to make a series of experiments in which the amplitude of the monsoon is modified and its impact on the phase and amplitude of the model ENSO cycle assessed.

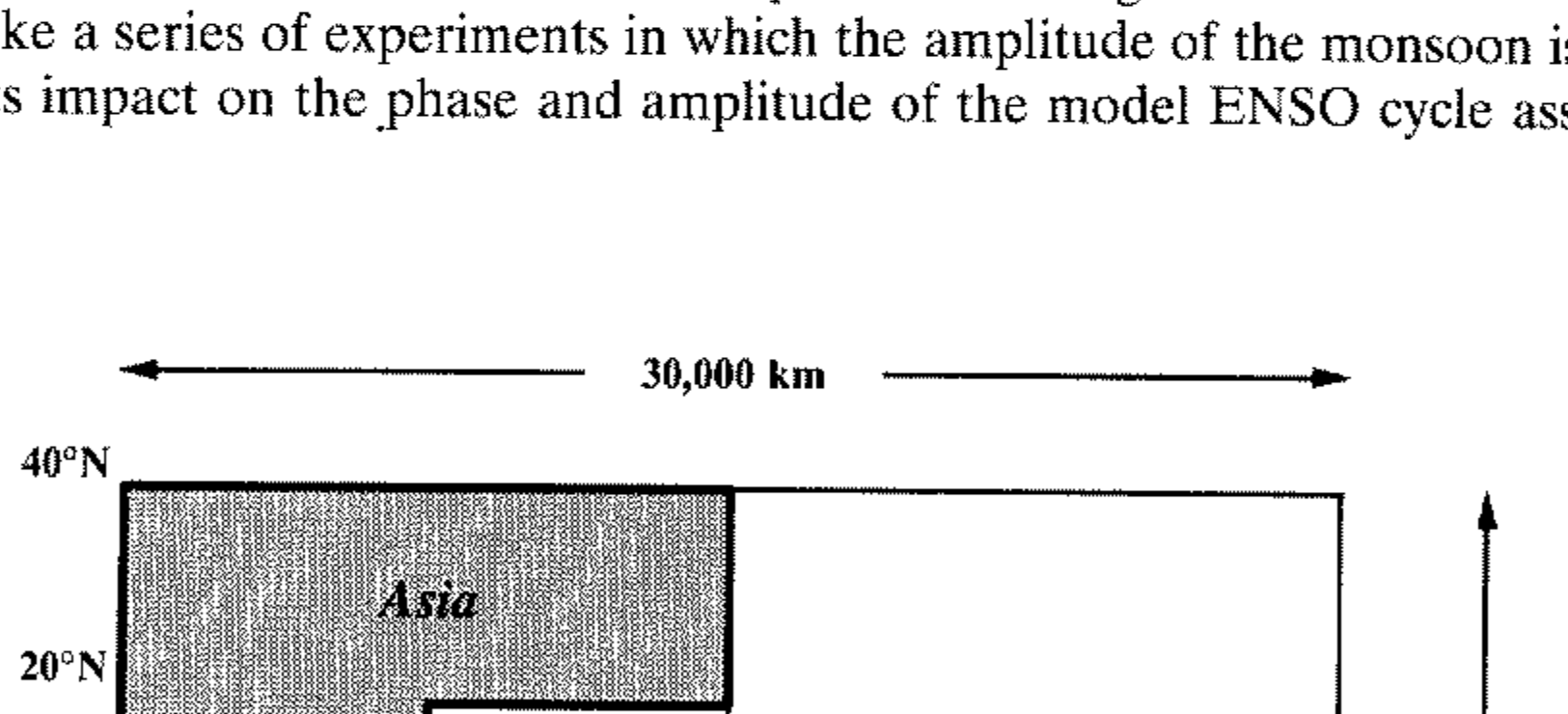

Figure B.1. Geography of the proposed model. The model consists of two independent oceans (the 'Pacific' and 'Indian') separated by a wall. A global atmosphere lies over the oceans and a continental complex aimed at providing an annual asymmetry to the solar heating. The atmosphere is linearized relative to an evolving zonally symmetric coupled model forced by an annual cycle in solar heating. Similarly, ocean and continental regions are also forced by a solar-heating function.

REFERENCES

Arkin, P. A. 1982 The relationship between interannual variability in the 200 mb tropical wind field and the Southern Oscillation. *Mon. Weather Rev.*, **110,** 1393–1404

Anderson, D. and McCreary, J. 1985 Slowly moving disturbances in a coupled ocean–atmosphere model. *J. Atmos. Sci.*, **42,** 615–629

Angell, J. K. 1981 Comparison of variations in atmospheric quantities with sea surface temperature variations in the equatorial eastern Pacific. *Mon. Weather Rev.*, **109,** 230–243

Barnett, T. P. 1984 Interaction of the monsoon and Pacific trade wind system at interannual time scales. Part III: A partial anatomy of the Southern Oscillation. *Mon. Weather Rev.*, **112,** 2388–2400

1985 Variations in near-global sea level pressure. *J. Atmos. Sci.*, **42,** 478–500

1991 The interaction of multiple time scales in the tropical climate system. *J. Climate*, **4,** 269–285

Barnett, T. P., Dumenil, L., Schlese, U., Roekner E. and Latif, M. 1989 The effect of Eurasian snow cover on regional and global climate variations. *J. Atmos. Sci.*, **46,** 661–685

Battisti, D. S. 1988 The dynamics and thermodynamics of a warming event in a coupled tropical atmosphere–ocean model. *J. Atmos. Sci.*, **45,** 2889–2919

Battisti, D. S. and Hirst, A. C. 1989 Interannual variability in the tropical atmosphere–ocean system: Influence of the basic state and ocean geometry. *J. Atmos. Sci.*, **46,** 1687–1712

Berlage, H. P. 1966 The Southern Oscillation and world weather. *K. Ned. Meteorol. Inst.*, Verh. **88,** 1–152

Bjerknes, J. 1969 Atmospheric teleconnections from the equatorial Pacific. *Mon. Weather Rev.*, **97,** 163–172

Blanford, H. F. 1884 On the connexion of Himalayan snowfall and seasons of drought in India. *Proc. R. Soc. London*, **37,** 3–22

Cane, M. A. 1991 Forecasting El Niño with a geographical model. Pp. 345–369 in Chapter 11, *Teleconnections connecting world-wide climate anomalies*. Eds. M. Glantz, R. Katz and N. Nicholls. Cambridge University Press

Cane, M. A. and Zebiak, S. E. 1985 A theory of El Niño and the Southern Oscillation. *Science*, **228,** 1085–1087

Cane, M. A., Dolan, S. C. and Zebiak, S. E. 1986 Experimental forecasts of the 1982/83 El Niño. *Nature* (*London*), **321,** 827–832

Dickson, R. R. 1984 Eurasian snow cover versus Indian monsoon rainfall—An extension of the Hahn–Shukla results. *J. Climate Appl. Meteorol.*, **23,** 171–173

Gill, A. E. 1980 Some simple solutions for heat induced tropical circulations. *Q. J. R. Meteorol. Soc.*, **106,** 447–462

Gill, A. E. and Rasmusson, E. M. 1983 The 1982–1983 climate anomaly in the equatorial Pacific. *Nature* (*London*), **305,** 229–234

Hahn, D. J. and Shukla, J. 1976 An apparent relationship between Eurasian snow cover and Indian monsoon rainfall. *J. Atmos. Sci.*, **33,** 2461–2462

Krishnamurti, T. N., Bedi, H. S. and Subramaniam, M. 1989a The summer monsoon of 1987. *J. Climate*, **2,** 321–340

1989b The summer monsoon of 1988. *Meteorol. Atmos. Phys.*, **42,** 19–37

Kutzbach, G. 1987 *Monsoons*, Eds. J. S. Fein and P. L. Stephens. Wiley–Interscience Publication. John Wiley and Sons

Latif, M. and Graham, N. E. 1991 How much predictive skill is contained in the thermal structure of an OGCM? *TOGA Notes*, **2,** 6–8

McCreary Jr, J. P. and Anderson, D. L. T. 1991 An overview of coupled ocean–atmosphere models of El Niño and the Southern Oscillation, *J. Geophys. Res.*, Special supplement, **96,** 3125–3150

Meehl, G. 1987 The annual cycle and interannual variability in the tropical Pacific and Indian Ocean region. *Mon. Weather Rev.*, **115,** 27–50

1989 The coupled ocean–atmosphere modeling problem in the tropical Pacific and Asian monsoon regions, *J. Climate*, **2,** 1146–1163

National Research Council 1990 TOGA: *A review of progress and future opportunities*. Report, Advisory panel for the Tropical Ocean/Global Atmosphere (TOGA) program. National Academy Press, Washington, D.C. (Available from the Board on Atmospheric Sciences and Climate, 2101 Constitution Ave., N.W., Washington, D.C., 20418)

Neelin, D. 1988 A simple model for surface stress and low level flow in the tropical atmosphere driven by prescribed heating. *Q. J. R. Meteorol. Soc.*, **114,** 747–770

Normand, C. 1953 Monsoon seasonal forecasting. *Q. J. R. Meteorol. Soc.*, **79,** 463–473

Philander, S. G. 1990 *El Niño, La Niña and the Southern Oscillation*. Vol. 46. International Geophysics Series. Academic Press

Ramage, C. 1971 *Monsoon meteorology*. Vol. 15. International Geophysics Series. Academic Press

Rasmusson, E. M. and Carpenter, T. H. 1983 The relationship between the eastern Pacific sea surface temperature and rainfall over India and Sri Lanka, *Mon. Weather Rev.*, **111,** 354–384

Rasmusson, E. M., Wang, X. and Ropelewski, C. F. 1990 The biennial component of ENSO variability. *J. Marine Systems*, **1,** 71–96

Richards, F. and Arkin, P. A. 1981 On the relationship between satellite-observed cloud cover and precipitation. *Mon. Weather Rev.*, **109,** 1081–1093

Ropelewski, C. F. and Halpert, M. S. 1987 Global and regional scale precipitation patterns associated with the El Niño/Southern Oscillation. *Mon. Weather Rev.*, **115,** 1606–1626

1989 Precipitation patterns associated with the high index phase of the Southern Oscillation. *J. Climate*, **2,** 268–284

Schopf, P. S. and Suarez, M. J. 1988 Vacillations in a coupled ocean–atmosphere model. *J. Atmos. Sci.*, **45,** 549–566

Shukla, J. 1987a Interannual variability of monsoons. Pp. 399–464 in *Monsoons*. Eds. J. S. Fein and P. L. Stephens. Wiley–Interscience Publication. John Wiley and Sons

1987b Long-range forecasting of monsoons. Pp. 523–548 in *Monsoons*. Eds. J. S. Fein and P. L. Stephens. Wiley–Interscience Publication. John Wiley and Sons

Shukla, J. and Mooley, D. A. 1987 Empirical prediction of the summer monsoon rainfall over India. *Mon. Weather Rev.*, **115,** 695–703

Shukla, J. and Paolino, D. A. 1983 The Southern Oscillation and long range forecasting of the summer monsoon rainfall over India. *Mon. Weather Rev.*, **111,** 1830–1837

Srinvasian, J., Gadgil, S. and Webster, P. J. 1992 Meridional propagation of large-scale monsoon convective zones. To appear in *Meteorol. Atmos. Phys.*

Trenberth, K. E. 1984 Signal versus noise in the Southern Oscillation. *Mon. Weather Rev.*, **112,** 326–332

Trenberth, K. E. and Olson, J. G. 1988 An evaluation and intercomparison of global analyses from the National Meteorological Center and the European Centre for Medium Range Weather Forecasts. *Bull. Am. Meteorol. Soc.*, **69,** 1047–1057

Troup, A. J. 1965 The Southern Oscillation. *Q. J. R. Meteorol. Soc.*, **91,** 490–506

Walker, G. T. 1923 Correlation in seasonal variations of weather. III: A preliminary study of world weather. *Mem. Indian Meteorol. Dept.*, **24,** 75–131

1924 Correlation in seasonal variations of weather. IV: A further study of world weather. *Mem. Indian Meteorol. Dept.*, **24,** 275–332

1928 World weather. III. *Mem. R. Meteorol. Soc.*, **2,** 97–106

Walker, G. T. and Bliss, E. W. 1932 World weather. V. *Mem. R. Meteorol. Soc.*, **4,** 53–84

Wallace, J. M. and Gutzler, D. S. 1981 Teleconnections in the geopotential height field during the Northern Hemisphere winter. *Mon. Weather Rev.*, **109,** 784–812

Webster, P. J. 1972 Response of the tropical atmosphere to local, steady, forcing. *Mon. Weather Rev.*, **100,** 518–540

1981 Mechanisms determining the atmospheric response to sea surface temperature anomalies. *J. Atmos. Sci.*, **38,** 554–571

Webster, P. J. 1983 Mechanisms of monsoon low-frequency variability: Surface hydrological effects. *J. Atmos. Sci.*, **40,** 2110–2124

1991 'Ocean–atmosphere interaction in the tropics'. Pp. 67–116 in Tropical extratropical interactions. ECMWF seminar proceedings, 10–14 September, 1990

Webster, P. J. and Dong, M. 1991 The structure of low frequency phenomena in the tropics and its interaction with the extratropics. *Adv. Atmos. Sci.*, **9,** 1–16

Webster, P. J. and Keller, J. 1975 Strong long-period tropospheric and stratospheric rhythm in the southern hemisphere. *Nature*, **248,** 212–213

Yang, S. and Webster, P. J. 1990 The effect of tropical heating in the adjacent hemisphere on the extratropical westerly jet streams. *J. Geophys. Res.*, **95,** D11, 18705–18721

Yasunari, T. 1987 Global structure of the El Niño/Southern Oscillation. Part II. Time evolution. *J. Meteorol. Soc. Japan*, **65,** 81–102

1991 The monsoon year—A new concept of the climate year in the tropics. *Bull. Am. Meteorol. Soc.*, **72,** 1331–1338

Zebiak, S. E. and Cane, M. A. 1987 A model El Niño–Southern Oscillation. *Mon. Weather Rev.*, **115,** 2262–2278